Magnetic exchange interactions out of equilibrium

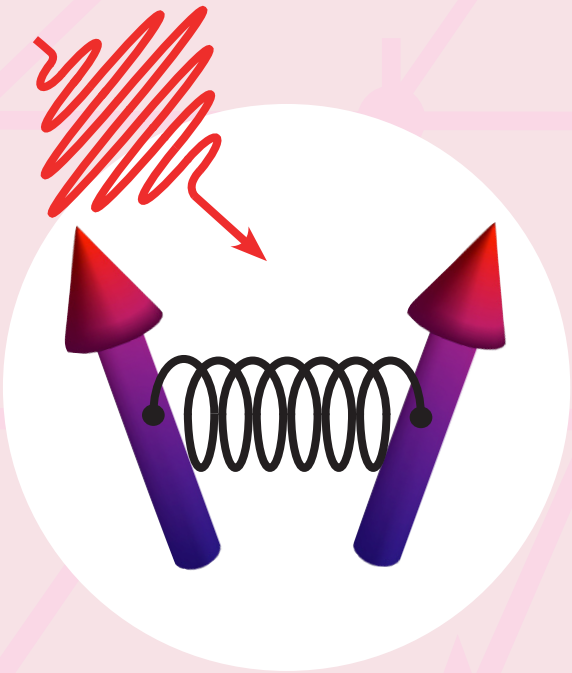

Marion Barbeau

MAGNETIC EXCHANGE INTERACTIONS OUT OF EQUILIBRIUM

Proefschrift
ter verkrijging van de graad van doctor
aan de Radboud Universiteit Nijmegen
op gezag van de rector magnificus prof. dr. J.H.J.M. van Krieken,
volgens besluit van het college van decanen
in het openbaar te verdedigen op dinsdag 30 september 2020
om 12.30 uur precies

door

Marion Michelle Séverine Barbeau

geboren op 30 juni 1992
te Nantes (Frankrijk)

Promotor: Prof. dr. M.I. Katsnelson

Copromotor: Dr. J.H. Mentink

Manuscriptcommissie:

Prof. dr. T.H.M. Rasing	
Prof. dr. M.V. Mostovoy	Rijksuniversiteit Groningen
Dr. A. Qaiumzadeh	Norges teknisk-naturvitenskapelige universitet, Trondheim, Noorwegen

The work described in this thesis was supported by the NWO via the Spinoza Prize, a VENI grant, by the European Research Council (ERC) Advanced Grant No. 338957 (FEMTO/NANO), and the Shell-NWO/FOM-initiative "Computational sciences for energy research" of Shell and Chemical Sciences, Earth and Life Sciences, Physical Sciences, FOM and STW.

Magnetic exchange interactions out of equilibrium
Thesis, Radboud University Nijmegen
ISBN 978-90-9033077-8

"N'oubliez jamais qu'il suffira d'une crise politique, économique ou religieuse pour que les droits des femmes soient remis en question."

– Simone de Beauvoir

CONTENTS

1 INTRODUCTION 1
1.1 Magnetism: macroscopic quantum physics . . . 2
1.2 Magnetism and technology . . . 3
1.3 Ultrafast spin dynamics . . . 3
1.4 Scope of the thesis . . . 4

2 METHODS 7
2.1 Introduction . . . 7
2.2 Hubbard model . . . 9
2.3 Exact diagonalization . . . 10
2.4 Generalized time-dependent canonical transformation . . . 10
2.4.1 Two-orbital Hamiltonian . . . 11
2.4.2 Projection operators . . . 11
2.4.3 Effective Hamiltonians . . . 14
2.5 Extended Dynamical Mean-Field Theory . . . 17
2.5.1 Mean-field approximation . . . 18
2.5.2 Interacting electron systems . . . 18
2.5.3 Bosonic and fermionic fields . . . 19
2.5.4 Cavity construction . . . 20
2.5.5 Comparison to the Anderson-Holstein model . . . 22
2.5.6 Self-consistencies . . . 25
2.5.7 Kadanoff-Baym contour and non-equilibrium dynamics . . . 26
2.6 Exchange interaction . . . 28
2.6.1 Exchange mechanism . . . 28
2.6.2 Formula for exchange with many-body formalism . . . 29

3 CONTROL OF COMPETING EXCHANGE INTERACTIONS IN TWO-ORBITAL SYSTEMS 33
3.1 Effective Hamiltonian . . . 35
3.2 Spin-one model . . . 36
3.3 Control of exchange interactions . . . 39

4 COHERENT SPIN-CHARGE COUPLING IN TWO-ORBITAL SYSTEMS 45
4.1 Beyond the spin-one model . . . 46
4.2 Time-dependent numerical simulations . . . 49

5 EFFECT OF DYNAMICAL SCREENING ON THE EXCHANGE INTERACTION 55
5.1 Introduction 55
5.2 Equilibrium screening of the exchange interaction 56
5.2.1 The DMFT limit 56
5.2.2 Screening by non-local correlations 57
5.3 Screening of exchange interactions out of equilibrium 59
5.3.1 Computation of the time-dependent exchange formula . . . 59
5.3.2 Non-equilibrium screening effects 61

6 STRAIN-CONTROL OF ANTISYMMETRIC EXCHANGE INTERACTION 63
6.1 Introduction 63
6.2 Modifications of Dzyaloshinskii-Moriya interaction 65
6.2.1 The model 66
6.2.2 Exchange interactions 68
6.2.3 Modification of the exchange interactions 72
6.3 Strain-induced modification of Dzyaloshinskii-Moriya interaction . 74
6.3.1 Multilayer structure for strain-wave generation 74
6.3.2 Strain-induced modification of exchange interactions 77
6.3.3 Dispersion effects 78
6.4 Effects of strain-induced changes of DMI on nucleation of Skyrmions 78

7 SUMMARY AND OUTLOOK 81

8 SAMENVATTING 85

9 RÉSUMÉ 89

10 ACKNOWLEDGMENTS 93

11 RESEARCH DATA MANAGEMENT 95

12 PUBLICATIONS 96

13 CURRICULUM VITAE 97

1

INTRODUCTION

In this chapter, we give an introduction to the basic principles of magnetism in magnetic materials. Specifically, we discuss how the exchange interaction determines the magnetic ordering of microscopic spins. Subsequently, we discuss the importance of magnetism in data storage technology. We highlight some of the challenges that industry faces with the development of the next generation of magnetic data storage devices. This is followed by an introduction to the field of ultrafast magnetism which potentially can overcome the limitations sets by the physics of conventional storage technology. We conclude that, in order to ultimately harness the potential of ultrafast magnetism, fundamental insight in the optical control of exchange interaction is highly desired. Finally, we discuss the scope and content of this thesis.

1.1 MAGNETISM: MACROSCOPIC QUANTUM PHYSICS

Magnetic materials are omnipresent in our lives, from the decorative magnets we put on the fridge to the advanced magnetic hard drive of our computers. Interestingly, the macroscopic effects of magnetism (the magnet is attracted by the surface of the fridge) come from the quantum properties of matter. Indeed, the origin of magnetism in materials lies in the intrinsic spin momentum carried by the electrons. For illustration, the spin of an electron is usally represented by an arrow and may be seen as a small magnet as illustrated in Figure 1.1a. The north pole of the magnet is represented by the top of the arrow (red) while the bottom of the arrow stands for the south pole (blue). Inside the fridge magnet, the spins points to the same direction leading to a total magnetic field strong enough to to stick the magnet to the metallic surface of the fridge instead of falling onto the ground due to gravity.

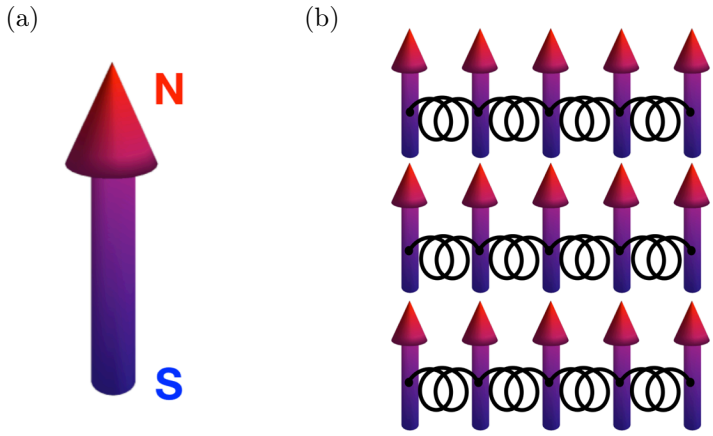

Figure 1.1: (a) Illustration of the spin of an electron as a small magnet. The magnet has two poles, a north pole represented in red and a south pole represented in blue. (b) Illustration of a magnetic order in a material. Arrows represents spins and black springs represent the exchange interactions responsible for the magnetic ordering.

The magnetic ordering in materials has its origin in quantum mechanics as well. Specifically, it stems from the interaction between the charge of the electrons and the symmetry of the quantum mechanical wavefunction under exchanging the position of electrons. The resulting force is called the exchange interaction. The exchange interaction is illustrated in Figure 1.1b by black springs which connect the spins leading to ordering of spins throughout the material (all spins point in the same direction). The exchange interaction is the strongest force in magnetic systems and is equal to about a thousand times that of a conventional magnetic field.

Therefore, there is huge interest among the scientific comunity to understand the exchange interaction and to ultimately control it in order to control the magnetic order.

1.2 MAGNETISM AND TECHNOLOGY

Nowadays the demand for magnetic data storage rapidly grows as a result of the increase of cloud storage, streaming video and social media. In 2012, this information and communication technology sector as a whole was consuming already up to 5% of the world electricity and continues to grow even further [1]. This growing need for digital data and corresponding increaseded energy cost calls for the development of not only faster but also more energy-efficient storage technology. This however, comprises a major challenge. The dominant storage technology is magnetic data storage. In magnetic hard drives, the data is stored in the form of bits 0 and 1 which represent the magnetization up or down of tiny magnets ($20\times20\text{nm}^2$). Currently, the magnetic orientation of these magnets is controlled by applying an external magnetic field. Therefore, the speed of writing information is determined by the field strength. The faster the magnetic bit switches, the stronger the magnetic field should be and therefore, more energy is needed. Hence, the current magnetic data storage technology faces physical limitations which stimulates scientists to look for alternative ways to control magnetism.

1.3 ULTRAFAST SPIN DYNAMICS

An intriguing possibility to overcome the physical limitations of magnetic field induced dynamics is the laser induced magnetism. Last century, it has been shown experimentally by Beaurepaire et al. [2] that the magnetism of nickel can be quenched on a sub-picosecond time scale following femtoseconds laser excitation. This dynamics is much faster than the usual nanosecond spin dynamics induced by a magnetic field. Subsequent works showed that the magnetization cannot only be quenched using light but can also be completely switched with a single femtosecond laser pulse [3–6].

At the microscopic scale, the exchange interaction plays a key role in this ultrafast magnetism. Therefore, the direct control of exchange is a very promising way to understand the ultrafast control of magnetic order, with potentially high energy efficiency. Recently, the direct ultrafast control of the exchange interaction by external laser pulses has received significant interest, both experimentally as well as in theory [7–19]. So far, modifications of exchange interaction of only a few percent were observed [13, 20]. Interestingly, many systems give rise to multiple exchange interactions (symmetric, antisymmetric, biquadratic,...). However, little is known about the effect of the control of the competition between these exchange interactions. Can it lead to a stronger and more efficient control of exchange interactions? Can it trigger additional spin dynamics? Can we make the perturbation

of the net exchange interaction stronger by investigating the competition between electronic interactions?

1.4 SCOPE OF THE THESIS

In this thesis, we theoretically study the control of exchange interactions in extentions of single-orbital systems either with additional orbitals or additional non-local Coulomb interaction. Specifically, we look for answers to three main problems:

- Despite existing studies on multi-orbital systems [21–24] the role of orbital dynamics in the control of exchange has not been fully revealed. Therefore, we want to know the influence of orbital dynamics on the direct control of the exchange interactions by an electric field in multi-orbital systems. In addition, are there any non-equilibrium phenomena which arise in multi-orbital systems and possibly compete or inhibit the control of exchange interactions?
- Another fundamental problem which arrises in the control of exchange is the effect of screening of the charge degrees of freedom. Even if screening effects are weak in equilibrium, do they remain weak out of equilibrium?
- Exchange interactions which lead to an antisymmetric spin ordering are responsible for exotic structures such as magnetic Skyrmions. Can we modify the antisymmetric exchange interaction in order to create/anihilate magnetic Skyrmions?

After this introduction, chapter 2 reviews the methods used in this thesis in order to study the control of exchange in condensed matter systems. After introducing the Hubbard model, we discuss the exact diagonalization as well as the generalized canonical transformation. Moreover, we discuss a diagrammatic method known as Extended Dynamical Mean-Field Theory (EDMFT). In addition, we discuss the exchange interaction and the techniques used in this thesis in order to calculate it.

Chapter 3 focuses on the control of competing exchange interactions in a two-orbital Mott-Hubbard system. Specificaly, we study the influence of the orbital dynamics on the control of exchange interactions with an external electric field.

In chapter 4, we continue studying the same system as in chapter 3 in a different regime for which a new spin-charge coupling phenomenon competes with the control of exchange interactions.

In chapter 5, we study the competition between the hopping and non-local Coulomb interaction leading to screening effects on the exchange interaction. First, we discuss the effects of screening in equilibrium. Then, we drive the system out of equilibrium using an external electric field and study the effects of dynamical screening on the exchange interaction.

Chapter 6 is dedicated to the control of antisymmetric exchange interaction with a strain wave created by an ultrafast laser pulse. We use a minimal model for a magnetic thin-film which exhibits both symmetric and antisymmetric exchange interactions. Using this model, we calculate the effect of displacement between the magnetic layer and the substrate on the exchange interactions. To simulate the

displacement, we study the propagation of a strain wave through the magnetic thin-film. Moreover, we draw a parallel between our calculations and results obtained with atomistic simulations targeted to the possibility of creating and annihilating magnetic Skyrmions with accoustic pulses.

In the two-orbital Mott-Hubbard system, a biquadratic exchange interaction arrises in addition to the Heisenberg exchange. As for the Heisenberg exchange, the biquadratic exchange interaction can be controlled by an electric field. In addition, we find that there is a field regime for which the exchange interactions strongly compete. Moreover, for a specific electric field regime, we discover a novel spin-charge coupling which allows non-resonant and reversible control of charge correlations in a spin state. The study of the screening of the exchange interaction leads to the observation that non-equilibrium screening effects are about ten times stronger than in equilibrium. In chapter 6, we investigate whether the modification of the antisymmetric exchange interaction with a strain wave is possible. The results suggest that the creation, annihilation of a magnetic Skyrmion is potentially feasible at the picosecond time scale with a femtojoule energy dissipation.

2

METHODS

2.1 INTRODUCTION

In condensed matter systems, dynamical quantum effects can be described by the time-dependent Schrödinger equation

$$i\hbar\frac{\partial|\psi(t)\rangle}{\partial t} = \hat{H}(t)|\psi(t)\rangle, \tag{2.1}$$

where $|\psi(t)\rangle$ is the wavefunction and $\hbar$ is the reduced Plank constant. Finding an exact solution for the Schrödinger equation is highly challenging. Hence, even for simple models of interest, analytical solutions are not available and despite the recent developments of supercomputers, obtaining an exact numerical description of condensed matter systems is practically impossible without resorting to approximations. In this chapter, we focus on a discussion of the analytical and numerical methods we used to study the exchange interactions.

The most accurate method for the study of solid states system is the exact diagonalization (ED). If the physics of interest is known to be captured by only a subspace of the total Hilbert space, approximate analytical methods can be usefull. A commonly used analytical method is the canonical transformation (CT) [25] and its extension to time-dependent systems [19, 21, 26–28]. The use of the CT leads to an effective model which describes the low energy subspace, capturing the effect of virtual excitation of high-energy states in effective parameters, such as the exchange interaction. Beyond the CT, diagrammatic methods are very useful for understanding many-body problems. These methods do not suffer from restrictions to specific subspaces of the Hilbert space and therefore, can be applied to arbitrary interaction strengths and external perturbations. Based on the many-body formalism, a Dynamical Mean-Field Theory (DMFT) has been developed and implemented [29–32]. Unlike ab initio techniques such as Density Functional Theory [33] which reduces many-body electronic interactions to an exactly solvable single-particle problem, DMFT maps an (infinitely) extended lattice onto a single-impurity model accounting for local many-body interactions. An interesting extension of DMFT, Extended DMFT (EDMFT), accounts not only for local electronic interactions but also non-local interactions between electrons in different lattice sites are taken into account [34]. Similarly as DMFT, the EDMFT has been generalized for the non-equilibrium case, allowing for the use of external driving such as electric fields [35]. To calculate effective exchange interactions from such many-body formalisms, analytical formulas have been derived both in equilbrium [36–38] as well as for time-dependent problems [39]. Furthermore,

these formulas have been implemented allowing for the study of non-equilibrium exchange interaction in strongly correlated systems [13, 18].

In this chapter, we review the methods which are used in this thesis to study condensed matter systems. In section 2.2, we discuss the Hubbard model and its extensions as used in this thesis. In section 2.3, we discuss the ED. In section 2.4, we discuss the CT as well as its generalization to a two-orbital oxide system under an external electric field. In section 2.5, we discuss the EDMFT as well as its extention to non-equilibrium dynamics. Finally, in section 2.6, we discuss the exchange interaction; how it can be derived and how it is evaluated.

Sections 2.2 and 2.4 of this chapters incorporates parts of the following publication: M.M.S. Barbeau, M. Eckstein, M.I. Katsnelson and J.H. Mentink, *"Optical control of competing exchange interactions and coherent spin-charge coupling in two-orbital Mott insulators"*, SciPost Phys. **6**, 027 (2019).

2.2 HUBBARD MODEL

The Hubbard model was first proposed in the early 1960s [40–43] to describe ferromagnetism in transition metals. The Hubbard model quickly raised interest for the description of strongly correlated systems, *e.g.* high-temperature superconductors [44, 45]. Nowadays, the Hubbard model and its extensions are still widely used in condensed matter systems as well as in cold atom systems [46]. In this section, we introduce the single-orbital Hubbard model and discuss its different limits. In addition, we discuss the Peierls substitution which allows to account for an external time-dependent electric field.

The Hubbard model is the simplest model which describes interacting electrons in lattices and reads

$$\hat{H} = -\sum_{<ij>,\sigma} t_{ij}\hat{c}^{\dagger}_{i\sigma}\hat{c}_{j\sigma} + U\sum_{i}\hat{n}_{i\uparrow}\hat{n}_{i\downarrow}, \tag{2.2}$$

where $\hat{c}^{\dagger}(\hat{c})$ are creation (anihilation) operators, i and j are site indices, $< ... >$ stands for nearest neigbhors, $\sigma = \uparrow, \downarrow$ are up and down spins, respectively, and $\hat{n}_{i\sigma}=\hat{c}^{\dagger}_{i\sigma}\hat{c}_{i\sigma}$.

The Hubbard model, Eq. (2.2), possesses two terms, (i) the kinetic term with the hopping amplitude t_{ij} which allows the electrons to move to different sites in the lattice, (ii) the Coulomb interaction U which is the energy required to have two electrons on one site. While the kinetic term tends to delocalize electrons in the lattice, the repulsive Coulomb interaction tends to localize them in order to minimize the potential energy cost. Therefore, by tuning the parameters t_{ij} and U, the Hubbard model allows two distinct phases:

• The limit for which $t_{ij} \gg U$ where the electrons are strongly delocalized on the lattice leading to a metallic phase.

• The limit for which $t_{ij} \ll U$ where the electrons are strongly localized on site leading to a Mott insulating phase.

In the vicinity of $t_{ij}/U \sim 1$, the system experiences what is called a Mott transition [47] where the system exhibits a first-order phase transition between a metallic and an insulating phase. In this thesis we study both the strongly correlated insulating phase and weakly correlated metallic phase, outside the region where the metal-insulator transition takes place.

Time-dependent electric fields can be included in Eq. (2.2) within the hopping matrix elements $t_{ij}=t_{ij}(t)$ via the Peierls substitution $t_{ij}(t)=t_0 e^{ieA_{ij}(t)}$ [18, 48, 49], where e is the electronic charge, $A_{ij}(t) = -\frac{1}{\omega}E_0\cos(\omega t)(R_i - R_j)$ is the projection of the vector potential along the direction from site i to j, where E_0 is the amplitude of the field. We define the parameter $\mathcal{E}=eaE_0/\omega$ which represents the driving strength, with $a=|R_i - R_j|$ and we take $t_0=1$ as a unit of energy.

In conclusion, we introduced the generic single-orbital Hubbard model. We discussed the limits in which the model displays different physics. Moreover, we

discussed the Peierls substitution commonly used to account for external electric fields.

2.3 EXACT DIAGONALIZATION

An exact solution of the many-body problem is obtained by expanding the Hamiltonian in a set of many-particle basis states constructed from single-particle basis states. In this section, we discuss the exact diagonalization (ED) technique which is used later in chapter 6

Let H be an Hamiltonian with basis states $|\phi_i\rangle$ belonging to the Hilbert space $\mathcal{H}$. The Hamiltonian H can be written in a matrix form as

$$H = \begin{pmatrix} H_{11} & H_{21} & H_{31} & \cdots & H_{k1} \\ H_{12} & H_{22} & H_{32} & \cdots & H_{k2} \\ H_{13} & H_{23} & H_{33} & \cdots & H_{k3} \\ \vdots & \vdots & \vdots & \ddots & \vdots \\ H_{1k} & H_{2k} & H_{3k} & \cdots & H_{kk} \end{pmatrix}, \tag{2.3}$$

where H_{ij} are matrix elements $H_{ij}=\langle\phi_i|H|\phi_j\rangle$.

The diagonalization is done by solving the eigenvalue problem

$$\det(H - \lambda) = 0. \tag{2.4}$$

After the diagonalization, the Hamiltonian is diagonal in the eigenvectors $|\tilde{\phi}_j>$ thus obtained: $<\tilde{\phi}_i|\hat{H}|\tilde{\phi}_j>=\delta_{ij}\lambda_j$, with eigenvalues λ_i, i=1, ..., k.

For the case of non-interacting particles, the ED can be used for large systems (millions of atoms [50]). However, our interest is in systems where the electrons are correlated which leads to many-particle states. Therefore, we restrict ourselves to systems with a small number of atoms.

2.4 GENERALIZED TIME-DEPENDENT CANONICAL TRANSFORMATION

The conventional way to derive a low energy effective Hamiltonian of the system is to use a canonical transformation (CT) also known as Schrieffer-Wolff transformation [25]. Unlike ED (see section 2.3) the CT gives a description of only a subspace of the total Hilbert space. Moreover, in practice analytical expressions for the CT are obtained using a perturbative expansion from a well-controlled limit. Eventually, the canonical transformation leads to the expression of an effective Hamiltonian which captures the low-energy properties of the system. The CT can be extended to time-dependent systems in case of perturbations by external electric fields [19, 21, 26–28]. With this extension, the time-dependent CT allows to approximate a generic time-dependent Hamiltonian by an effective Hamiltonian for a specific part

of the (perturbed) spectrum. This can be subsequently used to obtain expressions for exchange interactions. In this section, we generalize a time-dependent canonical transformation for the case of a two-orbital Mott-Hubbard model [51]. This allows us to capture properties of the system which not only involve the low-energy subspace, but also a coupling with high-energy states. The section is organized as follows: in subsection 2.4.1, we introduce the two-orbital Hamiltonian. In subsection 2.4.2, we derive projection operators. In subsection 2.4.3, we derive an effective Hamiltonian using the formalism of the generalized time-dependent CT.

2.4.1 *Two-orbital Hamiltonian*

In this subsection, we discuss the two-orbital Mott Hubbard Hamiltonian at half-filling. In addition, we discuss the time-dependent electric field included in the kinetic term of the Hamiltonian via the Peierls substitution [18, 48, 49].

The Hamiltonian is given by $\hat{H}(t)=\hat{H}_{\mathrm{U}}+\hat{H}_{\mathrm{kin}}(t)$, where $\hat{H}_{\mathrm{U}}=\hat{H}_{\mathrm{nn}}+\hat{H}_{\mathrm{sf}}$ [41]. Hamiltonians $\hat{H}_{\mathrm{nn}}$, $\hat{H}_{\mathrm{sf}}$ and $\hat{H}_{\mathrm{kin}}$ contain the density-density interaction, the spin-flip and pair hopping, and the intersite hopping, respectively:

$$\hat{H}_{\mathrm{nn}}=\sum_{i,\alpha} U\hat{n}_{i\alpha\uparrow}\hat{n}_{i\alpha\downarrow}+\sum_{i,\alpha\neq\beta,\sigma}\left\{\frac{(U-2J_H)}{2}\hat{n}_{i\alpha\sigma}\hat{n}_{i\beta\bar{\sigma}}+\frac{(U-3J_H)}{2}\hat{n}_{i\alpha\sigma}\hat{n}_{i\beta\sigma}\right\} \tag{2.5}$$

$$\hat{H}_{\mathrm{sf}}=-J_H\sum_{i,\alpha\neq\beta}\left(\hat{c}^{\dagger}_{i\alpha\uparrow}\hat{c}_{i\alpha\downarrow}\hat{c}^{\dagger}_{i\beta\downarrow}\hat{c}_{i\beta\uparrow}+\hat{c}^{\dagger}_{i\alpha\uparrow}\hat{c}_{i\beta\downarrow}\hat{c}^{\dagger}_{i\alpha\downarrow}\hat{c}_{i\beta\uparrow}\right) \tag{2.6}$$

$$\hat{H}_{\mathrm{kin}}(t)=-\sum_{<i,j>} t_{ij}(t)\sum_{\alpha,\sigma}\hat{c}^{\dagger}_{i\alpha\sigma}\hat{c}_{j\alpha\sigma}. \tag{2.7}$$

Here, $\alpha=a,b$ stands for the orbital degree of freedom and J_{H} is the Hund exchange interaction. In addition, we used the Peierls substitution for the hopping amplitude $t_{ij}(t)=t_0 e^{ieA_{ij}(t)}$, see section 2.2. Note that this system can be associated with the e_g band of an oxide compound and, since both e_g orbitals originate from d orbitals, no on-site electric dipole transitions are allowed.

Summarizing, we introduced the two-orbital Hubbard model which, unlike the single-orbital model, Eq. (2.2), possesses an additional Hund exchange interaction J_{H} which arises only in the case of multi-orbital systems.

2.4.2 *Projection operators*

To derive an effective Hamiltonian for a specific subspace of the Hilbert space, it is useful to define projection [52–56]. This is well-known for single-orbital models, but the two-orbital case is more involved due to the Hund interaction J_{H}.

To deal with this problem, we restrict the Hilbert space to blocks involving only two sites (ij). For all states $|\phi_k\rangle$ on the bond (ij), we then define projection

operators $\hat{P}_d^{\nu}(N,M)$ onto the following quantum numbers:

- Particle number:

$$(N-\hat{N})\ \hat{P}_d^{\nu}(N,M)\ |\phi_k\rangle = 0, \tag{2.8}$$

where $\hat{N}=\sum_{i\alpha\sigma}\hat{n}_{i\alpha\sigma}$ and N=0, ..., 8 the number of electrons which occupy the system.

- Total spin $\hat{S}^z$ component:

$$(M-\hat{S}^z_{\rm tot})\ \hat{P}_d^{\nu}(N,M)\ |\phi_k\rangle = 0, \tag{2.9}$$

where $\hat{S}^z_{\rm tot}=\sum_i(\hat{S}^z_{ia}+\hat{S}^z_{ib})$ and $M=-2, ..., 2$.

We are primarily interested in the case of half-filling, for which N=4. In addition, we consider an antiferromagnetic state such that M=0, and write $\hat{P}_d^{\nu}(N{=}4, M{=}0)\equiv\hat{P}_d^{\nu}$.

- Number of doubly occupied sites, i.e. number of doublons d:

$$(d-\hat{d})\ \hat{P}_d^{\nu}\ |\phi_k\rangle = 0, \tag{2.10}$$

where d=0, 1, 2 and $\hat{d}=\sum_{i\alpha}\hat{n}_{i\alpha\uparrow}\hat{n}_{i\alpha\downarrow}$. Hence, $\hat{P}_d^{\nu}$ projects onto states with d doublons.

- Hund rule violation:

$$(\nu-\hat{\nu})\ \hat{P}_d^{\nu}\ |\phi_k\rangle = 0, \tag{2.11}$$

with $\hat{\nu}=\sum_{i\alpha\neq\beta}\frac{1}{2}(\hat{n}_{i\alpha\uparrow}\hat{h}_{i\alpha\downarrow}\hat{h}_{i\beta\uparrow}\hat{n}_{i\beta\downarrow}+\hat{n}_{i\alpha\uparrow}\hat{n}_{i\alpha\downarrow}\hat{h}_{i\beta\uparrow}\hat{h}_{i\beta\downarrow})$, where $\hat{h}_{i\alpha\sigma}=(1-\hat{n}_{i\alpha\sigma})$. The value ν=0, 1 corresponds to configurations that satisfy or violate local spin alignment dictated by Hund exchange, respectively. For example, in the $\hat{P}_0^{\nu}$ sector, the states with ν=0 are $|\uparrow,\uparrow\rangle_i|\downarrow,\downarrow\rangle_j$, $|\downarrow,\downarrow\rangle_i|\uparrow,\uparrow\rangle_j$, and the ν=1 states are $|\uparrow,\downarrow\rangle_i|\uparrow,\downarrow\rangle_j$, $|\downarrow,\uparrow\rangle_i|\downarrow,\uparrow\rangle_j$, $|\uparrow,\downarrow\rangle_i|\downarrow,\uparrow\rangle_j$, $|\downarrow,\uparrow\rangle_i|\uparrow,\downarrow\rangle_j$, where $|\sigma_a,\sigma'_b\rangle_i=\hat{c}^{\dagger}_{ib\sigma'}\hat{c}^{\dagger}_{ia\sigma}|0\rangle$.

Although $\left[\hat{H}_{\rm sf},\hat{P}_d^{\nu}\right]$=0, the states $\hat{P}_d^{\nu}|\phi_k\rangle$, with ν=1 do not diagonalize $\hat{H}_{\rm sf}$. In principle, it is possible to further decompose $\hat{P}_d^{\nu}$ by introducing additional quantum numbers that project on states that simultaneously diagonalize $\hat{P}_d^{\nu}$ and $\hat{H}_{\rm sf}$. Here we restrict ourselves to the projectors $\hat{P}_d^{\nu}$, since this is already sufficient to describe the control of the biquadratic exchange interaction as well as the spin-charge coupling, as we discuss in more detail in chapters 3 and 4.

The explicit expressions for $\hat{P}_d^{\nu}(N,M)$ in terms of single-electron operators can be derived using

$$\hat{p}(i)=\prod_{\alpha,\sigma}(\hat{n}_{i\alpha\sigma}+\hat{h}_{i\alpha\sigma}). \tag{2.12}$$

With these definitions, the identity reads

$$1 = \hat{p}(i)\hat{p}(j) = \sum_{d,\nu,N,M} \hat{P}_d^\nu(N,M), \tag{2.13}$$

and we obtain the following expressions for $\hat{P}_d^\nu$

$$\hat{P}_0^0 = \sum_\sigma \hat{n}_{ia\sigma}\hat{h}_{ia\bar{\sigma}}\hat{n}_{ib\sigma}\hat{h}_{ib\bar{\sigma}}\hat{h}_{ja\sigma}\hat{n}_{ja\bar{\sigma}}\hat{h}_{jb\sigma}\hat{n}_{jb\bar{\sigma}}, \tag{2.14}$$

$$\hat{P}_0^1 = \sum_{\alpha\neq\beta} \hat{n}_{i\alpha\uparrow}\hat{h}_{i\alpha\downarrow}\hat{h}_{i\beta\uparrow}\hat{n}_{i\beta\downarrow}\big(\hat{n}_{j\alpha\uparrow}\hat{h}_{j\alpha\downarrow}\hat{h}_{j\beta\uparrow}\hat{n}_{j\beta\downarrow} + \hat{h}_{j\alpha\uparrow}\hat{n}_{j\alpha\downarrow}\hat{n}_{j\beta\uparrow}\hat{h}_{j\beta\downarrow}\big), \tag{2.15}$$

$$\begin{aligned}\hat{P}_1^0 = \sum_{<i,j>}\sum_{\alpha\neq\beta,\sigma} \hat{n}_{i\alpha\sigma}\hat{n}_{i\alpha\bar{\sigma}}\hat{n}_{i\beta\sigma}\hat{h}_{i\beta\bar{\sigma}}\big(\hat{h}_{j\alpha\sigma}\hat{h}_{j\alpha\bar{\sigma}}\hat{h}_{j\beta\sigma}\hat{n}_{j\beta\bar{\sigma}} \\ + \hat{h}_{j\alpha\sigma}\hat{n}_{j\alpha\bar{\sigma}}\hat{h}_{j\beta\sigma}\hat{h}_{j\beta\bar{\sigma}}\big),\end{aligned} \tag{2.16}$$

$$\hat{P}_1^1 = \sum_{<i,j>}\sum_{\alpha\neq\beta,\sigma} \hat{n}_{i\alpha\sigma}\hat{n}_{i\alpha\bar{\sigma}}\hat{h}_{i\beta\sigma}\hat{h}_{i\beta\bar{\sigma}}\hat{n}_{j\alpha\sigma}\hat{h}_{j\alpha\bar{\sigma}}\hat{h}_{j\beta\sigma}\hat{n}_{j\beta\bar{\sigma}}, \tag{2.17}$$

$$\hat{P}_2^0 = \sum_{<i,j>} \hat{h}_{ia\uparrow}\hat{h}_{ia\downarrow}\hat{h}_{ib\uparrow}\hat{h}_{ib\downarrow}\hat{n}_{ja\uparrow}\hat{n}_{ja\downarrow}\hat{n}_{jb\uparrow}\hat{n}_{jb\downarrow}, \tag{2.18}$$

$$\hat{P}_2^1 = \sum_{\alpha\neq\beta} \hat{n}_{i\alpha\uparrow}\hat{n}_{i\alpha\downarrow}\hat{h}_{i\beta\uparrow}\hat{h}_{i\beta\downarrow}\big(\hat{n}_{j\alpha\uparrow}\hat{n}_{j\alpha\downarrow}\hat{h}_{j\beta\uparrow}\hat{h}_{j\beta\downarrow} + \hat{h}_{j\alpha\uparrow}\hat{h}_{j\alpha\downarrow}\hat{n}_{j\beta\uparrow}\hat{n}_{j\beta\downarrow}\big). \tag{2.19}$$

While the interacting term of the two-orbital Hamiltonian Eq. (2.7) is diagonal in $\hat{P}_d^\nu$

$$\hat{H}_U = \sum_{d,\nu} \hat{P}_d^\nu \hat{H}_U \hat{P}_d^\nu, \tag{2.20}$$

the hopping $\hat{H}_{\mathsf{kin}}(t)$ term connects $\hat{P}_d^\nu$ with different d. It can be re-written in terms of operators $\hat{T}^{+1}(t)$, $\hat{T}^{-1}(t)$ and $\hat{T}^0(t)$ that change d by $+1$, -1 and 0 respectively

$$\hat{H}_{\mathsf{kin}}(t) = \hat{T}^{+1}(t) + \hat{T}^{-1}(t) + \hat{T}^0(t), \tag{2.21}$$

where

$$\hat{T}^{+1}(t) = \sum_{\nu=0,1} \big(\hat{P}_2^\nu \hat{H}_{\mathsf{kin}}(t)\hat{P}_1^0 + \hat{P}_1^0 \hat{H}_{\mathsf{kin}}(t)\hat{P}_0^\nu\big), \tag{2.22}$$

$$\hat{T}^{-1}(t) = \sum_{\nu=0,1} \big(\hat{P}_0^\nu \hat{H}_{\mathsf{kin}}(t)\hat{P}_1^0 + \hat{P}_1^0 \hat{H}_{\mathsf{kin}}(t)\hat{P}_2^\nu\big), \tag{2.23}$$

and

$$\hat{T}^0(t) = \hat{P}_1^0 \hat{H}_{\mathsf{kin}}(t)\hat{P}_1^1 + \hat{P}_1^1 \hat{H}_{\mathsf{kin}}(t)\hat{P}_1^0. \tag{2.24}$$

The projection operators $\hat{P}_d^\nu$ and hopping operators $\hat{T}^{+1}(t)$, $\hat{T}^{-1}(t)$, $\hat{T}^0(t)$ play an important role in the canonical transformation described in the next susbection.

Summarizing, we defined the projection operators $\hat{P}_d^\nu$ and showed their expressions in terms of fermionic operators. In addition, we identified that $\hat{H}_{\text{kin}}(t)$ changes the number of doublons d while $\hat{H}_U$ conserves d.

2.4.3 *Effective Hamiltonians*

The single-orbital model possesses only d=0 and d=1 subspaces while in the two-orbital case, we have an additional d=2 subspace. The standard Canonical Transformation (CT) gives rise to an effective Hamiltonian for the d=0 subspace only since the d=2 subspace is strongly gapped. However, out of equilibrium, the d=0 and d=2 subspaces can become (nearly) degenerate. Therefore generaliziation of the time-dependent CT is desired [51]. First, we introduce the conventional CT and the rotation of the Hamiltonian $\hat{H}$ by means of a unitary transformation. Second, we discuss the generalization of the CT using the projection operators $\hat{P}_d^\nu$ introduced in subsection 2.4.2. Third, we discuss the case of the driving with a time periodic electric field. Fourth, we discuss the energy approximation used to simplify the desciption of subspaces of the Hilbert space. Fifth, we derive an expression for a second and fourth order effective Hamiltonian.

The canonical transformation is a technique which enables the derivation of an effective Hamiltonian for the subspace of states $\hat{P}_d^\nu$ [19, 21, 25–28]. Formally, this is achieved by unitary transformation $\hat{V}(t)$=$e^{-i\hat{S}(t)}$ that transforms the Hamiltonian $\hat{H}(t)$ to a rotated frame. The effective Hamiltonian in the rotated frame reads

$$\hat{H}_{\text{eff}}(t) = \hat{V}^\dagger(t)(\hat{H}(t) - i\partial_t)\hat{V}(t). \tag{2.25}$$

The aim is to identify a suitable subspace (defined by values of d and ν) and determine $\hat{V}$ such that $\hat{H}_{\text{eff}}$ leaves this subspace invariant. To do this, we perform the unitary transformation perturbatively, treating the hopping parameter $t_0 \ll U$ as a perturbation. We expand $i\hat{S}(t)$ and $\hat{H}_{\text{eff}}(t)$ in terms of a Taylor series

$$i\hat{S}(t) = \sum_{n=1}^{\infty} i\hat{S}^{(n)}(t), \tag{2.26}$$

$$\hat{H}_{\text{eff}}(t) = \sum_{n=0}^{\infty} \hat{H}_{\text{eff}}^{(n)}(t), \tag{2.27}$$

where $\hat{S}^{(n)}$, $\hat{H}_{\text{eff}}^{(n)} \propto t_0^n$. For deriving a pure low energy model, one could construct the unitary transformation such that $\hat{H}_{\text{eff}}^{(n)}$ does not contain terms that change d [21, 25, 27, 57, 58], and obtain an effective Hamiltonian in the subspace d=0. Here, we enlarge our effective model and keep terms that change d by ± 2, while we design $\hat{P}_d^\nu i\hat{S}^{(n)}\hat{P}_{d'}^{\nu'}$ such that

$$\hat{P}_d^{\nu}\hat{H}_{\mathsf{eff}}^{(n)}(t)\hat{P}_{d\pm1}^{\nu'}=0. \tag{2.28}$$

At half filling and without inter-orbital hopping ($t_{\alpha\neq\beta}$=0), only odd orders of $i\hat{S}^{(n)}(t)\propto t_0^n$ remain,

$$i\hat{S}^{(n)}(t)=i\hat{S}^{(1)}(t)+i\hat{S}^{(3)}(t)+\mathcal{O}(t_0^5). \tag{2.29}$$

Eqs. (2.28) and (2.29) not only allow us to obtain an effective description of the low energy states $\hat{P}_0^{\nu}$, but also enable us to keep track of the coupling between the low energy space (spin: $\hat{P}_0^{\nu}$) and the space with the highest excited states (charge: $\hat{P}_2^{\nu}$).

We use the Baker–Campbell–Hausdorff formula to expand $\hat{H}_{\mathsf{eff}}(t)$, Eq. (2.25), in terms of nested commutators [57, 59] of $\hat{S}(t)$ and $\hat{H}(t)$

$$\begin{aligned}e^{i\hat{S}(t)}(\hat{H}(t)-i\partial_t)e^{-i\hat{S}(t)}=(\hat{H}(t)-i\partial_t)+\frac{1}{1!}[i\hat{S}(t),(\hat{H}(t)-i\partial_t)]\\+\frac{1}{2!}\big[i\hat{S}(t),[\hat{S}(t),(\hat{H}(t)-i\partial t)]\big]+...\end{aligned} \tag{2.30}$$

At the lowest order, the effective Hamiltonian yields

$$\hat{H}_{\text{eff}}^{(0)}=\hat{H}_{\text{nn}}+\hat{H}_{\text{sf}}. \tag{2.31}$$

Using the projection operators, we obtain the following equation for $i\hat{S}^{(1)}(t)$

$$\hat{P}_d^{\nu}\big[\hat{T}^{\pm1}(t)+[i\hat{S}^{(1)}(t),\hat{H}_U]-\partial_t i\hat{S}^{(1)}(t)\big]\hat{P}_{d\pm1}^{\nu'}=0. \tag{2.32}$$

In contrast to the zeroth order contribution $\hat{H}_{\text{eff}}^{(0)}$, Eq. (2.32) is a time-dependent equation. In principle, it is possible to solve this equation for arbitrary time-dependency, as worked out in [21]. Here we use a simpler algebraic solution that is feasible for time periodic driving and which is closely related to Floquet theory [18, 27, 57] and the high frequency expansion [26, 58, 60]. Given a time periodic electric field $E(t)$=$E(t+T)$ with a period $T=\frac{2\pi}{\omega}$, where ω is the frequency of the electric field, we can expand $\hat{T}^{\pm1}(t)$ and $i\hat{S}^{(n)}(t)$ in a Fourier series as follows

$$\hat{T}^{\pm1}(t)=\sum_{m=-\infty}^{\infty}\hat{T}_m^{\pm1}e^{im\omega t},\quad i\hat{S}^{(n)}(t)=\sum_{m=-\infty}^{\infty}i\hat{S}_m^{(n)}e^{im\omega t}, \tag{2.33}$$

where m is the Fourier index, which can be seen as the number of virtual photons absorbed or emitted by the system [57]. The expressions for $\hat{T}_m^{\pm1}$ in terms of single electron operators yield [1]

1 Note the factor $(-1)^m$ in front of expression $\hat{T}_m^{\pm1}$ is different from what has been written in [51].

$$\hat{T}_m^{+1} = -\,t_0 J_m(\mathcal{E}) \sum_{\alpha\neq\beta,\sigma} \big\{(-1)^m \hat{n}_{i\alpha\bar{\sigma}} \hat{c}^\dagger_{i\alpha\sigma} \hat{c}_{j\alpha\sigma} \hat{h}_{j\alpha\bar{\sigma}} (\hat{n}_{i\beta\bar{\sigma}} \hat{h}_{j\beta\bar{\sigma}} + \hat{h}_{i\beta\bar{\sigma}} \hat{n}_{j\beta\bar{\sigma}}) + \hat{n}_{j\alpha\bar{\sigma}} \hat{c}^\dagger_{j\alpha\sigma} \hat{c}_{i\alpha\sigma} \hat{h}_{i\alpha\bar{\sigma}} (\hat{n}_{j\beta\bar{\sigma}} \hat{h}_{i\beta\bar{\sigma}} + \hat{h}_{j\beta\bar{\sigma}} \hat{n}_{i\beta\bar{\sigma}})\big\}, \tag{2.34}$$

$$\hat{T}_m^{-1} = -\,t_0 J_m(\mathcal{E}) \sum_{\alpha\neq\beta,\sigma} \big\{(-1)^m \hat{h}_{i\alpha\bar{\sigma}} \hat{c}^\dagger_{i\alpha\sigma} \hat{c}_{j\alpha\sigma} \hat{n}_{j\alpha\bar{\sigma}} (\hat{n}_{i\beta\bar{\sigma}} \hat{h}_{j\beta\bar{\sigma}} + \hat{h}_{i\beta\bar{\sigma}} \hat{n}_{j\beta\bar{\sigma}}) + \hat{h}_{j\alpha\bar{\sigma}} \hat{c}^\dagger_{j\alpha\sigma} \hat{c}_{i\alpha\sigma} \hat{n}_{i\alpha\bar{\sigma}} (\hat{n}_{j\beta\bar{\sigma}} \hat{h}_{i\beta\bar{\sigma}} + \hat{h}_{j\beta\bar{\sigma}} \hat{n}_{i\beta\bar{\sigma}})\big\}, \tag{2.35}$$

where J_m is the Bessel function of order m and $\mathcal{E}{=}eaE_0/\omega$ represents the driving strenght, with e the electronic charge and a is the lattice constant. Using Eqs. (2.32) and (2.33), we obtain:

$$\hat{P}_d^\nu i\hat{S}_m^{(1)} \hat{P}_{d\pm1}^{\nu'} = C^{\nu\nu',\,m}_{dd\pm1} \hat{P}_d^\nu \hat{T}_m^{\pm1} \hat{P}_{d\pm1}^{\nu'}, \tag{2.36}$$

with $C^{\nu\nu',\,m}_{dd'}{=}(E_d^\nu - E_{d'}^{\nu'} + m\omega)^{-1}$ and

$$\hat{P}_d^\nu \hat{H}_{\mathrm{U}} \hat{P}_{d'}^{\nu'} = \delta_{dd'}\delta_{\nu\nu'} E_d^\nu \hat{P}_d^\nu. \tag{2.37}$$

For $\nu{=}1$, E_d^ν is a matrix in the single-electron basis and we would have to further decompose P_d^ν for the procedure to be exact. Here instead we use an approximation $E_d^\nu{=}\min\big(E_d^{\nu,\mu}\big)$, where $E_d^{\nu,\mu}$ are the eigenvalues obtained from diagonalizing $\big\langle\phi_k|\hat{P}_d^\nu \hat{H}_{\mathrm{U}} \hat{P}_d^\nu|\phi_{k'}\big\rangle$. This is a generalization of the energy approximation employed in [54], where E_d is approximated by the mean energy of all states for given d. In equilibrium, the present approximation is accurate for

$$|E_d^{\nu,\mu} - E_d^{\nu,\mu'}| \ll |E_d^\nu - E_{d'}^{\nu'}|, \tag{2.38}$$

where the number of doublons $d{\neq}d'$ and the Hund rule violation index $\nu{\neq}\nu'$.

The first order effective Hamiltonian $\hat{H}^{(1)}_{\mathrm{eff}}(t)$ vanishes because $\hat{T}^0(t){=}0$ for orbital-diagonal hopping $t_{\alpha\neq\beta}{=}0$. Eq. (2.36) allows us to compute higher order contributions to $\hat{H}_{\mathrm{eff}}(t)$ in a straightforward way. The second order contribution reads

$$\hat{P}_d^\nu \hat{H}^{(2)}_{\mathrm{eff}}(t) \hat{P}_{d'}^{\nu'} = \sum_{\substack{m=-\infty\\ k+l=m}}^{\infty} \hat{P}_d^\nu \frac{1}{2}\big[i\hat{S}_k^{(1)}, \hat{T}_l^{\pm1}\big] \hat{P}_{d'}^{\nu'} e^{im\omega t}, \tag{2.39}$$

where, $d, d'{=}0, 2$ and $\nu, \nu'{=}0, 1$.

The third order contribution to $\hat{H}_{\mathrm{eff}}(t)$ gives us an expression for $\hat{P}_d^\nu i\hat{S}_m^{(3)} \hat{P}_{d\pm1}^{\nu'}$:

$$\hat{P}_d^\nu i\hat{S}_m^{(3)} \hat{P}_{d\pm1}^{\nu'} {=} C^{\nu\nu',m}_{dd\pm1} \frac{1}{3} \sum_{p+q+r=m} \hat{P}_d^\nu \big[i\hat{S}_p^{(1)}, [i\hat{S}_q^{(1)}, \hat{T}_r^{\pm1}]\big] \hat{P}_{d\pm1}^{\nu'}. \tag{2.40}$$

This yields the following fourth order contribution to the effective Hamiltonian:

$$\hat{P}_d^{\nu}\hat{H}_{\text{eff}}^{(4)}(t)\hat{P}_{d'}^{\nu'} = \frac{1}{8}\sum_{\substack{p=-\infty \\ k+l+m+n=p}}^{\infty}\hat{P}_d^{\nu}\left[i\hat{S}_k^{(1)},\left[i\hat{S}_l^{(1)},[i\hat{S}_m^{(1)},\hat{T}_n^{\pm 1}]\right]\right]\hat{P}_{d'}^{\nu'}e^{ip\omega t}, \tag{2.41}$$

With Eqs. (2.25) and (2.41) we have derived the central result of this section, namely an effective Hamiltonian up to fourth order in the hopping.

Summarizing, we discussed the derivation an effective Hamiltonian for the subspaces d=0 and d=2 by means of a generalized time-dependent canonical transformation. This Hamiltonian will be used in chapters 3 and 4.

2.5 EXTENDED DYNAMICAL MEAN-FIELD THEORY

We have seen in the previous sections two methods which can both be used in order to study strongly correlated systems: ED and the generalized time-dependent CT. However, these methods encounter limitations in either the size of the system or the relative strength of the interactions. Alternatively, the Extended Dynamical Mean-Field Theory (EDMFT) [61, 62] is a method that maps the lattice problem to a single-impurity problem. Therefore, unlike the ED, it does not suffer from finite size problems. In addition, EDMFT is is based on a diagrammatic technique for the treatment of many-body correlations. Hence, unlike the CT which is restricted to a specific subspace of the Hilbert space, the EDMFT can be used for any interaction regimes. The EDMFT is an extention of the original Dynamical Mean-Field Theory (DMFT) [32] and accounts for non-local interactions between electrons. The EDMFT has already been succesfully applied to the study of charge-ordering and the Wigner-Mott transition [63, 64]. In addition, an EDMFT formalism was recently derived to account for time-dependent dynamics. This time-dependent EDMFT allowed the study of systems under non-equilibrium conditions leading to the study of charge relaxation and dynamical screening phenomena [35, 65] arising from the non-local correlations.

Distinct from the previous sections on ED and CT, we used EDMFT merely as a simulation tool. Therefore, we aim to outline only the main features of this method necessary to understand the physical effects it can describe. The section is organized as follows: in subsection 2.5.1, we discuss the mean-field approximation for the Ising model. In subsection 2.5.2, we introduce the diagrammatic formalism used in EDMFT. While subsection 2.5.3 focusses on the $U-V$ decoupling, subsection 2.5.4 shows that the EDMFT lattice problem can be reduced to a single-site problem using the "cavity construction". In subsection 2.5.5, we compare the effective single-site system to Anderson-Holstein model. In subsection 2.5.6, we briefly discuss the steps used to solve the fermionic and bosonic self-consistencies in EDMFT. Finally, in subsection 2.5.7, we introduce the Kadanoff-Baym formalism which is used in order to calculate non-equilibrium EDMFT equations.

2.5.1 *Mean-field approximation*

The idea of the mean-field approximation is to linearize the interaction term of the Hamiltonian which is usally quadratic (two-particle interaction). This is done by reducing the interactions with neighboring sites to an effective Weiss field h_{eff}. A generic example is the one of the Ising model

$$\hat{H}_{\text{Ising}} = \sum_{<ij>} J_{ij}\hat{S}_i\hat{S}_j - h\sum_i \hat{S}_i, \tag{2.42}$$

where $J_{ij}>0$ is the exchange interaction and h is an external magnetic field. First, we assume that $\langle\hat{S}_i\hat{S}_j\rangle \simeq \langle\hat{S}_i\rangle\langle\hat{S}_j\rangle$. To exploit this, we use that $\langle\hat{S}_i\rangle = m+\delta S_i$, where m is the magnetization and δS_i stands for the quantum spin fluctuations. Third, we expand $\langle\hat{S}_i\rangle\langle\hat{S}_j\rangle$ in terms of m and δS_i and remove terms quadratic in δS_i. This overall procedure is the equivalent of freezing spatial spin fluctuations and yields the mean-field Hamiltonian

$$H_{\text{MF}} = -\frac{J_{ij}m^2 z}{2} - h_{\text{eff}}S_i, \tag{2.43}$$

where m is the magnetization and z stands for the number of nearest neighbors. Here, the expression of the Weiss field is

$$h_{\text{eff}} = h - J_{ij}mz. \tag{2.44}$$

From this mean-field treatment, a self-consistent equation for the magnetization can be computed:

$$m = \tan(\beta h_{\text{eff}}). \tag{2.45}$$

In this subsection, we introduced the mean-field approximation. We have seen that, by freezing spacial spin fluctuations, we can compute an effective field which is commonly used to obtain the magnetic phase diagram of the Ising model.

2.5.2 *Interacting electron systems*

In the previous subsection, we have shown the mean-field treatment of a spin model. In this subsection, we interest ourselves to interacting electrons system which require a more advanced formalism involving functional integrals which can be expanded in terms of diagrams [66]. First, we introduce the expression for the expectation value of an observable which depends on the action of the system. Then, we show how the action is calculated and write it for the $U{-}V$ model.

Instead of solving for the many-body wavefunction in the Schrödinger picture, the diagrammatic formalism deals with the partition function of the system writen in terms of an integral with field operators in the Heisenberg picture [66]. The expression for the expectation value of an observable $\langle\hat{O}\rangle$ is

$$\langle \hat{O} \rangle = \frac{\mathrm{Tr}[e^S \hat{O}]}{Z}, \tag{2.46}$$

where $Z{=}\mathrm{Tr}[e^S]$ is the partition function and S is the action of the system. The action of a system is defined as an integral over the Lagrangian

$$S = \int_0^t \mathcal{L}(\phi_1, \phi_2, .., \bar{t}) d\bar{t}, \tag{2.47}$$

where ϕ_i are the variables of the system. Let us consider the $U{-}V$ Hubbard model

$$\hat{H} = -\sum_{<ij>,\sigma} t_{ij} \hat{c}^\dagger_{i\sigma} \hat{c}_{j\sigma} + U \sum_i \hat{n}_{i\uparrow} \hat{n}_{i\downarrow} - \mu \sum_i \hat{n}_i + \frac{V}{2} \sum_{<ij>} \hat{n}_i \hat{n}_j, \tag{2.48}$$

where μ is the onsite chemical potential, $\hat{n}_i{=}\hat{n}_{i\uparrow}{+}\hat{n}_{i\downarrow}$ and V represents the non-local interaction *i.e.* interaction between two electrons in nearest neighboring sites [67].

In equilibrium, it is convenient to define an imaginary time $\tau{=}it$ which is used as a variable in the interval $[0, \beta]$, $\beta{=}1/k_B T$. For quantum systems evolving along the imaginary time axis τ, the Lagrangien reads

$$\hat{\mathcal{L}} = \sum_{i,\sigma} \hat{c}^\dagger_{i\sigma}(\tau) \frac{\partial}{\partial \tau} \hat{c}_{i\sigma}(\tau) + \hat{H}. \tag{2.49}$$

This yields the action

$$S = \int_0^\beta d\tau \Big[\sum_{i,\sigma} \hat{c}^\dagger_{i\sigma}(\tau) \big(\frac{\partial}{\partial \tau} - \mu - \frac{U}{2} \big) \hat{c}_{i\sigma}(\tau) - \sum_{<ij>,\sigma} t_{ij} \hat{c}^\dagger_{i\sigma}(\tau) \hat{c}_{j\sigma}(\tau) + \frac{1}{2} \sum_{ij} v_{ij} \hat{n}_i(\tau) \hat{n}_j(\tau) \Big]. \tag{2.50}$$

where $v_{ij}{=}U\delta_{ij}{+}V\delta_{<ij>}$ [65, 67].

Summarizing, we showed how to calculate observables using a diagrammatic formalism. In addition, we have written the $U{-}V$ Hubbard model in terms of an action.

2.5.3 *Bosonic and fermionic fields*

In this subsection, we discuss the $U{-}V$ decoupling which is used in EDMFT in order to linearize the interaction term v_{ij} in the action Eq. (2.50).

The decoupling is done by applying the Hubbard-Stratonovich (HS) transformation to the partition function $Z{=}\mathrm{Tr}[e^S]$. The HS transformation reads [67]

$$e^{\left[\frac{1}{2}\int_0^\beta d\tau \sum_{ij} \hat{n}_i(\tau) v_{ij} \hat{n}_j(\tau)\right]} = \frac{1}{\sqrt{(2\pi)^2 \det(v)}} \int \mathcal{D}[\hat{\phi}_1, ..., \hat{\phi}_N] \times e^{\left[-\int_0^\beta d\tau \left\{ \frac{1}{2} \sum_{ij} \hat{\phi}_i(\tau) v_{ij}^{-1} \hat{\phi}_j(\tau) + i \sum_i \hat{\phi}_j(\tau) \hat{n}_j(\tau) \right\}\right]}. \tag{2.51}$$

The HS transformation replaces the on-site and inter-site interaction by a local coupling to a bosonic field ϕ [67]. Analogous to the mean-field solution of the spin model (subsection 2.5.1), this reduces the $U-V$ model to a problem in which interactions are linear in the fermionic and bosonic fields. After applying the HS transformation, the action reads

$$S = \int_0^\beta d\tau \Big[\sum_{ij,\sigma} \hat{c}_{i\sigma}^\dagger(\tau) (G_{ij}^0)^{-1} \hat{c}_{j\sigma}(\tau) + \frac{1}{2} \sum_{ij} v_{ij}^{-1} \hat{\phi}_i(\tau) \hat{\phi}_j(\tau) + i \sum_i \hat{\phi}_i(\tau) \hat{n}_i(\tau) \Big], \tag{2.52}$$

where

$$(G_{ij}^0)^{-1} = \big[(\frac{\partial}{\partial \tau} - \mu - \frac{U}{2}) \delta_{ij} - t_{ij} \delta_{<ij>} \big], \tag{2.53}$$

is the non-interacting lattice Green Function (GF). The hopping amplitude t_{ij} is 0 when i and j are not nearest neighbors. The bosonic field is represented by $\hat{\phi}^\dagger$, $\hat{\phi}$ while the fermionic field is represented by $\hat{c}^\dagger$, $\hat{c}$. Details of the HS transformation can be found in [65, 67].

Summarizing, we discussed the HS transformation and applied it to the action of the $U-V$ model in order to decouple fermionic and bosonic fields. In addition, we introduced the non-interacting lattice GF.

2.5.4 *Cavity construction*

In this subsection, we discuss the so called "cavity construction" which is used to approximate the infinite lattice system by a single-site problem.

The action of the $U-V$ model, Eq. (2.52), can be separated into three parts $S{=}S_0{+}S^{(0)}{+}\Delta S$, where S_0 is the action for site 0 and reads

$$S_0 = \int_0^\beta \Big[\sum_\sigma \hat{c}_{0\sigma}^\dagger(\tau) (G_{00}^0)^{-1} \hat{c}_{0\sigma}(\tau) + \frac{1}{2} v_{00}^{-1} \hat{\phi}_0(\tau) \hat{\phi}_0(\tau) + i \hat{\phi}_0(\tau) \hat{n}_0(\tau) \Big]. \tag{2.54}$$

The action for the lattice in the presence of the cavity, $S^{(0)}$ reads

$$S^{(0)} = \int_0^\beta \Big[\sum_{ij\neq 0,\sigma} \hat{c}^\dagger_{i\sigma}(\tau)(G^0_{ij})^{-1}\hat{c}_{j\sigma}(\tau) + \frac{1}{2}\sum_{ij\neq 0} v^{-1}_{ij}\hat{\phi}_i(\tau)\hat{\phi}_j(\tau) + i\sum_{i\neq 0}\hat{\phi}_i(\tau)\hat{n}_i(\tau)\Big]. \tag{2.55}$$

The cavity picture is illustrated in Figure 2.1 where the site 0 described by S_0 is removed from the lattice leading to a lattice in the presence of the cavity described by $S^{(0)}$.

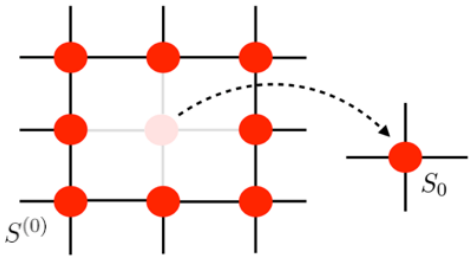

Figure 2.1: The cavity construction with site 0 and its nearest bonds with action removed from the lattice. The actions of site 0 and the lattice in the presence of the cavity are S_0 and $S^{(0)}$, respectively.

The remaining part ΔS which connects site 0 to the rest of the lattice reads

$$\Delta S = \int_0^\beta \Big[\sum_{i\neq 0,\sigma} t_{i0}\big(\hat{c}^\dagger_{0\sigma}\hat{c}_{i\sigma}(\tau) + \hat{c}^\dagger_{i\sigma}\hat{c}_{0\sigma}(\tau)\big) + \frac{1}{2}\sum_{i\neq 0} v^{-1}_{i0}\hat{\phi}_i(\tau)\hat{\phi}_0(\tau)\Big]. \tag{2.56}$$

In order to obtain an effective action for S_0 alone, we integrate out $S^{(0)}+\Delta S$. To do that, we write the partition function of the system

$$Z = \mathrm{Tr}[e^{S_0+S^{(0)}+\Delta S}], \tag{2.57}$$

and calculate the trace of Z only over $S^{(0)}$ and ΔS. Details of the caluculation of $\mathrm{Tr}[e^{S^{(0)}+\Delta S}]$ can be found in [65]. After integrating out $S^{(0)}+\Delta S$ over the fermionic field variables, we obtain an effective action which reads

$$S_{\mathrm{eff}} = S_0 - \int_0^\beta d\tau \int_0^\beta d\tau' \sum_\sigma \hat{c}^\dagger_{0\sigma}(\tau)\sum_{ij}\big[t_{i0}t_{j0}G^{(0)}_{ij}(\tau-\tau') + v^{-1}_{i0}v^{-1}_{j0}W^{(0)}_{ij}(\tau-\tau')\big]\hat{c}_{0\sigma}(\tau'), \tag{2.58}$$

where $G_{ij}^{(0)}$ and $W_{ij}^{(0)}$ are the lattice GF for fermions and bosons, respectively:

$$G_{ij}(\tau-\tau') = -\left\langle \hat{c}_{i\sigma}(\tau)\hat{c}_{j\sigma}^{\dagger}(\tau')\right\rangle \tag{2.59}$$

$$W_{ij}(\tau-\tau') = \left\langle \hat{\phi}_{i}(\tau)\hat{\phi}_{j}^{\dagger}(\tau')\right\rangle. \tag{2.60}$$

Note that Eq. (2.58) is an approximation which, for local interactions, in the limit of infinite dimensions and with a proper scaling of the hopping matrix elements becomes exact in the case of infinite dimensions [32, 68]. When we also integrate out the ϕ-field for convenience [67], the effective local action yields

$$S_{\text{eff}} = \int_{0}^{\beta} d\tau \left[\hat{c}_{0\sigma}^{\dagger}(\tau)\mathcal{G}^{-1}(\tau-\tau')\hat{c}_{0\sigma}(\tau) + \frac{1}{2}\mathcal{U}^{-1}(\tau-\tau')\hat{n}_{0}(\tau)\hat{n}_{0}(\tau')\right] - \frac{1}{2}\text{Tr}[\ln U], \tag{2.61}$$

where

$$\mathcal{G}^{-1}(\tau-\tau') = \frac{\partial}{\partial\tau} - \mu - \frac{U}{2} - \sum_{ij} t_{i0}t_{j0}G_{ij}^{(0)}(\tau-\tau') \tag{2.62}$$

$$\mathcal{U}^{-1}(\tau-\tau') = v_{00}^{-1} - \sum_{ij} v_{i0}^{-1}v_{j0}^{-1}W_{ij}^{(0)}(\tau-\tau'), \tag{2.63}$$

are the fermionic and bosonic Weiss field, respectively. The main difference between the Weiss field calculated in Subsection 2.5.1: h_{eff}, and $\mathcal{G}^{-1}(\tau-\tau')$, $\mathcal{U}^{-1}(\tau-\tau')$ is that the latter takes into account temporal fluctuations. Indeed, the field $\mathcal{G}^{-1}(\tau-\tau')$, $\mathcal{U}^{-1}(\tau-\tau')$ is equivalent to the amplitude for a fermion/boson coming from an external bath (the lattice in the presence of the cavity) to be created on site 0 at time τ' and being created back in the bath at time τ. Therefore, the Weiss fields can be considered as "dynamical" hence, the name of the extended Dynamical mean-field theory [32].

In conclusion, we have discussed the EDMFT infinite lattice problem can be reduced to a single-site problem using the cavity construction. This led the discussion of the analogue to the mean-field approximation for spins, for the case of a interacting electron systems.

2.5.5 *Comparison to the Anderson-Holstein model*

Given the EDMFT solution for the $U-V$ Hubbard model, we still need to evaluate the single-site problem, Eq. (2.61). Therefore, we need to compare the single-site problem to a model which can be solved: the Anderson-Holstein (AH) model

[69–71]. First, we write the EDMFT fermionic Green function in momentum space and we introduce the fermionic self-energy. Secondly, we introduce the AH model. Thirdly, we compare the fermionic part of the single-site effective problem to the single-impurity Anderson model (AM) [69, 72]. Fourthly, we use the bosonic part of the AH model to derive the retarded effective interaction.

To compare it with the single-impurity AM GF, we write the EDMFT fermionic GF in the momentum space:

$$G = \frac{1}{N}\sum_{\vec{k}} \frac{1}{i\omega_n + \mu - \epsilon - \Sigma(i\omega_n)}, \tag{2.64}$$

where ω_n=$(2n+1)\pi/\beta$ is the fermionic Matsubara frequency, N is the number of electrons in the system and ϵ is the kinetic energy which the site 0 exchanges with the rest of the lattice (electrons bath). An important quantity in Eq. (2.64) is the self-energy $\Sigma(i\omega_n)$=Σ:

$$\Sigma = (G^0)^{-1} - G^{-1} \tag{2.65}$$

where G_0 is the non-interacting GF. Hence, the self-energy describes the effect of the electron-electron interactions. Similarly, the bosonic self-energy Π which is equivalent to the polarization can be written as follows

$$\Pi = v^{-1} - W^{-1}, \tag{2.66}$$

and describes the boson-boson interactions. Note that v=v_{ij}.

In the previous subsection, we have seen that the U−V model can be reduced to a single-site effective problem. Therefore, within the EDMFT approximation, the self-energies are seen as local quantities *i.e.*

$$\Sigma_{ij} \simeq \Sigma\delta_{ij} \tag{2.67}$$
$$\Pi_{ij} \simeq \Pi\delta_{ij} \tag{2.68}$$

The AH model is the result of the single-impurity Anderson Model (AM) as well as a bosonic Holstein model:

$$\hat{H}_{AH} = \hat{H}_{AM} + \hat{H}_{\text{boson}} \tag{2.69}$$

First, let us consider $\hat{H}_{AM}$ [32, 69]. This model descibes a single impurity on site 0 coupled to an electronic bath. Its full Hamiltonian reads

$$\begin{aligned}\hat{H}_{AM} = \sum_{\sigma}(\epsilon_0 - \mu)\hat{c}^{\dagger}_{\sigma}\hat{c}_{\sigma} + U\hat{n}_{\uparrow}\hat{n}_{\downarrow} + \sum_{\vec{k},\sigma}\epsilon_b(\vec{k})\hat{a}^{\dagger}_{\sigma}(\vec{k})\hat{a}_{\sigma}(\vec{k}) \\ + \frac{1}{\sqrt{N}}\sum_{\vec{k},\sigma}\left(\tilde{V}(\vec{k})\hat{c}^{\dagger}_{\sigma}\hat{a}_{\sigma}(\vec{k}) + \tilde{V}(\vec{k})^{*}\hat{a}^{\dagger}_{\sigma}(\vec{k})\hat{c}_{\sigma}\right),\end{aligned} \tag{2.70}$$

where $\hat{a}^\dagger(\hat{a})$ is the creation (anihilation) operator for fermions in the bath and $\hat{c}^\dagger(\hat{c})$ is the creation (anihilation) operator for the impurity. The energy ϵ_0 is the kinetic energy on the impurity, $\epsilon_b(\vec{k})$ is the kinetic energy of an electron from the bath with momentum $\vec{k}$ and $\tilde{V}(\vec{k})$ is the hopping amplitude from the bath to the impurity and $V(\vec{k})^*$ is its conjugate. The single particle GF corresponding to the single-impurity AM reads

$$G^{AM} = \frac{1}{i\omega_n + \mu - \epsilon_0 - \Delta - \Sigma}, \tag{2.71}$$

where

$$\Delta = \frac{1}{N}\sum_{\vec{k}} \frac{|\tilde{V}(\vec{k})^2|}{i\omega_n - \epsilon_b(\vec{k})}, \tag{2.72}$$

is the hybridization between the impurity and the bath. Given that $\Delta{=}\epsilon{-}\epsilon_0$, the GFs G^{AM} and G are identical. Therefore, the single-site effective model is equivalent to the single-impurity AM. Hence, the single-site effective problem discussed in subsection 2.5.2 can be solved as a single Anderson impurity model for which reliable analytical as well as numerical solvers exist [32].

Second, we study the bosonic part of the AH model $\hat{H}_{\text{boson}}$ [65]. This system is described by the Hamiltonian

$$\hat{H}_{\text{boson}} = \sum_p \omega_p \hat{b}_p^\dagger \hat{b}_p + \sum_p \frac{\lambda_p}{\sqrt{2}} \hat{n}(\hat{b}_p^\dagger + \hat{b}_p), \tag{2.73}$$

where $\hat{b}_p^\dagger(\hat{b}_p)$ are creation (anihilation) operators for bosons in the bath, ω_p is the frequency mode of boson p, $\hat{n}{=}\hat{n}_\uparrow{+}\hat{n}_\downarrow$ stands for the fermionic impurity density and λ_p is the coupling strength between the impurity and the bosonic bath.

After writing $\hat{H}_{\text{boson}}$ in terms of an action and integrating out the bosonic degrees of freedom, we obtain [65]

$$S_{\text{boson}} = \frac{1}{\beta}\sum_m \hat{n}(i\nu_m)\Big\{ -\sum_p \lambda_p^2 \frac{2\omega_p}{(i\nu_m)^2 - \omega_p^2}\Big\}\hat{n}(-i\nu_m). \tag{2.74}$$

We define the retarded effective interaction as

$$\mathcal{D} = -\int d\omega \sum_p \lambda_p^2 \delta(\omega - \omega_p) \frac{2\omega}{(i\nu_m)^2 - \omega^2}, \tag{2.75}$$

which is the analogous to the fermionic hybridization function Δ [65].

Summarizing, we discussed the EDMFT approximation on the self-energies. We demonstrated the equivalence between the fermionic single-site effective fermionic problem and the single-impurity AM. In addition, we compared the bosonic part of EDMFT to an impurity coupled to a bosonic bath which allowed us to obtain an analog of the fermionic hybridization for bosons.

2.5.6 *Self-consistencies*

In subsections 2.5.4 and 2.5.5, we showed that the many-body lattice problem, Eq. (2.48), can be approximated by an Anderson-Holstein model. Therefore, the self-consistent equations which are solved are the one of the AH model. In this subsection, we sketch the steps needed to obtain a solution to the EDMFT equations [73].

1− Using an initial guess for the hybridization Δ and the retarded effective interaction $\mathcal{D}$, we calculate the impurity single-particle GFs:

$$G_{ii}(\tau - \tau') = -\left\langle \hat{c}_{i\sigma}(\tau)\hat{c}^{\dagger}_{i\sigma}(\tau')\right\rangle \tag{2.76}$$

$$W_{ii}(\tau - \tau') = \left\langle \hat{\phi}_i(\tau)\hat{\phi}^{\dagger}_i(\tau')\right\rangle. \tag{2.77}$$

2− We use Eq. (2.71) to calculate the fermionic self-energy Σ while its analogous for bosons Π is obtained via the relation

$$W = \mathcal{U}^{-1} - \Pi \tag{2.78}$$

However, due to interactions, obtaining exact expressions for Σ and Π is highly challenging. Therefore, we use the Non-Crossing Approximation (NCA) [74] which approximate the self-energies at the lowest order in Δ and $\mathcal{D}$.

3− Using the EDMFT approximation $\Sigma_{ij} \simeq \Sigma\delta_{ij}$, we calculate the lattice GFs:

$$G_{ij} = \left[(G^0_{ij})^{-1} - \Sigma\right]^{-1} \tag{2.79}$$

$$W_{ij} = \left[v^{-1}_{ij} - \Pi\right]^{-1} \tag{2.80}$$

$$\tag{2.81}$$

4− Then, we use Eq. (2.71) to calculate a new value for the hybridization Δ as well as the relation

$$\mathcal{U} = U + \mathcal{D}, \tag{2.82}$$

in order to obtain a new value for $\mathcal{D}$, where U is the Coulomb interaction.

Once step 4 has been implemented, the self-consistency goes back to step 1 and iterates until convergence is obtained.

One of the most important quantities to be computed in EDMFT are the GFs. In this thesis, we mainly focus on the fermionic GFs. The lattice GF, $G_{<ij>}(i\omega_n)$, includes $\langle S_i\rangle\langle S_j\rangle$ in the classical regime while the local fermionic GF, $G_{ii}(i\omega_n)$, corresponds to the magnetic moment $m_i{=}\langle S_i\rangle$ [32].

Summarizing, we sketched how to solve both the fermionic as well as the bosonic self-consistencies in EDMFT.

2.5.7 *Kadanoff-Baym contour and non-equilibrium dynamics*

So far, we have considered only imaginary time-dynamics within the framework of EDMFT. Here, we explain how the diagrammatic formalism for correlated systems can be generalized to the case of dynamical phenomena in real time. To this end, this subsection is dedicated to the non-equilibrium framework and the Kadanoff-Baym contour [73] which is generic for EDMFT.

Under non-equilibrium conditions, a physical system evolves in time leading to the need of developing a framework able to capture this time-evolution. For instance, the expression for the average value of an observable $\hat{O}$, Eq. (2.46), is extended to the time-dependent regime and reads [73]

$$\langle \hat{O}(t) \rangle = \frac{\mathrm{Tr}\big[\mathcal{T}_c e^{S(t)} \hat{O}(t)\big]}{Z(t)}, \tag{2.83}$$

where $S(t)$ is the action of the time-dependent system, $Z(t)$=Tr$[e^{S(t)}]$ is its partition function and $\mathcal{T}_c$ ensures time-ordering since the Hamiltonian of the system at t_1, $\hat{H}(t_1)$ does not comute with $\hat{H}(t_2)$. For instance let $\hat{O}(t)$=$\hat{A}(t_1)\hat{B}(t_2)$, $\mathcal{T}_c\hat{A}(t_1)\hat{B}(t_2)$=$\hat{B}(t_2)\hat{A}(t_1)$ if t_2 appears later than t_1 on the contour [74]. Therefore, within the time-dependent formalism, the time translation invariance is lost.

For the case of EDMFT, the time-dependent action $S(t)$ reads

$$S = -i \int_c dt \Big[\sum_{i,\sigma} \hat{c}^\dagger_{i\sigma}(t) \big(-i\frac{\partial}{\partial t} - \mu - \frac{U}{2} \big) \hat{c}_{i\sigma}(t) - \sum_{<ij>,\sigma} t_{ij}(t) \hat{c}^\dagger_{i\sigma}(t) \hat{c}_{j\sigma}(t) + \frac{1}{2} \sum_{ij} v_{ij}(t) \hat{n}_i(t) \hat{n}_j(t) \Big], \tag{2.84}$$

where and $v_{ij}(t)$=$U(t)\delta_{ij}$+$V(t)\delta_{<ij>}$. The time-dependent hopping between neighboring sites $t_{ij}(t)$ is used to capture the effects of a perturbation such as an in-plane electric field [35]. The time integral $\int_c$ is over the Kadanoff-Baym (KB) contour [75]. To illustrate the KB contour, we sketch how the average value of $\hat{O}(t)$ is calculated. The formal solution of $\hat{O}(t)$ reads

$$\hat{O}(t) = \hat{U}(t_0, t) \hat{O} \hat{U}(t, t_0), \tag{2.85}$$

where $\hat{U}(t, t')$ is the evolution operator

$$\hat{U}(t, t') = \Theta(t - t') \mathcal{T}_c \Big(-i \int_{t'}^{t} d\bar{t} \hat{H}(\bar{t}) \Big) + \Theta(t' - t) \tilde{\mathcal{T}}_c \Big(-i \int_{t'}^{t} d\bar{t} \hat{H}(\bar{t}) \Big), \tag{2.86}$$

with Θ the step function and $\tilde{\mathcal{T}}_c$ is the inverse time ordering operator.

The calculation of $\langle \hat{O}(t) \rangle$, Eq. (2.83), requires the system to evolve in a complex time domain. The contour which the system follows is the KB contour. We illustrate the KB contour in the expression of $\langle \hat{O}(t) \rangle$ by writing its numerator is expressed in terms of evolution operators

$$Tr\left[\mathcal{T}_c e^{S(t)} \hat{O}(t)\right] = Tr\left[\hat{U}(t_0 - i\beta)\hat{U}(t_0, t)\hat{O}\hat{U}(t, \infty)\hat{U}(\infty, t_0)\right]. \tag{2.87}$$

The KB contour followed by the system is represented in Figure 2.2. Starting from time t_0, the system evolves along the real time axis (blue lines) to infinite time $\hat{U}(\infty, t_0)$ and backward to time t, via $\hat{U}(t, \infty)$, where the observable $\hat{O}$ is measured. Then the systems returns to t_0, $\hat{U}(t_0, t)$. As a last step, the system evolves along the imaginary time axis towards $t_0 - i\beta$. Note that, Eq. (2.83) reduces to Eq. (2.46) in the equilibrium limit. Therefore, the time-dependent many-body formalism on the KB contour generalizes to the equilibrium formalism of the two times objects $A(t, t')$.

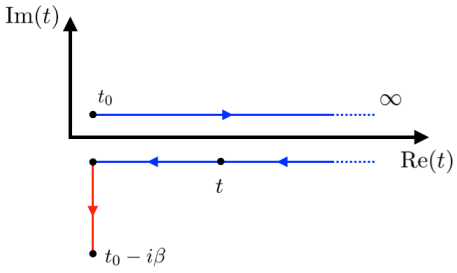

Figure 2.2: Sketch of the complex plan in which the KB contour applies. Blue arrows represent the two real time branches, from t_0 to infinity ∞ and backward. The red arrow represents the imaginary time branch, from t_0 to $t_0 - i\beta$.

The KB contour formalism lead the EDMFT self-consistency equations, see subsection 2.5.3, to be real time-dependent *e.g.* $G(t, t')$, $W(t, t')$, $\Sigma(t, t')$. The computation of these quantities is more involved since they acount for different components which are the result of the KB contour calculations (Matsubara, retarded, greater, lesser...), see [73] for a more extensive treatment. In this thesis, we focus on extracting the Matsubara as well as the retarded component of the KB quantities for the calculation of the exchange interaction. Matsubara quantities on their own are sufficient for equilibrium calculations.

In conclusion, we introduced the time-dependent diagrammatic formalism as well as the KB contour used to calculate the EDMFT equations. In addition, we briefly discussed the complex structure of the quantities which are solutions of the time-dependent EDMFT.

2.6 EXCHANGE INTERACTION

So far, we considered only elecronic systems. Here, we explain how to derive an equation for the exchange interactions from these systems by decoupling the spin and electronic degrees of freedom and map the system onto a spin model. In this section, we focus on the Heisenberg exchange interactions J_{ex}

$$\hat{H} = J_{\mathrm{ex}} \sum_{<ij>} \hat{\vec{S}}_i \cdot \hat{\vec{S}}_j. \tag{2.88}$$

The operators $\hat{\vec{S}}_i$ represent either (i) spin operators with the on-site spin multiplicity of system S (S=1/2 and S=1 in this thesis), see chapters 3 and 5 (ii) or classical spins $\vec{S}$= $<\hat{\vec{S}}_i>$, see chapter 6.

In this section, we discuss two techniques which are used in this thesis in order to obtain J_{ex}. In the first part, we discuss the mapping onto a spin model from the effective Hamiltonian of a single-orbital Hubbard model obtained with the CT technique. This method is restricted by the perturbative solution of the CT and therefore accurate in the limit $U \gg t$ only. Hence, in the second part, we sketch the derivation of a formula for exchange for arbitrary interaction strength. This derivation is based on the diagrammatic formalism used in EDMFT and is applicable both in equilibrium and for the non-equilibrium case [20, 39].

2.6.1 *Exchange mechanism*

In this subsection, we calculate the Heisenberg exchange interaction in a two sites (ij) single-orbital Hubbard system at half-filling and describe the exchange mechanism [76].

As mentioned in subsection 2.2, the generic Hamiltonian for strongly correlated system is the single-orbial Hubbard model, see Eq. (2.2). Using the CT technique, one can calculate the low-energy effective Hamiltonian for the Hubbard model:

$$\hat{H}_{\mathrm{eff}} = -\frac{2t_0^2}{U} \sum_{<ij>} \left(\hat{n}_{i\uparrow}\hat{n}_{j\downarrow} - \hat{c}^{\dagger}_{i\uparrow}\hat{c}_{i\downarrow}\hat{c}^{\dagger}_{j\uparrow}\hat{c}_{j\downarrow} \right). \tag{2.89}$$

Using the spin 1/2 operators

$$\hat{S}^x = \frac{1}{2}(\hat{c}^{\dagger}_{i\uparrow}\hat{c}_{i\downarrow} + \hat{c}^{\dagger}_{i\downarrow}\hat{c}_{i\uparrow}), \tag{2.90}$$

$$\hat{S}^y = -\frac{i}{2}(\hat{c}^{\dagger}_{i\uparrow}\hat{c}_{i\downarrow} - \hat{c}^{\dagger}_{i\downarrow}\hat{c}_{i\uparrow}), \tag{2.91}$$

$$\hat{S}^z = \frac{1}{2}(\hat{n}_{i\uparrow} - \hat{n}_{i\downarrow}), \tag{2.92}$$

we obtain the effective spin Hamiltonian

$$\hat{H}_{\text{eff}} = J_{\text{ex}} \sum_{<ij>} \Big(\hat{\vec{S}}_i \cdot \hat{\vec{S}}_j - \frac{\hat{n}_i \hat{n}_j}{4} \Big), \tag{2.93}$$

where $\frac{\hat{n}_i \hat{n}_j}{4}$ is a density term whith $\hat{n}_i = \hat{n}_{i\uparrow} + \hat{n}_{i\downarrow}$, which equals 1/4 in the half-filled case. The exchange interaction J_{ex} reads

$$J_{\text{ex}} = \frac{2t_0^2}{U}. \tag{2.94}$$

It is the energy associated with the exchange mechanism illustrated in Figure 2.3 where the dashed lines represent a virtual hopping of spin down ($\downarrow$) from the ground state to an excited state and back [76].

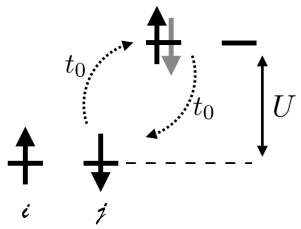

Figure 2.3: Exchange mechanism on two sites i and j, t_0 is the hopping and U is the Coulomb interaction. Arrows $\uparrow$ ($\downarrow$) represent spin up(down).

Summarizing, using a mapping of the effective single-orbital Hubbard Hamiltonian onto a spin 1/2, we obtained an expression for the Heisenberg exchange interaction J_{ex}. In addition, we illustrated the exchange mechanism at the origin of the Heisenberg exchange in the Hubbard model at half-filling.

2.6.2 *Formula for exchange with many-body formalism*

In this subsection, we sketch the main steps in the derivation of non-equilibrium exchange interactions using the diagrammatic formalism [20, 39]. In addition, we give the expression of the exchange formula in the equilibrium limit and illustrate its physical meaning with the example of the single-band Hubbard model.

The derivation of the exchange formula begins by taking a general system descibed by the time-dependent Hamiltonian:

$$\hat{H}(t) = \hat{H}_{\text{kin}}(t) + \hat{H}_{\text{U}} \tag{2.95}$$

where $\hat{H}_{\text{kin}}(t)$ is the single-particle Hamiltonian which includes the effect of an external time-dependent perturbation [39]. The second term of Eq. (2.95), $\hat{H}_{\text{U}}$ is the two-particles interaction term. Note, that the Hamiltonian Eq. (2.95), is an electronic Hamiltonian. Therefore, $\hat{H}(t)$ is written in terms of single particle fermionic operators $\hat{c}^\dagger$, $\hat{c}$. The action $S[\hat{c}^\dagger, \hat{c}]$ corresponding to $\hat{H}(t)$ can be easily derived using Eqs. (2.47) and (2.49).

The first step in the derivation of an exchange formula for many-body systems is to rotate the fermionic fields of the action $S[\hat{c}^\dagger, \hat{c}]$ of the system using a bosonic field Γ :

$$S[\hat{c}^\dagger, \hat{c}] \overset{HP}{=} S[\psi^*, \psi, \Gamma^*, \Gamma], \tag{2.96}$$

where ψ^*, ψ are rotated fermionic Grassmann fields and Γ^* is the complex conjugate of the bosonic field. Here, we chose the Holstein–Primakoff (HP) transformation [77] for the rotation of the fermionic fields:

$$R_i(t) = \begin{pmatrix} \sqrt{1 - |\Gamma_i(t)|^2} & \Gamma_i^*(t) \\ -\Gamma_i(t) & \sqrt{1 - |\Gamma_i(t)|^2} \end{pmatrix}. \tag{2.97}$$

The bosonic field $\Gamma_i(t)$ reads [39]

$$\Gamma_i(t) = -e^{i\phi_i(t)} \sin\big[\theta_i(t_c)/2\big], \tag{2.98}$$

where i is the cite index, ϕ_i and θ_i are the angles which determine the spin axis at time t on the KB contour, see subsection 2.5.7.

To give a better understanding of the meaning of the HP transformation, we compare the unit spin vector $\vec{S}_i$ before and after the HP transformation. In terms of units vectors $\vec{u}$ in the three dimensional space, the unit spin vector reads

$$\vec{S}_i = \cos(\phi_i)\sin(\theta_i)\vec{u}_x + \sin(\phi_i)\sin(\theta_i)\vec{u}_y + \cos(\theta_i)\vec{u}_z. \tag{2.99}$$

After the HP tranformation *i.e.* after using Eq. (2.98), $\vec{S}_i$ can be written as

$$\vec{S}_i = \sqrt{1 - |\Gamma_i|^2}\big[-(\Gamma_i + \Gamma_i^*)\vec{u}_x + i(\Gamma_i - \Gamma_i^*)\vec{u}_y\big] + (1 - 2|\Gamma_i|^2)\vec{u}_z. \tag{2.100}$$

Note that we drop the t dependency of the bosonic field Γ for notational convenience.

The next step in the calculation of the exchange formula is to integrate out the fermionic fields $\psi^\dagger$ and ψ in the rotated action $S[\psi^\dagger, \psi, \Gamma^*, \Gamma]$ such that we obtain an action in terms of bosonic fields Γ, Γ^* only

$$\tilde{S} = \tilde{S}(\Gamma, \Gamma^*). \tag{2.101}$$

However, obtaining an exact expression for arbitrary bosonic fields is highly challenging. Therefore, to proceed, a suitable small parameter needs to be chosen. The small parameter used in subsection 2.6.1 for the downfolding procedure was

the ratio $t_0/U \ll 1$. Here, a small angle deviation from a colinear reference spin configuration is assumed within the time accessible with the EDMFT method. Within a small angle approximation, the polar angle θ_i is the small parameter and the rotation matrix can be approximated as [39]

$$R_i \simeq \begin{pmatrix} 1 - \frac{|\Gamma_i|}{2} & \Gamma_i^* \\ -\Gamma_i & 1 - \frac{|\Gamma_i|}{2} \end{pmatrix}. \tag{2.102}$$

After a perturbation, the exchange process is fast (process involving electronic virtual excitations, see Figure (2.3)) with respect to the spin precession around the equilibrium configuration. Within this adiabatic limit, we expect to recover the spin-model alone. However, the diagrammatic formalism allows to evaluate the effective exchange even in cases when it is not clear that a spin-model alone is sufficient to describe the spin dynamcis of the many-body system.

The integration over fermionic fields itself is technically challenging, we refer to [39] for further details. The action thus obtained is quadratic in the bosonic fields. By comparing with the terms that would emerge from a pure spin model, several different exchange interactions can be extracted. For us, the most important contribution is the Heisenberg term [20]

$$J_{ij}(t) = \frac{1}{4m(t)^2} \int_0^\infty ds \mathrm{Im}\big[A_{ij}^R(t, t-s)\big], \tag{2.103}$$

where $m(t)$ is the magnetization. The retarded object $A_{ij}^R(t, t-s)$ is a product between single-particle GFs and self-energies Σ.

From a physical point of view, the object $A_{ij}^R(t, t')$ corresponds to the coupling between spin rotations at different times and different sites. Its integration over time s approximates the exchange interaction to its slow dynamics and therefore integrates out the fast oscillations [20].

In equilibrium, the formula Eq. (2.103) reduces to [39]

$$J_{ij} = -\frac{1}{4m^2} \sum_{n=-\infty}^{+\infty} \mathrm{Re}\big[A_{ij}(\omega_n)\big], \tag{2.104}$$

where ω_n is the fermionic Matsubara frequency.

In the case of the single-orbital Hubbard model, the equilibrium exchange interaction reads [39, 78]

$$J_{ij} = -\frac{1}{m^2} \sum_{n=-\infty}^{+\infty} \Sigma_i^S(\omega_n) G_{ij}^{\downarrow}(\omega_n) \Sigma_j^S(\omega_n) G_{ji}^{\uparrow}(\omega_n), \tag{2.105}$$

where $\Sigma_i^S = (\Sigma_i^{\uparrow} - \Sigma_i^{\downarrow})/2$ represents the on-site exchange. The GF G_{ij}^{σ} stands for the amplitude of an electron of spin σ to propagate from site i to site j. Thus, the

physical meaning of J_{ij} is the energy which is required for the on-site spin moment at site i with spin down to propagate to site j and back with the opposite spin [78].

To conclude, we higlighted the main assumptions in the derivation of a many-body exchange formula which can be applied in equilibrium as well as non-equilibrium cases [20]. Moreover, we illustrated the physical meaning of the exchange formula using the case of the single-band Hubbard model.

3

CONTROL OF COMPETING EXCHANGE INTERACTIONS IN TWO-ORBITAL SYSTEMS

In order to have a better understanding of the influence of orbital dynamics on the ultrafast and reversible control of exchange, we report the study of a two-orbital Mott Hubbard system at half filling under the effect of a periodic electric field, see subsection 2.4.1. There are two main differences between single and multi-orbital systems which are already captured in the two-orbital case. First, there is the Hund interaction J_{H} that directly arises from inter-orbital exchange on the same site. At half filling and for $J_{\mathrm{H}}>0$, each orbital is singly occupied and the low-energy degrees of freedom are spin-one states which interact both via a normal Heisenberg exchange $J_{\mathrm{ex}}\vec{S}_i\cdot\vec{S}_j$ and with a biquadratic exchange interaction $B_{\mathrm{ex}}(\vec{S}_i\cdot\vec{S}_j)^2$. While J_{ex} favors collinear spin order at neighboring sites, for $B_{\mathrm{ex}}>0$, non-collinear spin order can become preferential. For classical spins, the presence of biquadratic exchange interaction can lead to spin spiral states [79]. For quantum spins in low dimentional systems, the presence of B_{ex} can give rise to disordered phases such as dimerized or quadrupolar phase [80–82]. Second, as illustrated in Figure 3.1, the two-orbital model has excited states which are doubly ionized and strongly gapped with respect to states with only one electron in each orbital (we will refer to configurations with one electron in each orbital as singly occupied states). The doubly ionized states are charge states, which are coupled to singly occupied states by two subsequent hopping processes.

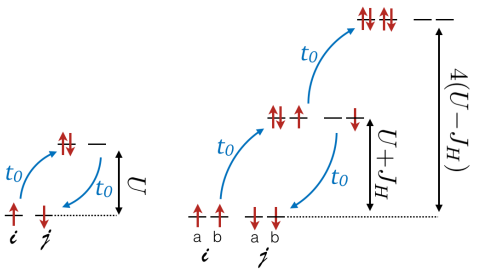

Figure 3.1: Sketch of virtual hopping processes t_0 (in blue) between site i and j with different number of doublons d in the case of a single orbital (left) and a two-orbital (a and b) model (right). Small red arrows indicate the spins of electrons. U denotes the Coulomb repulsion and J_H is the on-site Hund exchange interaction. The energies represented between different states correspond to what is written in the single and two-orbtial Hamiltonians, Eqs. 2.2 and 2.5, respectively.

In this chapter we present the results obtained with the projection operators of subsection 2.4.2 and the effective Hamiltonian introduced in subsection 2.4.1. First, we derive the effective Hamiltonian in the $d = 0$ sector which requires a second time-dependent canonical transformation (CT). Second, we show that the low-energy effective Hamiltonian can be mapped onto an effective spin-one (S=1) model. This requires a third time-dependent CT which specializes to the S=1 states only. Third, in the effective spin-one Hamiltonian, we extract the Heisenberg $J_{\rm ex}(\mathcal{E}, \omega)$ and biquadratic $B_{\rm ex}(\mathcal{E}, \omega)$ exchange interactions and study their behavior.

This chapter is based on the following publication: M.M.S. Barbeau, M. Eckstein, M.I. Katsnelson and J.H. Mentink, *"Optical control of competing exchange interactions and coherent spin-charge coupling in two-orbital Mott insulators"*, SciPost Phys. **6**, 027 (2019).

3.1 EFFECTIVE HAMILTONIAN

In this section we study the low energy effective Hamiltonian up to fourth order in the hopping. According to condition Eq. (2.28), the full effective Hamiltonian yields

$$\sum_{n=2,4}\hat{H}^{(n)}_{\rm eff}(t)=\sum_{\substack{n=2,4\\ \nu\nu'}}\Big\{\hat{P}^{\nu}_0\hat{H}^{(n)}_{\rm eff}(t)\hat{P}^{\nu'}_0+\hat{P}^{\nu}_2\hat{H}^{(n)}_{\rm eff}(t)\hat{P}^{\nu'}_2+\hat{P}^{\nu}_0\hat{H}^{(n)}_{\rm eff}(t)\hat{P}^{\nu'}_2+\hat{P}^{\nu}_2\hat{H}^{(n)}_{\rm eff}(t)\hat{P}^{\nu'}_0\Big\}, \tag{3.1}$$

In the derivation of a low energy effective model, we have to consider the sector $\hat{P}^{\nu}_2$ as a high energy sector and perform a second time-dependent CT, illustrated in Figure 3.2b, in order to project out states for which d=2:

$$\hat{H}^{d=0}_{\rm eff}(t)=\sum_{\nu\nu'}\hat{P}^{\nu}_0\Big\{\hat{H}^{(2)}_{\rm eff}(t)+\hat{H}^{(4)}_{\rm eff}(t)+\tilde{H}^{(4)}_{\rm eff}(t)\Big\}\hat{P}^{\nu'}_0, \tag{3.2}$$

with

$$\sum_{\nu,\nu'}\hat{P}^{\nu}_0\tilde{H}^{(4)}_{\rm eff}(t)\hat{P}^{\nu'}_0=\frac{1}{2}\sum_{\nu,\nu'}\sum_{m,m'=-\infty}^{\infty}\hat{P}^{\nu}_0\big[i\tilde{S}^{(1)}_m(t),\tilde{T}^{\pm1}_{m'}(t)\big]\hat{P}^{\nu'}_0, \tag{3.3}$$

where $\hat{P}^{\nu}_d i\tilde{S}^{(1)}_m(t)\hat{P}^{\nu'}_{d'}=C^{\nu\nu',m}_{dd'}\hat{P}^{\nu}_d\tilde{T}^{\pm1}_m(t)\hat{P}^{\nu'}_{d'}$ and $C^{\nu\nu',m}_{dd'}=(E^{\nu}_d-E^{\nu'}_{d'}+m\omega)^{-1}$.

Note that $E^{\nu}_d=E^{\nu(0)}_d+E^{\nu(2)}_d$, where $E^{\nu(n)}_d$ is the energy contribution to E^{ν}_d of order t^n_0. We use $E^{\nu}_d\simeq E^{\nu(0)}_d$ and do not take into account second order contribution $E^{\nu(2)}_d$ since it leads to 6^{th} order corrections to $\hat{P}^{\nu}_0\tilde{H}^{(4)}_{\rm eff}(t)\hat{P}^{\nu'}_0$. The effective hoppings $\tilde{T}^{\pm1}_m(t)$ in the second CT are determined by second order off-diagonal contributions to $\hat{H}^{(2)}_{\rm eff}$:

$$\tilde{T}^{+1}_m(t)=\sum_{\nu\nu'}\hat{P}^{\nu}_2\hat{H}^{(2)}_{{\rm eff},m}(t)\hat{P}^{\nu'}_0,\quad \tilde{T}^{-1}_m(t)=\sum_{\nu\nu'}\hat{P}^{\nu}_0\hat{H}^{(2)}_{{\rm eff},m}(t)\hat{P}^{\nu'}_2. \tag{3.4}$$

This leads to:

$$\sum_{\nu,\nu'}\hat{P}^{\nu}_0\tilde{H}^{(4)}_{\rm eff}(t)\hat{P}^{\nu'}_0=\sum_{\nu''}\sum_{m,m'=-\infty}^{\infty}C^{\nu'0,m}_{20}\hat{P}^{\nu}_0\hat{H}^{(2)}_{{\rm eff},m}(t)\hat{P}^{\nu''}_2\hat{H}^{(2)}_{{\rm eff},m'}(t)\hat{P}^{\nu'}_0, \tag{3.5}$$

where we used that $C^{\nu0,m}_{d0}=C^{\nu1,m}_{d0}$. Note that this CT includes all modes m from the first CT. Detailed expressions for $\hat{P}^{\nu}_d\tilde{H}^{(2)}_{\rm eff}(t)\hat{P}^{\nu'}_{d'}$ and $\hat{P}^{\nu}_0\tilde{H}^{(4)}_{\rm eff}(t)\hat{P}^{\nu'}_0$ can be found in [51]. We would like to point out that in the full lattice, additional 4^{th} order interactions occur, such as ring-exchange terms, spin chirality terms [27] as well

as additional 4^{th} order contribution to the Heisenberg and biquadratic exchange interactions. Since we restrict ourselves to a two site model, such processes are not taken into account in our calculations.

In conclusion, we obtained an expression of the effective Hamiltonian up to fourth order in the hopping and used a second time-dependent canonical transformation to project out states with doubly occupied sites d=0.

3.2 SPIN-ONE MODEL

In this section, we map the electronic effective Hamiltonian, Eq. (3.2), onto a spin-one model. In addition, we do a third time-dependent canonical tranformation within the d=0 sector wich leads an additional contribution to the biquadratic exchange.

Hamiltonian Eq. (3.2), can be written in terms of spin-one (S=1) operators as described before in [83, 84]. In general, S=1 operators can be defined using many-electron operators [85]. Here, we define their projection onto local spin states $|S, M_S\rangle$

$$|S, M_s\rangle_i = \Big\{|1,1\rangle_i, |1,0\rangle_i, |1,-1\rangle_i\Big\}. \tag{3.6}$$

Then, we can write the spin-one states in terms of single electron states using suitable Clebsh-Gordan coefficients

$$|1,1\rangle_i = |\uparrow,\uparrow\rangle_i, \quad |1,0\rangle_i = \frac{1}{\sqrt{2}}(|\uparrow,\downarrow\rangle_i + |\downarrow,\uparrow\rangle_i), \quad |1,-1\rangle_i = |\downarrow,\downarrow\rangle_i, \tag{3.7}$$

where $|\sigma_a, \sigma'_b\rangle_i = \hat{c}^\dagger_{ib\sigma'}\hat{c}^\dagger_{ia\sigma}|0\rangle$. Using the relation [85]

$$\hat{S}^q_i|S, M_S\rangle_i = \sqrt{S(S+1)}C^{SM_S+q}_{SM_S,1q}|S, M_S+q\rangle_i, \tag{3.8}$$

one can write $\hat{S}^q$ in terms of single electron operators (index i is omitted for brevity), which yields

$$\hat{S}^{+1} = -\frac{1}{\sqrt{2}}\sum_{\alpha\neq\beta}\hat{c}^\dagger_{\alpha\uparrow}\hat{c}_{\alpha\downarrow}(\hat{n}_{\beta\uparrow}\hat{h}_{\beta\downarrow} + \hat{h}_{\beta\uparrow}\hat{n}_{\beta\downarrow}), \tag{3.9}$$

$$\hat{S}^{-1} = \frac{1}{\sqrt{2}}\sum_{\alpha\neq\beta}\hat{c}^\dagger_{\alpha\downarrow}\hat{c}_{\alpha\uparrow}(\hat{n}_{\beta\uparrow}\hat{h}_{\beta\downarrow} + \hat{h}_{\beta\uparrow}\hat{n}_{\beta\downarrow}), \tag{3.10}$$

$$\hat{S}^0 = \hat{n}_{a\uparrow}\hat{h}_{a\downarrow}\hat{n}_{b\uparrow}\hat{h}_{b\downarrow} - \hat{h}_{a\uparrow}\hat{n}_{a\downarrow}\hat{h}_{b\uparrow}\hat{n}_{b\downarrow}. \tag{3.11}$$

Using the definition $\hat{S}^{\pm1} = \mp\frac{1}{\sqrt{2}}(\hat{S}^x \pm i\hat{S}^y)$ for the spin-one spin flip terms [85], one can compute the product $\vec{S}_i\cdot\vec{S}_j$ as well as $(\vec{S}_i\cdot\vec{S}_j)^2$ in terms of single electron operators and identify them with the terms of Eq. (3.2). Subsequently, by time averaging $\bar{H}^{d=0}_{\text{eff}} = \frac{1}{T}\int_0^T \hat{H}^{d=0}_{\text{eff}}(t)dt$, we obtain an effective time-independent Hamiltonian:

$$\bar{H}^{d=0}_{\text{eff}} = \sum_{<i,j>} \Big\{ K_1(\mathcal{E},\omega)\big(\vec{S}_i\cdot\vec{S}_j + \hat{R}^1_{ij}\big) + K_2(\mathcal{E},\omega)\big(\vec{S}_i\cdot\vec{S}_j + \hat{R}^1_{ij}\big)^2 + K_3(\mathcal{E},\omega)\big((\vec{S}_i\cdot\vec{S}_j)^2 + \hat{R}^2_{ij}\big)\Big\}, \tag{3.12}$$

$K_1(\mathcal{E},\omega)$ corresponds to the exchange $J_{\text{ex}}(\mathcal{E},\omega)$ up to second order in the hopping. $K_2(\mathcal{E},\omega)$ gives a fourth order contribution to $J_{\text{ex}}(\mathcal{E},\omega)$ as well as the biquadratic exchange $B_{\text{ex}}(\mathcal{E},\omega)$. $K_3(\mathcal{E},\omega)$ gives a contribution directly to $B_{\text{ex}}(\mathcal{E},\omega)$.

The remaining term $\hat{R}^2_{ij}$ describes orbital resolved spin dynamics that strictly goes beyond a spin-one model. Their expression in terms of fermionic operators can be found in [51]. To arrive at an effective spin-one model only, we perform a third time-dependent CT to account for the coupling between the spin-one and the non spin-one state of $\hat{P}^\nu_0$ that is described by $\hat{R}^1_{ij}$.

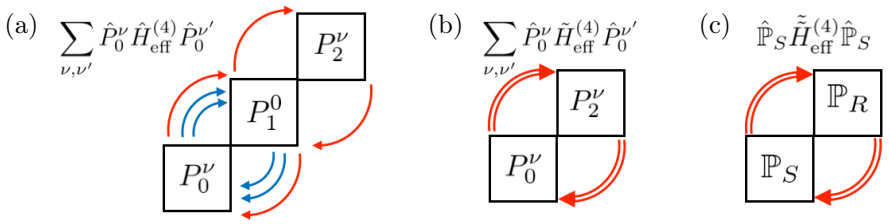

Figure 3.2: Diagrams illustrating the fourth order hopping process of (a) the first CT via the $\hat{P}^\nu_0$ sector in blue and via the $\hat{P}^\nu_2$ sector in red. (b) The second CT via the $\hat{P}^\nu_2$ sector and (c) the third CT between the spin one sector $\mathbb{P}_S$ and a the non spin-one sector $\mathbb{P}_R$ from the $\hat{P}^\nu_0$ sector. Red and blue arrows represent first order hopping processes in (a), double arrows represent second order hopping processes.

In order to do the third time-dependent CT, we use the basis transformation which allows one to go from an electron occupation number basis to the angular momentum basis is the following

$$|S, M_S, S_i, S_j\rangle = \sum_{M_i, M_j} C^{SM}_{S_i M_i, S_j M_j} |S_i, M_i, S_j, M_j\rangle, \tag{3.13}$$

where $C^{SM_S}_{S_i M_i, S_j M_j}$ are Clebsch-Gordan coefficients. From this basis transformation, we obtain three spin-one states, namely a singlet (S=0), a triplet (S=1) and a quintet state (S=2)

$$|0,0,1,1\rangle = \frac{1}{2\sqrt{3}}\Big\{2|\uparrow,\uparrow\rangle_i|\downarrow,\downarrow\rangle_j + 2|\downarrow,\downarrow\rangle_i|\uparrow,\uparrow\rangle_j - |\uparrow,\downarrow\rangle_i|\uparrow,\downarrow\rangle_j - |\downarrow,\uparrow\rangle_i|\downarrow,\uparrow\rangle_j - |\uparrow,\downarrow\rangle_i|\downarrow,\uparrow\rangle_j - |\downarrow,\uparrow\rangle_i|\uparrow,\downarrow\rangle_j\Big\}, \tag{3.14}$$

$$|1,0,1,1\rangle = \frac{1}{\sqrt{2}}\Big\{|\uparrow,\uparrow\rangle_i|\downarrow,\downarrow\rangle_j - |\downarrow,\downarrow\rangle_i|\uparrow,\uparrow\rangle_j\Big\}, \tag{3.15}$$

and

$$\begin{aligned}|2,0,1,1\rangle=\frac{1}{\sqrt{6}}\Big\{&|\uparrow,\uparrow\rangle_i|\downarrow,\downarrow\rangle_j+|\downarrow,\downarrow\rangle_i|\uparrow,\uparrow\rangle_j+|\uparrow,\downarrow\rangle_i|\uparrow,\downarrow\rangle_j+|\downarrow,\uparrow\rangle_i|\downarrow,\uparrow\rangle_j\\ &+|\uparrow,\downarrow\rangle_i|\downarrow,\uparrow\rangle_j+|\downarrow,\uparrow\rangle_i|\uparrow,\downarrow\rangle_j\Big\},\end{aligned} \tag{3.16}$$

and three states which are non spin-one states. We define spin-one projection operators such that $\sum_\nu \hat{P}_0^\nu = \hat{\mathbb{P}}_S + \hat{\mathbb{P}}_R$, where subscripts S and R refere to $S=1$ and $S\neq 1$ states respectively [83]. The third CT, illustrated in Figure 3.2c, takes $\hat{\mathbb{P}}_R$ as a high energy sector. This transformation leads to the following fourth order contribution to the effective Hamiltonian

$$\tilde{\hat{H}}^{(4)}_{\text{eff}}(t) = -\sum_{m,m'=-\infty}^{\infty} \frac{\hat{\mathbb{P}}_S \hat{H}^{(2)}_{\text{eff},m} \hat{\mathbb{P}}_R \hat{H}^{(2)}_{\text{eff},m'} \hat{\mathbb{P}}_S}{E_R - E_S + m\omega} e^{i(m+m')\omega t}, \tag{3.17}$$

where, E_S and E_R are energies of the $S=1$ and $S\neq 1$ states, respectively. The coupling between the $\hat{\mathbb{P}}_S$ and $\hat{\mathbb{P}}_R$ subspaces only involves the singlet state $|0,0,1,1\rangle$ and the $S\neq 1$ state $|0,0,0,0\rangle$

$$|0,0,0,0\rangle = \frac{1}{2}\Big\{|\uparrow,\downarrow\rangle_i|\uparrow,\downarrow\rangle_j + |\downarrow,\uparrow\rangle_i|\downarrow,\uparrow\rangle_j - |\uparrow,\downarrow\rangle_i|\downarrow,\uparrow\rangle_j - |\downarrow,\uparrow\rangle_i|\uparrow,\downarrow\rangle_j\Big\}. \tag{3.18}$$

Note that, the energy approximation of Eq. (2.38) is only for $d\neq d'$. Here, within the $d=0$ sector, we take the exact value for the energies of $|0,0,1,1\rangle$ and $|0,0,0,0\rangle$, 0 and $4J_{\text{H}}$ respectively. After time averaging and projection onto the singlet state, this yields

$$\begin{aligned}\tilde{\hat{E}}^{(4)}_{\text{Singlet}} = -\frac{3}{2}t_0^4 {\sum_{k,l,m,n}}' J_k(\mathcal{E})J_l(\mathcal{E})J_m(\mathcal{E})J_n(\mathcal{E})(C_{01}^{00,k}-C_{10}^{00,l})(C_{01}^{00,m}-C_{10}^{00,n})\\ \times \frac{(-1)^k\big((-1)^m+(-1)^n\big)}{(4J_H+(k+l)\omega)},\end{aligned} \tag{3.19}$$

where ${\sum_{k,l,m,n}}'$ is the sum over all k,l, m and n from $-\infty$ to $+\infty$ where $k+l+m+n=0$, $\tilde{\hat{E}}^{(4)}_{\text{Singlet}}$ is the additional fourth order energy contribution to the singlet state due

to the additional downfolding of $\hat{P}_0^{\nu}$ and J_m is a Bessel function of order m and . Using the spin-one Hamiltonian

$$\hat{H}_{\text{spin}} = E_0 + \sum_{<i,j>} \{ J_{\text{ex}} \vec{S}_i \cdot \vec{S}_j + B_{\text{ex}} (\vec{S}_i \cdot \vec{S}_j)^2 \}, \tag{3.20}$$

one can obtain a relation between J_{ex} and B_{ex} and the spin-one state energies

$$J_{\text{ex}} = (E_{\text{Quintet}} - E_{\text{Triplet}})/4, \tag{3.21}$$

$$B_{\text{ex}} = (E_{\text{Quintet}} - E_{\text{Triplet}})/4 - (E_{\text{Quintet}} - E_{\text{Singlet}})/6. \tag{3.22}$$

Since the additional downfolding of $\hat{P}_0^{\nu}$ gives rise to an energy contribution for the singlet state only, the third time-dependent CT yields an additional energy contribution to the biquadratic exchange interaction B_{ex}.

Summarizing, we mapped the effective model obtained in subsection 3.1 onto an S=1 model. Moreover, we obtained an additional contribution to the biquadratic exchange interaction by performing a third time-dependent canonical transformation.

3.3 CONTROL OF EXCHANGE INTERACTIONS

In section 3.2, we obtained an effective spin-one model

$$\hat{H}_{\text{ex}} = J_{\text{ex}} \vec{S}_i \cdot \vec{S}_j + B_{\text{ex}} (\vec{S}_i \cdot \vec{S}_j)^2. \tag{3.23}$$

In this section, we write the expressions for the Heisenberg J_{ex} and biquadratic B_{ex} exchange interactions. We study the behavior of J_{ex} as well as the different biquadratic exchange paths contributing to B_{ex}. In addition, we study the behavior of the ratio $B_{\text{ex}}/J_{\text{ex}}$ for a broad range of frequency ω and strength $\mathcal{E}$ of the external electric field.

The Heisenberg exchange reads

$$\begin{aligned} J_{\text{ex}}(\mathcal{E},\omega) = \sum_{m=-\infty}^{\infty} \frac{t_0^2 J_m^2(\mathcal{E})}{U + J_H + m\omega} - 2t_0^4 {\sum_{k,l,m,n}}' J_k(\mathcal{E}) J_l(\mathcal{E}) J_m(\mathcal{E}) J_n(\mathcal{E}) \\ \times (-1)^k \left[(-1)^m + (-1)^n \right] C_{01}^{00,k} C_{10}^{00,l} C_{01}^{00,m}, \end{aligned} \tag{3.24}$$

where the first term of Eq.(3.24) corresponds to $K_1(\mathcal{E},\omega)$ and the second term is a contribution from $K_2(\mathcal{E},\omega)$.

We now would like to compare the behavior of the second order $J_{\text{ex}}(\mathcal{E},\omega)$ in single and two-orbital systems. $J_{\text{ex}}(\mathcal{E},\omega)$ for single-orbital systems reads

$$J_{\text{ex}}^{\text{single}}(\mathcal{E},\omega) = \sum_{m=-\infty}^{\infty} \frac{2t_0^2 J_m^2(\mathcal{E})}{U + m\omega}. \tag{3.25}$$

We can see that $J_{\rm ex}(\mathcal{E},\omega)$ in the two-orbital model, Eq. (3.24), has an additional factor 1/2 as compared to $J_{\rm ex}^{\rm single}$. This is due to the inter-orbital hopping $t_{\alpha\beta}$=0 which changes the prefactor of $J_{\rm ex}(\mathcal{E},\omega)$ as compared to the single-orbital case. For $t_{\alpha\beta}$=$t_{\alpha\alpha}$=t_0, the second order contribution of the single and two-orbital model would have the same prefactor. However, the relative modification of the exchange $\Delta J_{\rm ex}(\mathcal{E},\omega)/J_{\rm ex}(\mathcal{E},\omega)$ is the same and therefore, orbital dynamics does not change the control of $J_{\rm ex}(\mathcal{E},\omega)$.

The biquadratic exchange interaction can be writen as a sum of six contributions:

$$B_{\rm ex}(\mathcal{E},\omega)=B_{\rm ex}^{[1]}(\hat{P}_0)+B_{\rm ex}^{[1]}(\hat{P}_2^0)+B_{\rm ex}^{[1]}(\hat{P}_2^1)+B_{\rm ex}^{[2]}(\hat{P}_2^0)+B_{\rm ex}^{[2]}(\hat{P}_2^1)+B_{\rm ex}^{[3]}(\hat{P}_0), \quad (3.26)$$

where

$$B_{\rm ex}^{[1]}(\hat{P}_0) = 2{\sum_{k,l,m,n}}' A^1_{klmn}(\mathcal{E})C_{01}^{00,k}C_{10}^{00,l}C_{01}^{00,m}, \quad (3.27)$$

$$B_{\rm ex}^{[1]}(\hat{P}_2^0) = {\sum_{k,l,m,n}}' A^2_{klmn}(\mathcal{E})C_{01}^{00,k}C_{12}^{00,l}(C_{21}^{00,m}-3C_{10}^{00,m}), \quad (3.28)$$

$$B_{\rm ex}^{[1]}(\hat{P}_2^1) = \frac{1}{2}{\sum_{k,l,m,n}}' A^1_{klmn}(\mathcal{E})C_{01}^{00,k}C_{12}^{01,l}(C_{21}^{10,m}-3C_{10}^{00,m}), \quad (3.29)$$

$$B_{\rm ex}^{[2]}(\hat{P}_2^0) = {\sum_{k,l,m,n}}' A^2_{klmn}(\mathcal{E})C_{02}^{00,k+l}(C_{01}^{00,k}-C_{12}^{00,k})(C_{21}^{00,m}-C_{10}^{00,m}), \quad (3.30)$$

$$B_{\rm ex}^{[2]}(\hat{P}_2^1) = \frac{1}{2}{\sum_{k,l,m,n}}' A^1_{klmn}(\mathcal{E})C_{02}^{01,k+l}(C_{01}^{00,k}-C_{12}^{01,k})(C_{21}^{10,m}-C_{10}^{00,m}), \quad (3.31)$$

$$B_{\rm ex}^{[3]}(\hat{P}_0) = -{\sum_{k,l,m,n}}' A^1_{klmn}(\mathcal{E})\frac{(C_{01}^{00,k}-C_{10}^{00,l})(C_{01}^{00,m}-C_{10}^{00,n})}{4(4J_H+(k+l)\omega)}, \quad (3.32)$$

with

$$A^1_{klmn}(\mathcal{E}) = t_0^4(-1)^k\left[(-1)^m+(-1)^n\right]J_k(\mathcal{E})J_l(\mathcal{E})J_m(\mathcal{E})J_n(\mathcal{E}), \quad (3.33)$$

$$A^2_{klmn}(\mathcal{E}) = t_0^4(-1)^{k+l}J_k(\mathcal{E})J_l(\mathcal{E})J_m(\mathcal{E})J_n(\mathcal{E}). \quad (3.34)$$

We used the notation $B_{\rm ex}^{[i]}(\hat{P}_d^\nu)$ to denote the first, second and third canonical transformation via the $\hat{P}_d^\nu$ sector, for i=1, 2, 3, repsectively. Since the energy approximation Eq.(2.38) leads to a same energy for both $\hat{P}_0^0$ and $\hat{P}_0^1$, we group the biquadratic paths via these two sectors into one path via the $\hat{P}_0$ sector, $B_{\rm ex}^{[i]}(\hat{P}_0)=\sum_\nu B_{\rm ex}^{[i]}(\hat{P}_0^\nu)$, where ν=0, 1. In deriving Eqs.(3.27)-(3.32), one obtains

factors which contain k, l, m and n indices, see Eqs. (3.33) and (3.34). These directly arise from the canonical transformation and come from Bessel functions J_{-m} which are symmetric for even m but anti-symmetric for odd m. In addition, we used that $C_{d0}^{\nu 0,m}=C_{d0}^{\nu 1,m}$. In principle, the factor C_{12}^{10} present in $B_{\rm ex}^{[2]}(\hat{P}_2^1)$ violates Eq. (2.38) since a state of $\hat{P}_0^1$ has the same energy as a state of $\hat{P}_2^1$. However, in our case, the energy approximation Eq. (2.38) still holds since the exchange interactions are studied in the spin space which has the energy $E=\min(E_0^\nu) \neq \min(E_2^1)$.

Figure 3.3 shows the behavior of the Heisenberg exchange and the biquadratic exchange interaction in the two-orbital model as a function of the driving strength $\mathcal{E}$. The upper panel of Figure 3.3a shows the typical behavior of $J_{\rm ex}(\mathcal{E})$ while the lower panel shows behavior of $B_{\rm ex}(\mathcal{E})$ for frequencies ω=9, 18 and 25. We observe that $J_{\rm ex}(\mathcal{E},\omega)$ can be controlled with the strength $\mathcal{E}$ and frequency ω of the electric field similarly as found in [18] for the single-orbital system *i.e.* $J_{\rm ex}(\mathcal{E})$ can be reduced for frequencies above the Mott gap $U+J_H$ (ω=18 and ω=25), enhanced for frequencies below the gap (ω=9) and reversed for stronger driving field $\mathcal{E}$. The major contribution to $J_{\rm ex}(\mathcal{E})$ comes from the second order contribution in the hopping.

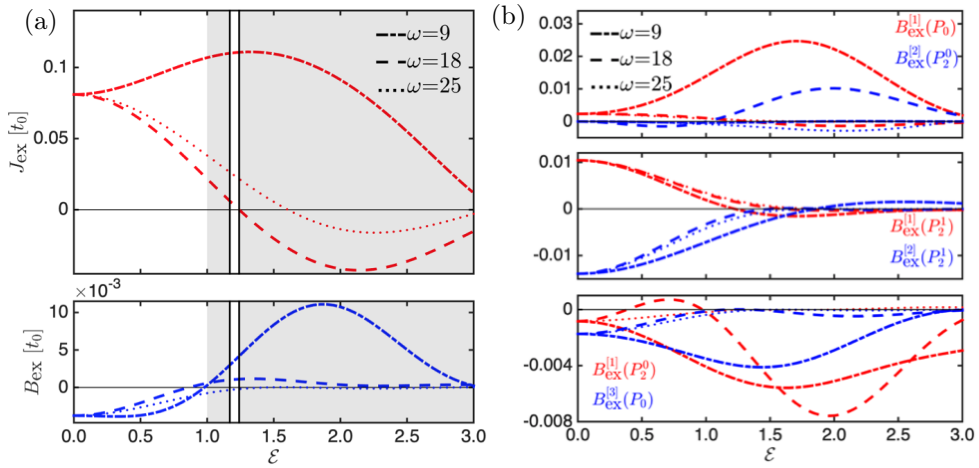

Figure 3.3: (a) $J_{\rm ex}(\mathcal{E},\omega)$ in the upper panel and $B_{\rm ex}(\mathcal{E},\omega)$ in the lower panel as a function of $\mathcal{E}$, the grey area represents regime for which both $J_{\rm ex}(\mathcal{E},\omega)$ and $B_{\rm ex}(\mathcal{E},\omega)$ are positive for ω=9 and the rectangular box represents the regime for which $|J_{ex}(\mathcal{E},\omega)|\sim|B_{\rm ex}(\mathcal{E},\omega)|$ for ω=18. (b) Biquadratic exchange paths $B_{\rm ex}^{[i]}(\mathcal{E})$ as a function of $\mathcal{E}$, where i=1, 2, 3 indicates the canonical transformation order set in Section 3.2. Results are computed for ω=9 (dash-dot line), ω=18 (dashed line) and ω=25 (dots), the frequency ω is expressed in units of the hopping t_0. Parameters for the Figure: U/t_0=10, J_H/t_0=2.

Figure 3.3b shows the contributions of the different biquadratic paths $B_{\rm ex}^{[i]}(\hat{P}_d^\nu)$ as a function of the driving strength $\mathcal{E}$. The top panel shows $B_{\rm ex}^{[1]}(\hat{P}_0^\nu)$ in red and

$B_{\rm ex}^{[2]}(\hat{P}_2^0)$ in blue which are the strongest contributions to the biquadratic exchange. The middle panel displays $B_{\rm ex}^{[1]}(\hat{P}_2^1)$ in red and $B_{\rm ex}^{[2]}(\hat{P}_2^1)$ in blue. On the bottom panel, we plotted the weakest contributions to the biquadratic exchange: $B_{\rm ex}^{[1]}(\hat{P}_2^0)$ in red and $B_{\rm ex}^{[2]}(\hat{P}_0)$ in blue. By summing up all the $B_{\rm ex}^{[i]}(\hat{P}_d^\nu)$ paths the biquadratic exchange $B_{\rm ex}(\mathcal{E})$ is obtained as shown in the bottom panel of Figure 3.3a. In equilibrium, $B_{\rm ex}(\mathcal{E}{=}0){<}0$ favors a collinear alignment of spins in the classical limit and $|B_{\rm ex}(\mathcal{E}{=}0)|$ is weak as compared to $|J_{\rm ex}(\mathcal{E}{=}0)|$.

We observe that analogous to $J_{\rm ex}(\mathcal{E},\omega)$, also $B_{\rm ex}(\mathcal{E},\omega)$ can be controlled by the electric field strength and frequency. In the regime of low driving field strength $\mathcal{E}{\ll}1$, $|B_{\rm ex}(\mathcal{E},\omega)|$ is reduced for frequencies above the Mott gap, $\omega{=}18$ and 25, and enhanced for the frequency below the gap, shown here for $\omega{=}9$. The enhancement of $|B_{\rm ex}(\mathcal{E})|$ can be understood from Figure 3.3b where $|B_{\rm ex}^{[1]}(\hat{P}_2^0)|$ and $|B_{\rm ex}^{[3]}(\hat{P}_0)|$ are both enhanced at low driving field. In addition, the sum of $B_{\rm ex}^{[1]}(\hat{P}_2^1)$ and $B_{\rm ex}^{[2]}(\hat{P}_2^1)$ gives a reduction of $B_{\rm ex}$. Eventually, the sum of these four contributions dominates over the large enhancement of the $B_{\rm ex}^{[1]}(\hat{P}_0)$ contribution, leading to an enhancement of $|B_{\rm ex}(\mathcal{E})|$. The physical mechanism behind the increase/reduction of $|B_{\rm ex}(\mathcal{E},\omega)|$ for low driving field strength can be explained as follows: the virtual hopping to $m\omega$ high energy states is enhanced or reduced as compare to equilibrium. This leads to an increase, decrease or change of sign of the $C_{dd'}^{\nu\nu',m}$ products in different biquadratic paths $B_{\rm ex}^{[i]}(\hat{P}_d^\nu)$, Eqs.(3.27-3.28). Summing all the biquadratic paths, the total $|B_{\rm ex}(\mathcal{E},\omega)|$ is enhanced or reduced as compare to its equilibrium value.

For larger driving field strenght $\mathcal{E}{\gtrsim}1$, the reduction of photo-assisted hopping as well as the oscillatory origin of the Bessel function can lead to a change of sign of $B_{\rm ex}(\mathcal{E},\omega)$. Interestingly, for frequency $\omega{=}9$, we identify a regime for which both $J_{\rm ex}(\mathcal{E})$ and $B_{\rm ex}(\mathcal{E})$ are positive for a range of driving field strenght $\mathcal{E}{>}1$, this regime is diplayed with a gray area in Figure 3.3a. At $\omega{=}18$, the rectangle box in Figure 3.3a shows a regime for which $J_{\rm ex}(\mathcal{E}){\sim}B_{\rm ex}(\mathcal{E}){>}0$. Within this regime, both $J_{\rm ex}(\mathcal{E})$ and $B_{\rm ex}(\mathcal{E})$ are positive which leads to a competition between the exchange interactions. We note that our results suggest that in principle it is possible to change the ratio of $J_{\rm ex}(\mathcal{E}){\sim}B_{\rm ex}(\mathcal{E})$ over a large range, where the equilibrium phase diagram in 1D shows several distinct quantum phases. It will be very interesting to study the feasibility of dynamical transitions between such phases in future work. Analogously, it might be very interesting to study the emergence of non-collinear order in classical spin systems by perturbation of the ratio $J_{\rm ex}(\mathcal{E}){\sim}B_{\rm ex}(\mathcal{E})$. For resonant photo-excitation, this problem has been studied recently and it was indeed found that the non-collinear phase can emerge [79].

Next, we study the possible enhancement of $B_{\rm ex}(\mathcal{E},\omega)/J_{\rm ex}(\mathcal{E},\omega)$ for a wider range of freqeuncies ($9{\leq}\omega{\leq}40$) where $\omega{=}40$ is larger than the highest energy of the undriven system $E_2^0{-}E_0^0$. The result is shown in Figure 3.4 as a color map as a function of $\mathcal{E},\omega$. Positive values of the ratio are shown in yellow and negative values are shown in blue. Below the Mott gap ($\omega{=}12$), accurate results can only be obtained in a frequency range $9{\leq}\omega{\leq}9.5$. Below and above this range

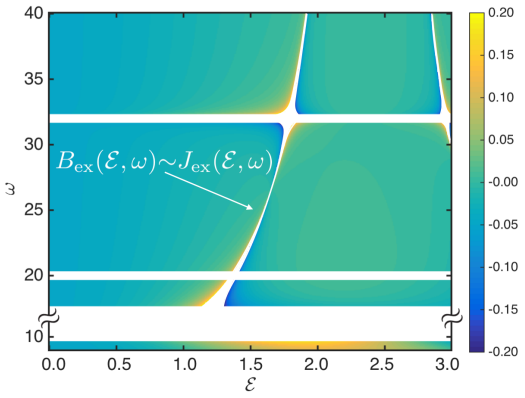

Figure 3.4: Value of the exchange ratio $B_{ex}(\mathcal{E},\omega)/J_{ex}(\mathcal{E},\omega)$ for frequencies $9{\leq}\omega{\leq}40$ and driving amplitude $\mathcal{E}$ up to 3. The white band for ω between 10 and 16 and the white lines in the vicinity of $\omega = 20$ and 32 are centered around frequencies at which the canonical transformation diverges. The frequency range $11{\leq}\omega{\leq}17$ is not displayed in the figure since the biquadratic formula is not accurate in this range. White curved areas correspond to points for which $B_{ex}(\mathcal{E},\omega){\sim}J_{ex}(\mathcal{E},\omega)$. Parameters: $U/t_0{=}10$, $J_H/t_0{=}2$. For clarity, $B_{ex}(\mathcal{E},\omega)/J_{ex}(\mathcal{E},\omega)$ is restricted to -0.23 to 0.23.

until $\omega{\simeq}17$, the energy approximation Eq.(2.38) breaks down and orbital resolved spin dynamics [83] is required to have an accurate description of the exchange interactions. Therefore, the frequency range $10{\leq}\omega{\leq}17$ is not shown. Figure 3.4 clearly demonstrates that the exchange ratio can be enhanced as well as reduced depending on ω and $\mathcal{E}$. The parameters for which $B_{ex}(\mathcal{E},\omega)/J_{ex}(\mathcal{E},\omega)$ is strongly enhanced correspond to three types of situations:

• Frequencies for which $\omega{=}E_d^{\nu}{-}E_{d'}^{\nu'}{+}m\omega$, this corresponds to white lines at $\omega{=}10, 12, 16$, 20 and 32. At these frequencies, $B_{ex}(\mathcal{E},\omega)$ diverges, such that the canonical transformation breaks down. Note that $\omega{=}32$ is the frequency that separates spin states from the doubly ionized state, such that a coupling appears close to this frequency. This coupling leads to charge dynamics and therefore, the spin-one model is not accurate in this region. This coupling to charge states is studied in detail in the next section.

• Field parameters ω and $\mathcal{E}$ for which $B_{ex}(\mathcal{E},\omega){\sim}J_{ex}(\mathcal{E},\omega)$ are indicated in white curved areas. For this regime, the exchange ratio $|B_{ex}(\mathcal{E},\omega)/J_{ex}(\mathcal{E},\omega)|$ is enhanced since $J_{ex}(\mathcal{E},\omega){\simeq}0$. This leads to a regime where $B_{ex}(\mathcal{E},\omega){>}J_{ex}(\mathcal{E},\omega)$ is realised however, $B_{ex}(\mathcal{E},\omega)$ itself remains small as compared to $J_{ex}(\mathcal{E}{=}0)$.

• Parameters ω and $\mathcal{E}$ for which the relative sign of $B_{ex}(\mathcal{E},\omega)/J_{ex}(\mathcal{E},\omega)$ is changed due to the change of sign of $B_{ex}(\mathcal{E},\omega)$ leading to a slight enhancement of $B_{ex}(\mathcal{E},\omega)/J_{ex}(\mathcal{E},\omega)$. This can be clearly seen for frequency $\omega{\simeq}9$ at $\mathcal{E}{\simeq}2$ (yellow region in Figure 3.4).

Summarizing, we obtained an expression for both $J_{\rm ex}(\mathcal{E},\omega)$ and $B_{\rm ex}(\mathcal{E},\omega)$. In addition, showed that orbital degrees of freedom do not change the behavior of $J_{\rm ex}(\mathcal{E},\omega)$. Moreover, both sign and strength of $J_{\rm ex}(\mathcal{E},\omega)$ and $B_{\rm ex}(\mathcal{E},\omega)$ as well as their relative sign can be controlled by driving the system with an external electric field, while the regime for which $B_{\rm ex}(\mathcal{E},\omega)\sim J_{\rm ex}(\mathcal{E},\omega)$ is reached only for $J_{\rm ex}(\mathcal{E},\omega)\ll J_{\rm ex}(\mathcal{E}=0)$. In condensed matter systems, a driving field strenght of $\mathcal{E}>1$ is required in order to have acess to the regime for which $J_{\rm ex}$ and $B_{\rm ex}$ compete. This regime seems not accesssible with the current experimental techiques. Nevertheless, driving strength $\mathcal{E}\sim 0.1$ is accessible experimentally and would lead to a relative change of $J_{\rm ex}$ of about 1%, similarly as for the single orbital model [18], while for $B_{\rm ex}$ it corresponds to a change of up to 2%.

4

COHERENT SPIN-CHARGE COUPLING IN TWO-ORBITAL SYSTEMS

In the previous chapter, we studied a regime for which the exchange interactions dominate. In this chapter, we interest ourselves in a regime for which a new type of spin-charge coupling phenomenon overcomes the exchange interaction.

As illustrated in Figure 3.1, the doubly ionized states (states with two doublons d=2) are strongly gapped with respect to singly occupied states. However, we show that with a non-resonant driving field, the doubly ionized states (charge state) can hybridize with singly occupied states (spin state) [51]. This yields a spin-charge coupling at leading order in the field and second order in the hopping.

In this chapter, we show that the spin-charge coupling is well captured by the time-dependent extended canonical transformation. Then, we confirm the analytical results with time-evolution of the system under electric field driving leading to a reversible transfer between spin and charge degrees of freedom.

This chapter is based on the following publication: M.M.S. Barbeau, M. Eckstein, M.I. Katsnelson and J.H. Mentink, *Optical control of competing exchange interactions and coherent spin-charge coupling in two-orbital Mott insulators*, SciPost Phys. **6**, 027 (2019).

4.1 BEYOND THE SPIN-ONE MODEL

In this chapter, we investigate the spin-charge coupling which goes beyond the spin model description alone, see section 3.2.

To study the spin-charge coupling, we use the time-dependent extended canonical transformation to study the coupling to the doubly ionized charge sector (d=2), which is irrelevant in equilibrium due to the large energy difference between the sectors. Under non-equilibrium conditions, the spin-charge coupling reads

$$\hat{H}^{(n)}_{\mathrm{sc}}(t) = \sum_{n} \sum_{\nu=0,1} \hat{P}^{\nu}_{0} \hat{H}^{(n)}_{\mathrm{eff}}(t) \hat{P}^{\nu'}_{2} + h.c.. \tag{4.1}$$

We now study the regime for which $\hat{P}^{\nu}_{0}$ and $\hat{P}^{\nu'}_{2}$ from different m sectors overlap. This overlap appears for frequencies ω close to E^{ν}_{0}=E^{ν}_{2}+$m\omega$. Although this seems a resonant condition, a direct optical transition is not possible since two hoppings are required to go from the $\hat{P}^{\nu}_{0}$ sector to the $\hat{P}^{\nu'}_{2}$ sector. Equation (4.1) can be divided into contributions $\sum_{m} \hat{H}^{(n)}_{\mathrm{sc},\Delta m=0}$ and $\sum_{m} \hat{H}^{(n)}_{\mathrm{sc},\Delta m\neq 0}$. The first contribution represents the coupling within one Fourier sector m. This contribution remains weak since $\hat{P}^{\nu}_{0}$ and $\hat{P}^{\nu'}_{2}$ states are strongly gapped when they belong to the same Fourier sector. We therefore focus on the second term that allows coupling between the spin sector $\hat{P}^{\nu}_{0}$ and the charge sector $\hat{P}^{\nu'}_{2}$ with different m. For small $\mathcal{E}$, the leading contribution to Eq. (4.1) arises from n=2 and Δm=$\pm$1. Here we restrict to the coupling between between $\hat{P}^{\nu}_{0}$ from m=0 and $\hat{P}^{\nu'}_{2}$ from m=$-$1 sector. This yields

$$\begin{aligned} \hat{H}^{(2)}_{\mathrm{sc},|\Delta m|=1}(t) = \frac{1}{2} \sum_{k=-\infty}^{\infty} \Big(\frac{1}{3U - 5J_H - k\omega} - \frac{1}{U + J_H - k\omega} \Big) \\ \times \Big[\sum_{\nu,\nu'} \hat{P}^{\nu}_{0} \hat{T}^{-1}_{k} \hat{P}^{0}_{1} \hat{T}^{-1}_{1-k} \hat{P}^{\nu'}_{2} e^{-i\omega t} \Big] + h.c. \sim \mathcal{E}, \end{aligned} \tag{4.2}$$

To illustrate the spin-charge coupling, we restrict ourselves to the space ν'=0. These are two states that have all electrons either on site i or on site j.

The effective Hamiltonian, Eq 4.2, forms a 8×8 matrix in the occupation number basis states $|\phi_k\rangle$ of the $\hat{P}^{\nu}_{0}$+$\hat{P}^{0}_{2}$ sector, which yields the following matrix structure

$$\begin{pmatrix}
-4t_0^2F & 0 & 0 & 0 & 2t_0^2F & 2t_0^2F & \vdots & -t_0^2I & t_0^2I \\
0 & -4t_0^2F & 0 & 0 & 2t_0^2F & 2t_0^2F & \vdots & -t_0^2I & t_0^2I \\
0 & 0 & 2J_H & 0 & -J_H & -J_H & \vdots & 0 & 0 \\
0 & 0 & 0 & 2J_H & -J_H & -J_H & \vdots & 0 & 0 \\
2t_0^2F & 2t_0^2F & -J_H & -J_H & 2J_H{-}4t_0^2F & 0 & \vdots & t_0^2I & -t_0^2I \\
2t_0^2F & 2t_0^2F & -J_H & -J_H & 0 & 2J_H{-}4t_0^2F & \vdots & t_0^2I & -t_0^2I \\
\cdots & \cdots & \cdots & \cdots & \cdots & \cdots & \cdots & \cdots & \cdots \\
-t_0^2I^* & -t_0^2I^* & 0 & 0 & t_0^2I^* & t_0^2I^* & \vdots & E_I{-}\omega{+}4t_0^2G & 0 \\
t_0^2I^* & t_0^2I^* & 0 & 0 & -t_0^2I^* & -t_0^2I^* & \vdots & 0 & E_I{-}\omega{+}4t_0^2G
\end{pmatrix}, \tag{4.3}$$

where

$$F{=}\sum_{m=-\infty}^{\infty}\frac{J_{|m|}(\mathcal{E})^2}{2(U+J_H+m\omega)}, \tag{4.4}$$

$$G{=}\sum_{m=-\infty}^{\infty}\frac{J_{|m|}(\mathcal{E})^2}{2(3U-5J_H+m\omega)}, \tag{4.5}$$

$$I{=}I(t){=}\sum_{k=-\infty}^{\infty}(-1)^{k+1}J_k(\mathcal{E})J_{k+1}(\mathcal{E})\Big\{\frac{1}{3U-5J_H+k\omega}-\frac{1}{U+J_H+k\omega}\Big\}e^{-i\omega t}. \tag{4.6}$$

I^* is the complex conjugate of I and $E_I{=}4(U{-}J_{\rm H})$ is the energy of the doubly ionized states [1]. The upper left block of the matrix Eq. (4.3) corresponds to the effective Hamiltonian in $\hat{P}_0^{\nu}$ sector with $m{=}0$ where the basis states are

$$h_{d=0}=\Big\{|\uparrow,\uparrow\rangle_i|\downarrow,\downarrow\rangle_j,|\downarrow,\downarrow\rangle_i|\uparrow,\uparrow\rangle_j,|\uparrow,\downarrow\rangle_i|\uparrow,\downarrow\rangle_j, \tag{4.7}$$

$$|\downarrow,\uparrow\rangle_i|\downarrow,\uparrow\rangle_j,|\uparrow,\downarrow\rangle_i|\downarrow,\uparrow\rangle_j,|\downarrow,\uparrow\rangle_i|\uparrow,\downarrow\rangle_j\Big\}, \tag{4.8}$$

where $|\sigma_a,\sigma'_b\rangle_i{=}\hat{c}^{\dagger}_{ib\sigma'}\hat{c}^{\dagger}_{ia\sigma}|0\rangle$. The lower right block of the matrix corresponds to the effective Hamiltonian in $\hat{P}_2^0$ sector with$m{=}{-}1$ where the basis is the following

$$h_{d=2}=\Big\{|\uparrow\downarrow,\uparrow\downarrow\rangle_i|0,0\rangle_j,|0,0\rangle_i|\uparrow\downarrow,\uparrow\downarrow\rangle_j\Big\}. \tag{4.9}$$

We diagonalize the matrix, Eq. (4.3) and, after time averaging, obtain the spectrum shown in Figure 4.1 for $\omega{=}\omega_0{+}\delta\omega$, where $\omega_0{=}|E_0^{\nu}{-}E_2^0|$ and $\delta\omega{=}0.5$. We emphasize

1 Note the factor $(-1)^{k+1}$ in front of Eq. (4.6) is different from what has been written in [51].

that the diagonalization and time averaging do not commute e.g. $\frac{1}{T}\int_0^T I(t)dt=0$ which washes out the coupling.

In Figure 4.1, the lowest energy state is a singlet state that couples to the two charge states of $\hat{P}_2^0$. The latter are degenerate up to t_0^4 since four hoppings are needed in order to transfer the four electrons from one atom to the other one. Black lines, from top to bottom, show the quintet state (S=2) and the triplet state (S=1) that are not involved in the spin-charge coupling. The black dashed line shows the behavior of the spin state which is a singlet state from sector m=0. The dotted lines show the behavior of the charge states from m=−1. The thick red and blue lines show the spin and charge states, respectively and are obtained by diagonalizing the full $\hat{H}_{\rm eff}^{(2)}$, Eq. 4.3. The eigen-energies show an avoided crossing, which reveals a hybridization between the spin and charge states. For driving frequencies far away from ω_0, the spin-charge coupling terms $\hat{H}^{(2)}_{{\rm sc},|\Delta m|=1}(t)$ remain small and for these frequencies, the spin and charge states are gapped. Therefore, the hybridization is negligible and we recover the regime for which the effective spin model is valid. However, in the regime $\omega\sim\omega_0$, the hybridization between the spin and charge states cannot be neglected and the exchange interaction formula obtained in the previous section are no longer accurate.

To sketch the hybridization process, let us take the equilibrium ground state state of the system which is the singlet state (spin state). After switching on the electric field and by slowly changing the field amplitude ($\partial_t E_0/E_0 \ll \omega$), one anticipates that the system starts in a pure spin state and, approaching the avoided-crossing regime, charge states are mixed to the state. For strong $\mathcal{E}$, the spin state becomes a pure charge state.

In the literature, a time-dependent traverse of an avoided crossing is widely studied. The basic example is the Landau-Zener (LZ) effect [86, 87]. Also condensed matter systems can exhibit LZ physics. For instance, the Zener breakdown has been studied [88, 89] in semiconductors and more recently in Mott insulators [90]. Nonetheless, distinct from these LZ effects which involve changes of the electrical conductivity, here we report coherent transfer of spin to charge degrees of freedom that keep the system in an insulating regime.

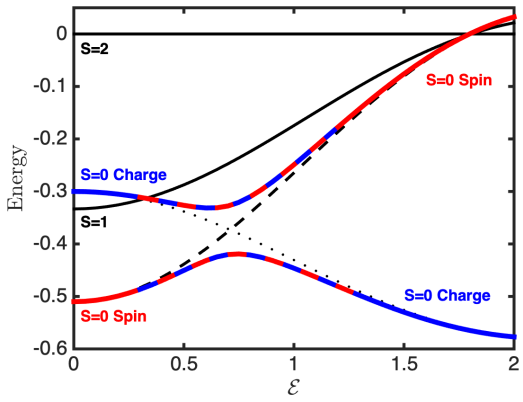

Figure 4.1: Low energy spectrum as a function of the driving amplitude $\mathcal{E}$. The spectrum is restricted to the spin states of the m=0 sector and the highest excited state of the sector m=−1. Upper and lower thin black lines represent the quintet state and the triplet state. The thin black dots and the dashed line represent the charge multiplet and the singlet without spin-charge coupling, respectively. Blue to red thick line represents the charge ($\mathcal{E}$<0.5) to spin ($\mathcal{E}$>1) state and the red to blue thick line represents the spin ($\mathcal{E}$<0.5) to charge ($\mathcal{E}$>1) state. Parameters: U/t_0=10, J_{H}/t_0=2 and ω=ω_0+0.5.

Summarizing, orbital dynamics gives access to charge states that are not accessible in equilibrium. The spin-charge coupling offers the possibility to induce coherent charge dynamics in the system. This phenomenon appears in the non-equilibrium low-energy spectrum as an avoided crossing. We stress that it is quite distinct from spin-orbit coupling since here we have an interplay with Coulomb and Hund interaction with the driving field. The spin-charge coupling is not present in single band systems, and we expect it to be universal for multi-orbital systems. Indeed, since multi-orbital systems offer the possibility of having multiple excited states (multiple doublons), multi-doublon excitation should be possible for multi-orbital systems in general. Note that here we did not study $\hat{P}_2^1$ states, they are nonetheless very interesting since they have a lower energy (at and below the energy of the gap U+J_H) and therefore are reachable with lower frequencies ω.

4.2 TIME-DEPENDENT NUMERICAL SIMULATIONS

In the previous section, we showed that the generalized canonical transformation can capture a qualitatively new phenomenon that couples the spin and doubly ionized charge sector. To further support this finding, we perform an exact time propagation of a cluster of two sites described by the Mott-Hubbard Hamiltonian. We focus our attention on the coherent transfer of spin to charge degrees of freedom. In order to describe the charge dynamics, we define pseudo-spin one operators $\hat{\mathcal{T}}^0$ that are

composed of Anderson pseudo-spin 1/2 operators $\hat{\tau}^{+}_{i\alpha}=\hat{c}^{\dagger}_{i\alpha\uparrow}\hat{c}^{\dagger}_{i\alpha\downarrow}$ ($\hat{\tau}^{-}_{i\alpha}=\hat{c}_{i\alpha\downarrow}\hat{c}_{i\alpha\uparrow}$) [91, 92]. The construction of $\hat{\mathcal{T}}^0$ is inspired by the expression of the spin-one operator $\hat{S}^0$. By using a similar procedure with $\hat{\mathcal{T}}^0$ and pseudo-spin 1/2 operators, we obtain

$$\hat{\mathcal{T}}^0 = \hat{\tau}^{+}_{a}\hat{\tau}^{-}_{a}\hat{\tau}^{+}_{b}\hat{\tau}^{-}_{b} - \hat{\tau}^{-}_{a}\hat{\tau}^{+}_{a}\hat{\tau}^{-}_{b}\hat{\tau}^{+}_{b} = \hat{n}_{a\uparrow}\hat{n}_{a\downarrow}\hat{n}_{b\uparrow}\hat{n}_{b\downarrow} + \hat{h}_{a\uparrow}\hat{h}_{a\downarrow}\hat{h}_{b\uparrow}\hat{h}_{b\downarrow}, \tag{4.10}$$

that characterizes fully occupied and completely empty sites from the $\hat{P}^0_2$ sector. Operators $\hat{\mathcal{T}}^{+1}$ and $\hat{\mathcal{T}}^{-1}$ can be defined analogously [51].

To solve the time-dependent Schrödinger equation, we use a second order commutator-free approximation of the time-propagator [93] and we compute the time-dependent wavefunction $|\Psi(t)\rangle$ and evaluate observables as

$$\langle\hat{O}\rangle=\langle\Psi(t))|\hat{O}|\Psi(t)\rangle. \tag{4.11}$$

We focus on three different observables: First, the spin correlation $\langle\vec{S}_i\cdot\vec{S}_j\rangle$ to show the spin dynamics during the laser pulse. Second, we characterize the charge states $\hat{P}^0_2$ with $\langle\hat{\mathcal{T}}^0_i\hat{\mathcal{T}}^0_j\rangle$. Finally, to probe the states that possess one doublon d=1, we evaluate $\langle\hat{N}_{d=1}\rangle$, where $\hat{N}_{d=1}=\hat{P}^0_1\hat{d}\hat{P}^0_1$.

Figure 4.2 shows simulated spin-charge dynamics for an electric field

$$E(t)=E_0\cos(\omega t)\exp\left(-(t-t_*)^2/\tau^2\right), \tag{4.12}$$

where E_0 is the amplitude of the field, t_* is the time at which $E(t)$ peaks and τ is the pulse width.

We choose a Gaussian envelope with $\tau=4000\pi/\omega$, $\omega=\omega_0+\delta\omega$, with $\delta\omega$=0.5, such that $\tau\times\omega_{sc}\gg1$ where $\omega_{\rm sc}\simeq0.1$ is the energy splitting of the avoided crossing (see Figure 4.1). It has been shown that the effective Hamiltonian picture can break down for long-time dynamics in the thermodynamic limit, because the system heats up to infinite temperature [94]. Here we restrict ourselves to a two-site system to mimic the dynamics of a large system at relatively short timescales. However, for generic systems it is shown that heating can occur at short timescale since the adiabatic limit of Floquet does not exists [95]. Nevertheless, here the use of Floquet restricts to the derivation of an effective Hamiltonian which gives a qualitative picture of the avoided-crossing. We confirm the reversibility of the spin-charge coupling phenomenon within the two-site system with the time-dependent numerical simulations displayed in Figure 4.2.

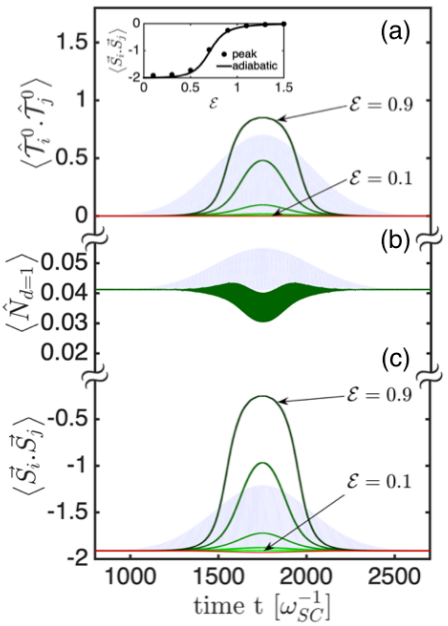

Figure 4.2: (a) and (c) Spin $\langle \vec{S}_i \cdot \vec{S}_j \rangle$ and charge $\langle \hat{\mathcal{T}}_i^0 \hat{\mathcal{T}}_j^0 \rangle$ dynamics as a function of time in orange and green, respectively. The dynamics is computed for driving strengths $\mathcal{E}$ from 0.1 to 0.9 with steps $\Delta\mathcal{E}$=0.2 represented by different color shades. Note that in equilibrium $\langle \vec{S}_i \cdot \vec{S}_j \rangle$ is negative. (b) Single doublon number $\langle \hat{N}_{d=1} \rangle$ in blue, for $\mathcal{E}$=0.7. The amplitude of the electric field envelop is shown in Figure (a),(b) and (c) by a light blue Gaussian, each laser pulse contains 4000 cycles. Parameters U/t_0=10 and J_H/t_0=2, for an electric field frequency ω=ω_0+0.5. The inset shows a comparison between the time evolution (dots) and the analytical calculation in the adiabatic limit for the field envelope (solid line). Red lines in (a) and (c) represent the spin and charge dynamics for frequency ω=ω_0+3 and $\mathcal{E}$=0.7, away from the hybridization.

Figure 4.2a, c show the plot of the charge and spin observables respectively, for different driving strength $\mathcal{E}$ from 0.1 to 1.5. The time-dependent electric field is represented in light blue and the results are computed for U/t_0=10 and J_H/t_0=2.

Figure 4.2c shows $\langle \vec{S}_i \cdot \vec{S}_j \rangle$ for different $\mathcal{E}$. In equilibrium and for small $\mathcal{E}$, $\langle \vec{S}_i \cdot \vec{S}_j \rangle \simeq -1.9$, which slightly deviates from the pure spin case ($\langle \vec{S}_i \cdot \vec{S}_j \rangle = -2$) due to hybridization with $\hat{P}_0^\nu$, $\hat{P}_1^0$ and $\hat{P}_2^0$ sectors. Figure 4.2c shows that, with increasing $\mathcal{E}$ the state has less spin characteristics. Moreover, it is observed in Figure 4.2a that with increasing $\mathcal{E}$, the state has more charge characteristics $\langle \hat{\mathcal{T}}_i^0 \hat{\mathcal{T}}_j^0 \rangle$. In addition, after the laser pulse, both charge excitation and the spin correlations return to their initial value, demonstrating that the coupling is reversible.

Further, we confirm that for frequencies away from ω_0 the spin-charge coupling dynamics is not present. This is shown in Figure 4.2a,c where the charge and spin dynamics are plotted in red lines for $\delta\omega$=3. In this case, no enhancement is observed. Similarly, in Figure 4.2c, the spin correlations are not diminished. Moreover, we show the single doublon states dynamics $\langle \hat{N}_{d=1} \rangle$ in Figure 4.2b, for a field strength $\mathcal{E}$=0.7. We observe that the laser pulse does not trigger any positive excitation of $\hat{P}_1^0$ states. This means that enhancement of charge dynamics is not due to resonant excitation of the intermediate excited states $\hat{P}_1^0$. Interestingly, we actually observe depopulation of the $\hat{P}_1^0$ states during the laser pulse. This means that more $\hat{P}_1^0$ states are virtually excited to the doubly inonized sector than spin states excited to the $\hat{P}_1^0$ sector. Finally, the inset of Figure 4.2a shows values of the peak of the spin correlations $\langle \vec{S}_i \cdot \vec{S}_j \rangle_{t_{\text{peak}}}$ for each $\mathcal{E}$ in dots and values of the spin correlations $\langle \vec{S}_i \cdot \vec{S}_j \rangle$ as a function of $\mathcal{E}$ is obtained from the anaytical calculation of Section 4.1. Good agreement between analytical and numerical results is found, which confirms the predictions of the analytical theory. The slight discrepancies between $\langle \vec{S}_i \cdot \vec{S}_j \rangle_{\mathcal{E}}$ and $\langle \vec{S}_i \cdot \vec{S}_j \rangle_{t_{\text{peak}}}$ at zero field $\mathcal{E}$ can be reduced by taking into account higher order terms in the effective Hamiltonain as well as the spin-charge coupling dynamics to the full P_2^ν sector. In addition, we note that with careful tuning of $\delta\omega$, the reduction of $|\langle \vec{S}_i \cdot \vec{S}_j \rangle|$ as a function of $\mathcal{E}$ at small $\mathcal{E}$ can be made even stronger *e.g.* by increasing $\delta\omega$, one can move the avoided-crossing closer to $\mathcal{E}$=0 which enhances hybridization with the charge states at small $\mathcal{E}$.

As a conclusion, a new coupling between spin and charge states is confirmed by simulating electron dynamics on a two-site cluster. This coupling leads to a hybridization between spin and charge states for frequencies close to the spin-charge gap. In contrast to a common charge excitation by resonant photo-absorption, the spin-charge coupling allows non-resonant and reversible coupling to charge degrees of freedom. Natural extension of this work are numerical studies for extended systems. This could be possible for example using multiband extensions of nonequilibrium Dynamical Mean-Field Theory (DMFT) [73, 74, 96–98]. We emphasize that, besides the possibility to induce coherent charge dynamics, the presence of the spin-charge coupling should also be visible for short pulses, enabling the excitation of doubly ionized states which could remain coherent due to the gapping with the normal Mott-Hubbard gap. This suggests interesting perspectives for enhancing electronic coherence in correlated electron systems. In this context, it will be interesting to explore the applicability of the two-orbital model to experimental spin-one systems such as $KNiF_3$ [14], which in the literature are considered as prototypical S=1 systems. We would like to point out that modification of the charge occupation is known to systematically influence phonon excitation. Since we did not take into account electron-phonon interactions in our model, an outlook would be to study phonon excitation induced by the spin-charge coupling. In addition, interesting prospect of this work is the two-orbital system under arbitrary fields similarly to what is done in [84] and, since our approach with the canonical transformation

can also be applied for arbitrary time-dependent fields [21]. Its extention to more exotic forms of time-dependent fields seems feasible and is left for future work. Finally, we hope that our work can find applications in cold atoms systems, where multi-orbital systems can nowadays be engineered [99, 100]. With an adiabatic ramping of the electric field strength, the fully reversible spin-to-charge conversion might be directly observed in double-well systems.

5

EFFECT OF DYNAMICAL SCREENING ON THE EXCHANGE INTERACTION

5.1 INTRODUCTION

In condensed matter systems, the distribution of electrons in the system tends to minimize the potential energy leading to screening effects. For instance, it is observed in metalic systems that the on-site electron-electron potential is strongly screened by the (other) itinerant electrons. As a consequence, the effective Coulomb interaction between electrons is small. In the case of Mott insulators for which electrons are imobile, screening effects are smaller. However, driving a Mott insulator out of equilibrium with resonant pulse leads to the creation of non-thermal metallic states. Therefore, these photo-doped systems can exhibit screening effects. This has been predicted for NiO where the effective Coulomb interaction is dynamically screened by thermal electrons [101].

An interesting consequence of screening in materials is its implication in magnetism. Since the exchange interaction originates from the Pauli principle and the Coulomb energy, potentially strong perturbation of the exchange interaction are expected due to the screening.

One way to study screening effects in insulating systems is to account for a nearest neighbore interaction V, see subsection 2.5.2. These interactions modify the potential energy landscape of the lattice leading to an additional screening of the local Coulomb interaction [64, 65, 102–104]. In the case of non-equilibrium dynamics, the non-local interactions play a role in the excitation as well as in the relaxation processes where they allow additional thermalization channels [35].

In this chapter, we study the screening of the Heisenberg exchange interaction by the non-local correlations V using the $U-V$ Hubbard model, as introduced in subsection 2.5.2. The calculations are performed using a non-equilibrium version of the EDMFT formalism developed by Golež and Werner [35, 65]. The system considered is a two-dimensional antiferromagnetic (AFM) square lattice at half-filling. The exchange interactions are calculated from the non-equilibrium Green functions obtained with EDMFT based on the formalism developed by [39] and implemented for time-dependent exchange by Mentink et al. [18, 20], see subsection 2.6.2. Using this implementation, we can evaluate the exchange formula Eq. (2.103) which reduces to Eq. (2.104) in equilibrium. Firstly, we discuss the screening of the exchange interactions by the non-local correlations in equilibrium. Secondly, we study the effect of the screening on the exchange interactions when the system is pumped by an external electric field.

5.2 EQUILIBRIUM SCREENING OF THE EXCHANGE INTERACTION

In this section, we study the exchange interaction and the effects of the screening by the non-local correlations V in equilibrium. First of all, we study the limit $V = 0$, for which the EDMFT coincides with DMFT. Then, we study the limit for which $U \to \infty$ and compare the results with the exchange formula to leading order in the hopping t_0 obtained with the downfolding technique

$$J_{\text{ex}} = \frac{2t_0^2}{U}, \tag{5.1}$$

see subsection 2.6.1. Subsequently, we study the screened exchange interaction and compare these results with the exchange formula obtained with the downfolding technique for the $U - V$ model [105].

5.2.1 *The DMFT limit*

In the DMFT limit and in the limit of large U, the exchange formula calculated with the GF formalism J_{ij}, Eq. (2.104), and the exchange formula obtained with the downfolding technique, see subsection 2.6.1, are expected to give similar results:

$$\lim_{U\to\infty} U J_{ij} \simeq 2t_{ij}^2. \tag{5.2}$$

However, the (E)DMFT exchange J_{ij} is extracted from the product between the impurity GF and the self-energy which includes the neighbors

$$[G \star \Sigma]_{ij} = \sum_{<i>_j} G_{ij} t_{ji}. \tag{5.3}$$

where $\sum_{<i>_j} t_{ji}{=}zt_0$, with z, the number of nearest neighbors. This leads the exchange J_{ij} to scale as

$$\lim_{U\to\infty} J_{ij} \simeq \frac{2z^2 t_0^2}{U}. \tag{5.4}$$

The hopping t_0 is taken as a unit of energy in the EDMFT calculations. In order to obtain values of the exchange interaction on the bond ij, J_{ij}^0, we rescale J_{ij} as follows

$$J_{ij}^0 = \frac{1}{z^2} J_{ij}. \tag{5.5}$$

We consider the 2D lattice: $z{=}4$, which leads the rescaling $J_{ij}^0{=}J_{ij}/16$. Results of the numerical calculations are shown in Figure 5.1. We compare values of J_{ij}^0 (dots) with the downfolding formula J_{ex} (dashed lines) as a function of the temperature T for $U{=}12$, 18 and 24. We observe that the values of J_{ij}^0 decrease with increasing U and resemble the perturbative result more accurately at large U, as expected

and previously reported with DMFT for the Bethe lattice [20]. Above $T{\sim}0.15$, the values of the Matsubara exchange J_{ij}^0 slightly increases for each value of U. In the vicinity of the Néel temperature, the AFM order melts and the ordered moment vanishes and it is not possible to use the formula for the exchange J_{ij}, Eq. (2.103).

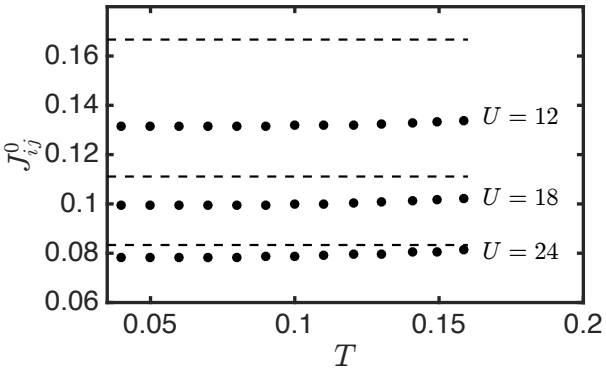

Figure 5.1: The Matsubara exchange interaction J_{ij} for $V = 0$ as a function of the temperature T for $U = 12$, 18 and 24 in dots. Dashed lines represent values for the downfolding formula $J_{\rm ex} = 2t_0^2/U$.

As a conclusion, we studied the exchange interaction in the DMFT limit. After an appropriate rescaling, we found that the exchange J_{ij}^0 resembles the perturbative results for large U confirming what has been observed previously [20].

5.2.2 *Screening by non-local correlations*

In this subsection, we study the behavior of the exchange interaction J_{ij}^0 as a function of U for $V{=}0$, 1 and 2. In addition, we compare the EDMFT exchange with the exchange obtained with the downfolding formula.

The formula for the exchange in the $U{-}V$ model obtained with a canonical transformation reads [105]

$$J_{\rm ex} = \frac{2t_0^2}{U_{\rm eff}}, \tag{5.6}$$

where $U_{\rm eff}{=}U{-}V$ is the effective Coulomb interaction. Note that Eq. (5.6) reduces to Eq. (5.1) at $V{=}0$.

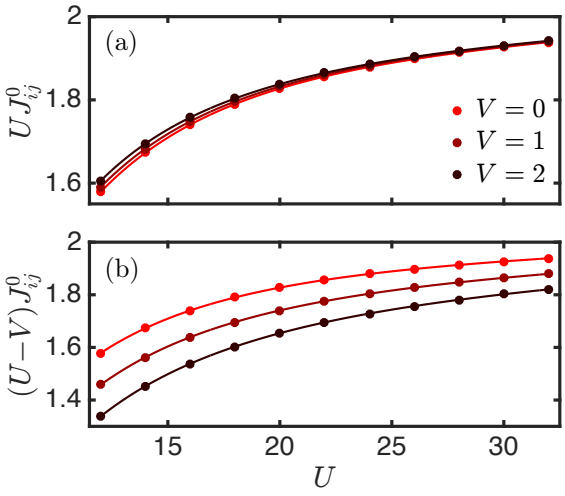

Figure 5.2: (a) UJ^0_{ij} and (b) $(U-V)J^0_{ij}$ as a function of U. Light to dark red indicates V=0, 1, 2, respectively. Dots show the data points and the lines represent the polynomial fitting of the data points.

Figure 5.2a shows the quantity UJ^0_{ij} as a function of U for V=0, 1 and 2. The results where computed until the largest U for which we could obtain an accurate closure of the self-consistency. Despite the fact that the values of UJ^0_{ij} for different V are very similar, we observe that the effects of the non-local correlations are larger at smaller U which lead to larger discrepancies between the values of UJ^0_{ij}. Therefore, screening effects due to non-local interactions on the exchange interaction are stronger for smaller values of U. For instance, at U=12, we obtain $\Delta J^0_{ij}\sim$1.7% for ΔV=2. However, these results obtained with EDMFT are not consistent with the perturbative formula, Eq. (5.6). This inconsistency is particularly visible in Figure 5.2b which shows the quantity $(U-V)J^0_{ij}$ as a function of U for V=0, 1 and 2. We observe that, the values of $(U-V)J^0_{ij}$ are very diffferent for different V. Especially, their are more differences between the values of $(U-V)J^0_{ij}$ than between the values of UJ^0_{ij} for different V. This means that the EDMFT results do not coincide with the perturbative results Eq. (5.6). This can be understood from the perspective of the impurity model in EDMFT. In EDMFT, the effective Coulomb interaction in the self-consistency is not a constant as for DMFT, but depends on the Matsubara frequency $U_{\text{eff}}(\omega_n)$ due to V:

$$U_{\text{eff}}(\omega_n) = U - \Lambda(\omega_n), \tag{5.7}$$

where $\Lambda(\omega_m)\sim V^2$ in the limit $V/U\ll 1$ [102, 103]. Therefore, the exchange interaction does not scale as $(U-V)^{-1}$ but as $(U-\Lambda(\omega_n))^{-1}$. This is analogous to an EDMFT impurity problem which does not account for inter-site correlations in the

charge sector. Hence, the EDMFT does not fully describe the screening effects due to non-local interactions V in the exchange mechanism.

Sumarizing, we studied the behavior of the equilibrium exchange interaction for different values of the Coulomb interaction U as well as different values of the non-local correlations V. We have shown that despite the scaling of U_{eff} with V^2, we observe a screening of J_{ij}^0 which effect is larger with smaller U and goes up to $\sim$1.7% for ΔV=2.

5.3 SCREENING OF EXCHANGE INTERACTIONS OUT OF EQUILIBRIUM

Despite the limitations for recovering the static limit, the presence of dynamical effects $\Lambda(\omega_m)$ might have a non-trivial effect out of equilibrium. In order to study the screening of the exchange interactions out of equilibrium, we use an external electric field. We choose the electric field to be resonant with the Mott-Hubbard gap in order to create non-thermal states most effeciently. In this section, we study the effect of the dynamical screening of the exchange by the non-local correlations V in excitation and relaxation processes. First, we explain how the exchange interaction $J_{ij}(t)$ is computed from $\mathrm{Im}\big[A_{ij}^R(t,t-s)\big]$, see subsection 2.6.2. In addition, we show that the effect of non-local dynamical correlations can already be observed in $\mathrm{Im}\big[A_{ij}^R(t,t-s)\big]$ without an excitation pulse. Second, we study the behavior of the magnetization, the double occupancy and exchange interaction as a function of the electric field amplitude. Third, we study the effect of the non-local correlations on these quantities.

5.3.1 *Computation of the time-dependent exchange formula*

In this subsection, we discuss the behavior of $\mathrm{Im}\big[A_{ij}^R(t,t-s)\big]$ without any electric field excitation. In addition, we explain how the time-dependent exchange interaction is computed from the data obtained with EDMFT.

Figure 5.3 shows the imaginary part of the quantity $A_{ij}^R(t_m,t_m-s)$, see Eq. (2.103), at T=0.1, U=12, 18 and 24 for V from 0 to 2 shown with color from light to dark. Transient oscillations at small time comprises the main contribution to the exchange interaction. The number of these oscillations increases for increasing U while the value of the exchange interaction decreases for increasing U, see Figure (5.1). Additional smaller oscillations are observed for longer times ($t\gtrsim$4) and their amplitude decreases with increasing U. At small time, the most pronounced difference between $\mathrm{Im}\big[A_{ij}^R(t_m,t_m-s)\big]$ for different V is the amplitude of the oscillations. At any U studied, the larger V, the smaller the amplitude of the oscillations. However, this effect seems to be reversed for times $\gtrsim$4 where the oscillations appear slightly larger for larger V. An additional effect of the non-local interaction on $\mathrm{Im}\big[A_{ij}^R(t_m,t_m-s)\big]$ is the phase-shift of the oscillations which can easly be observed for times $\gtrsim$ 4. The phase-shift effect seem to be more pronounced

for smaller U, which is consistent with what is observed in Figure 5.2 where the effect of V on the Matsubara exchange interaction is larger for smaller U.

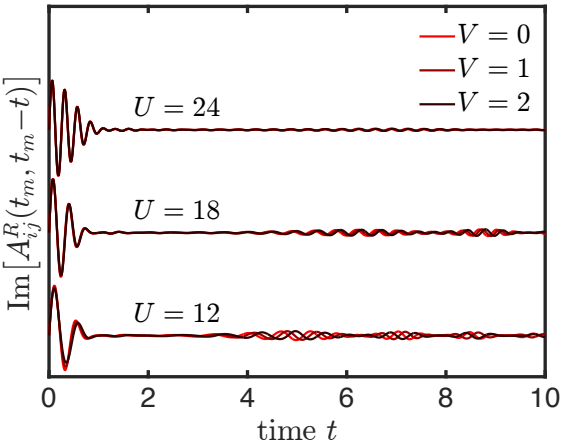

Figure 5.3: The quantity $\mathrm{Im}\left[A^R_{ij}(t_m, t_m - t)\right]$ as a function of time t. The calulations are done at zero field, U=12, 18 and 24, T=0.1, colors from light to dark correspond to values of V=0, 1, 2. Time t_m=10 is the maximum time up to which the dynamics is computed.

Since the effects of non-local correlations V are larger at smaller U, we consider U=12 for the rest of the calculations in this chapter. The exchange interaction at t_m=10 is obtained by integrating $\mathrm{Im}\left[A^R_{ij}(t_m, t_m - s)\right]$ over time s and dividing out by $4m(t_m)^2$, see Eq. (2.103). This leads to a value of $J_{ij}(t_m)$ that closely resembles the Matsubara exchange interaction with a $\sim$1% error. In principle, $J_{ij}(t)$ can be evaluated for any time t. However, in practice we attribute a finite initial t_i for which we do the numerical time-integration of $J_{ij}(t)$:

$$J_{ij}(t) = \int_0^t ds\ \mathrm{Im}\left[A^R_{ij}(t_m, t_m - s)\right]. \tag{5.8}$$

The initial time $t = t_i \simeq 1.5$ was chosen so that $J_{ij}(t)$ captures the initial transient oscillations of $\mathrm{Im}\left[A^R_{ij}(t_m, t_m - s)\right]$, see Figure 5.3.

Summarizing, we have studied the behavior of $\mathrm{Im}\left[A^R_{ij}(t_m, t_m - t)\right]$ where the effects of the non-local correlations are already observed. In addition, we discussed the computation of the time-dependent exchange $J_{ij}(t)$ from an initial time different to that of the begining of the dynamics.

5.3.2 *Non-equilibrium screening effects*

In this subsection, we study non-equilibrium dynamics and the effects of the non-local correlations on the screening of the exchange interactions.

We chose a single cycle electric field pulse with a Gaussian envelope as used in [35]. The field is of the form

$$E(t) = E_0 \sin\big(\omega(t - t_*)\big) e^{-4.6(t-t_*)^2/t_*^2}, \tag{5.9}$$

where E_0 is the amplitude of the field, ω is the frequency and $t_*{=}2\pi/\omega$ is the width of the pulse. The electric field $E(t){=}{-}\partial_t A(t)$ enters $t_{ij}(t)$ via the Peierls substitution, see Eq. (2.84) [35].

Figure 5.4 shows *(i)* the magnetization $m{=}(n_\uparrow{-}n_\downarrow)/2$ in red in the top panels, *(ii)* the double occupancy $n_\uparrow n_\downarrow$ in blue in the middle panels. This quantity measures the number of sites which possess two electrons. *(iii)* The exchange interaction $J^0_{ij}{=}J_{ij}(t)/z^2$ is displayed in green in the bottom panel. These three quantitties are plotted as a function of time. The electric field is represented in black dots in Figure 5.4a top and middle panel to indicate the begining of the dynamics.

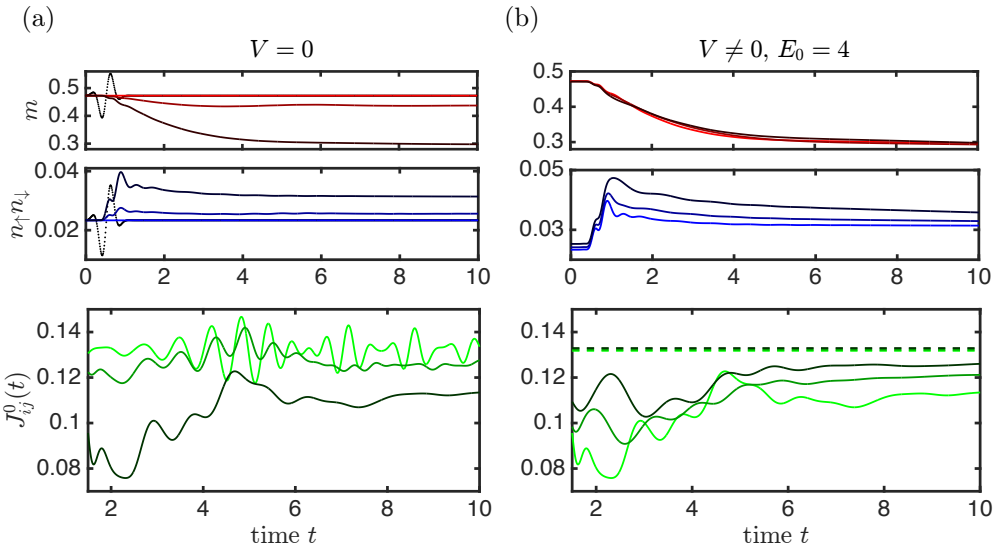

Figure 5.4: From top to bottom panel, the magnetization, the double occupancy $n_\uparrow n_\downarrow$ as a function of time and the exchange $J^0_{ij}(t)$ for $U{=}12$ and $T{=}0.1$, (a) at $V{=}0$ with light to dark color indicating electric field amplitude $E_0{=}0$, 2 and 4, (b) for $E_0{=}4$, light to dark color indicates V from 0 to 2. The electric field is resonant with the Mott-Hubbard gap: $\omega{=}12{=}U$. The electric field is displayed in black dots in the top and middle panel of (a) as an indicator for the start of the dynamics. Values of the Matsubara exchange interaction is indicated with dashed lines in the bottom panel of (b).

Figure 5.4a shows non-equilibrium dynamics of m, $n_\uparrow n_\downarrow$ and $J^0_{ij}(t)$ at U=12, T=0.1 and V=0. Electric field amplitude E_0=0, 2 and 4 correspond to colors from light to dark. The electric field pulse gives rise to a decrease of the magnetic moment m which is stronger for larger E_0. Unlike the magnetization, the double occupancy increases for increasing E_0. This comes from the fact that the electric field excites electrons creating doublons and holons and therefore, increases the double occupancy. At large time, the system reaches a quasi-thermal state where the double occupancy is quasi-constant. Note that the exchange interaction $J_{ij}(t)$ changes by up to 10% at zero field due to the long-time oscillations of $\mathrm{Im}\big[A^R_{ij}(t,t-s)\big]$, see Figure (5.3). At larger E_0 and short time, the effects of the electric field are more pronounced since the value of exchange decreases with increasing E_0. At larger time, $J^0_{ij}(t)$ relaxes to a quasi-thermal state where the oscillations observed for E_0=0 and 1 are not present at larger E_0.

Figure 5.4b shows the dynamics of m, $n_\uparrow n_\downarrow$ and $J^0_{ij}(t)$ at U=12, T=0.1 and E_0=4. Light to dark color represent V=0, 1 and 2. Different values of V do not seem to have an effect in the reduction of the magnetization m. Indeed, m does not only reaches similar values at large time for different V but also, the speed of the demagnetization is similar for all the V considered. However, the non-local correlations V seem to have a larger effect on the double occupancy. At $t\simeq 0$, the values of the double occupancy increases with increasing V. At $t\simeq 1.5$, the excitation of $n_\uparrow n_\downarrow$ is larger for larger V as observed previously for the paramagnetic phase in [35]. In addition, the $1/U$ oscillations which appear at time $\sim$1.5 for V=0 [20] disappear when $V\neq 0$. For each V and at t_i, the exchange interaction $J^0_{ij}(t)$ decrease by about 30% as compared to its equilibrium value displayed in dashed lines. However, as for the magnetization, we do not see large differences in the thermalization speed of $J^0_{ij}(t)$ when $V\neq 0$. Nevertheless, we observe that at large time ($t\gtrsim 6$), the difference between values of exchange for different V in the quasi-thermal state is larger than in equilibrium (dashed lines). Indeed, for ΔV=2, $\Delta J^0_{ij}\simeq 0.9\%$ in equilibrium while $\Delta J^0_{ij}(t$=10) goes up to 11%. Therefore, the dynamical screening effects are stronger out of equilibrium than what we observe in equilibrium.

As a conclusion, we studied the exchange interactions out of equilibrium. Despite the presence of additional relaxation channels by the non-local interactions, the effect of screening on the relaxation speed of exchange is only a small correction. Even without correct static contribution, the dynamical effects of V in nonequilibrium are larger than in equilibrium. Our calculations show that transient changes $\Delta J_{ij}(t)/J^0_{ij}\sim 11\%$ are feasible for eaE_0=$4t_0$ and $t_m\sim 10/t_0$. Taking $t_0\sim$0.1 eV, $a\sim$2 Å and a laser pulse duration dt=10 fs we find that this might be accessible for a laser fluence $\sim$5 mJ/cm^2. Since the EDMFT allows the study of the time-dependent effective Coulomb interactions $U_{\mathrm{eff}}(t)$ [35], an interesting next step to our work would be to study the correlations between $U_{\mathrm{eff}}(t)$ and the exchange interactions $J_{ij}(t)$.

6

STRAIN-CONTROL OF ANTISYMMETRIC EXCHANGE INTERACTION

6.1 INTRODUCTION

A magnetic Skyrmion is a particle-like object defined by a topological spin texture with a structure that is similar to a vortex. With sizes down to few nanometers and high controllability by external fields, Skyrmions are attractive candidates for future processing and storage technology [106–108].

Nowadays, an interesting challenge is to find ways to switch magnetic Skyrmions on ultrashort time-scales and with a low energy dissipation. The first evidence of the nucleation and annihilation of magnetic Skyrmions in a thin film was found by Romming *et al.* [109]. Later, the switching of magnetic Skyrmions attracted a lot of attention using not only electric currents [110–112], but also spin-polarized currents [113], magnetic fields [114] as well as ultrafast laser pulses [115–117]. Recently, strain-mediated voltage-control of Skyrmion switching [118] was theoretically predicted, leading to an unprecendented low energy dissipation of a few femtojoules per Skyrmion. However, the energy efficiency of Skyrmion switching hardly combines with ultrashort time-scales.

In principle, the ultimate speed limit of switching may be achieved with a direct control of the magnetic exchange interactions responsible for the stabilization of Skyrmions. In most of the cases, this stability is due to the Dzyaloshinskii-Moriya interaction (DMI), which is an antisymmetric exchange interaction. The DMI between the spin of two atoms requires a third atom which possess spin-orbit coupling. In addition, the system has to break inverstion symmetry in order to give rise to DMI. Recently, the ultrafast optical control of the ratio of DMI and symmetric Heisenberg exchange interactions was demonstrated in oxides systems [13]. However, a direct extension of these results to metallic ferromagnets (FM) is difficult since in the latter, laser heating dominates the physics. Alternatively, magnetic interactions can be controlled by strain-waves, avoiding the direct heating of the magnetic material. So far, it was shown that strain can be used to modify the magnetic anisotropy [119–121], which can even lead to magnetization switching [122]. However, the effect of strain on the DMI has not so far been studied. Here we theoretically explore modifications of DMI induced by strain-waves.

This chapter is organized as follows. First, we introduce a minimal model for the calculation of DMI in transition metal thin films. Second, we evaluate DMI as a function of electronic hybridization and lattice displacement. Third, we extract time-dependent changes of DMI by solving the strain-wave propagation in a multilayer structure. Finally, we discuss the relation of our results to recent atomistic

spin dynamics simulations [123], suggesting that nucleation and annihilation of Skyrmions by strain-induced changes of DMI might be feasible.

6.2 MODIFICATIONS OF DZYALOSHINSKII-MORIYA INTERACTION

A minimal model for DMI in transition metals was derived in [124] and consists of a three-atom trimer system. This model was found to compare qualitatively well with ab initio calculations, capturing both the effects of spin orbit coupling and electronic structure. Here, we use the trimer system to study the changes of DMI due to the displacement d. First, we introduce the model. Second, we calculate the Heisenberg exchange interaction as well as the DMI by mapping the electronic model onto a classical Heisenberg spin model. Third, we study the modifications of DMI with d.

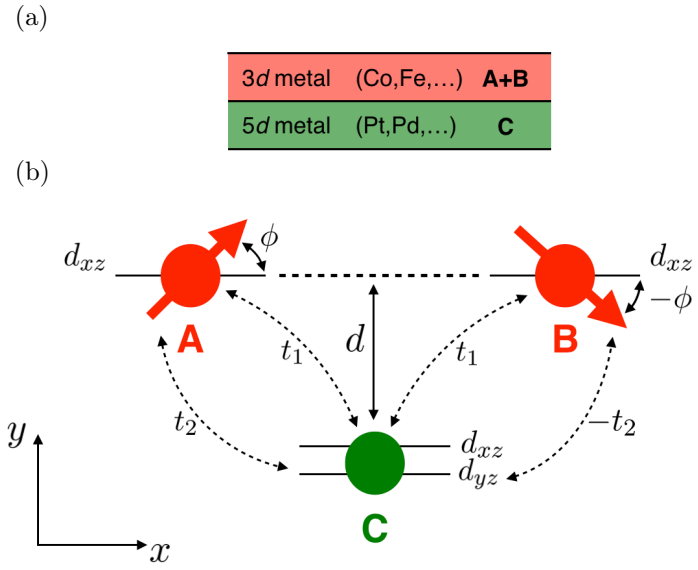

Figure 6.1: (a) Illustration of a magnetic thin film with a $3d$-metal magnetic layer (red) and a $5d$ metallic layer (green). The trimer model consists of two magnetic atoms A and B from the red layer and one non-magnetic atom C from the green layer. (b) Illustration of the trimer system where the orientation of the magnetic moments of atoms A and B are determined by the angle ϕ with respect to the x axis. These magnetic atoms are modeled by a single orbital d_{xz}, while two orbitals d_{xz} and d_{yz} are taken into account for atom C. Hopping between A, C and B, C is indicated with dashed arrows, with hopping amplitudes $t_{1,2}$ and d is the distance between atom C and the atoms in the magnetic layer.

6.2.1 *The model*

In this section, we introduce the electronic Hamiltonian of the trimer system which is illustrated in Figure 6.1 and was originally introduced in [124]. The generic expression for this Hamiltonian reads:

$$\hat{H}_{\text{elec}} = \hat{H}_0 + \hat{H}_{\text{hop}} + \hat{H}_{\text{soc}} + \hat{H}_{\text{mag}}. \tag{6.1}$$

The first term of Eq. (6.1) describes the on-site energies

$$\hat{H}_0 = \sum_{i=A,B,C} \sum_{\alpha,\sigma} E_i \hat{n}_{i\alpha\sigma}, \tag{6.2}$$

where $\hat{n}_{i\alpha\sigma}{=}\hat{c}^{\dagger}_{i\alpha\sigma}\hat{c}_{i\alpha\sigma}$. The index α stands for the orbital d_{xz}, d_{yz}, σ corresponds to the spin index: $\uparrow$, $\downarrow$ and A, B and C are the atoms of the system. The hybridization between the atoms is determined by the energy differences between E_A, E_B and E_C. We use $E_A{=}E_B$ such that the only parameter which determines the hybridization is $|E_A{-}E_C|$. The smaller $|E_A{-}E_C|$, the larger the hybridization.

It is well established that one of the key ingredient for DMI is inversion symmetry breaking. Here, the inversion symmetry breaking is induced by electron hoppings from the orbital d_{xz} of the magnetic atoms to orbitals d_{xz} and d_{yz} of atom C. These hoppings are described by the following Hamiltonian:

$$\hat{H}_{\text{hop}} = t_1\hat{h}_1 + t_2\hat{h}_2, \tag{6.3}$$

where $\hat{h}_1$ describes hopping between the same type of orbitals while $\hat{h}_2$ describes hopping between d_{xz} and d_{yz} orbitals:

$$\hat{h}_1{=}\sum_{\sigma}\left[\hat{c}^{\dagger}_{A,d_{xz},\sigma}\hat{c}_{C,d_{xz},\sigma} + \hat{c}^{\dagger}_{C,d_{xz},\sigma}\hat{c}_{A,d_{xz},\sigma} + \hat{c}^{\dagger}_{B,d_{xz},\sigma}\hat{c}_{C,d_{xz},\sigma} + \hat{c}^{\dagger}_{C,d_{xz},\sigma}\hat{c}_{B,d_{xz},\sigma}\right], \tag{6.4}$$

$$\hat{h}_2{=}\sum_{\sigma}\left[\hat{c}^{\dagger}_{A,d_{xz},\sigma}\hat{c}_{C,d_{yz},\sigma} + \hat{c}^{\dagger}_{C,d_{yz},\sigma}\hat{c}_{A,d_{xz},\sigma} - \hat{c}^{\dagger}_{B,d_{xz},\sigma}\hat{c}_{C,d_{yz},\sigma} - \hat{c}^{\dagger}_{C,d_{yz},\sigma}\hat{c}_{B,d_{xz},\sigma}\right]. \tag{6.5}$$

Values for hopping amplitudes t_1 and t_2 are Slater-Koster matrix elements between orbitals of the atoms in the system:

$$t_1 = V_{dd\pi}R_x^2 + V_{dd\delta}R_y^2 \tag{6.6}$$

$$t_2 = (V_{dd\pi} - V_{dd\delta})R_xR_y, \tag{6.7}$$

where R_x and R_y are the direction cosines:

$$R_x = \frac{x_{AB}}{2|\vec{r}_{AC}|},\ R_y = -\frac{d}{|\vec{r}_{AC}|}, \tag{6.8}$$

where x_{AB} is the distance between atom A and atom B, $\vec{r}_{AC}$ is the vector from atom A to atom C, d is the distance which separates the $3d$ atoms from atom C and $|\vec{r}_{AC}|=\sqrt{(x_{AB}/2)^2+d^2}$. Note that the minus sign obtained for the hopping $\hat{h}_2$ in Eq. (6.5) comes from the direction cosine R_y which becomes $-R_y$ in the direction C to B. This leads to inversion symmetry braking in the system.

We choose parameters relevant for 3d-5d metallic thin films. Specifically, taking FePt as a representative example we have d=2.44 Å and x_{AB}=2.77 Å for iron on top of Pt(111) [124]. The Slater-Koster coefficients are $V_{dd\pi}$=0.8 eV and $V_{dd\delta}$=−0.07 eV [124] .

Another essential ingredient for DMI is spin-orbit coupling (SOC) where a generic Hamiltonian for SOC reads

$$\hat{H}_{\rm soc} = \frac{\xi}{2}\vec{L}_C \cdot \hat{\vec{\sigma}}, \tag{6.9}$$

where ξ is the SOC constant, $\vec{L}$ is the orbital moment of atom C and $\hat{\vec{\sigma}}=(\hat{\sigma}_x, \hat{\sigma}_y, \hat{\sigma}_z)$ is the Pauli vector.

To give rise to non-zero DMI, spin-flip transition matrix elements in SOC are needed *e.g.* $\langle C, d_{xz}, \uparrow \mid \vec{L}_C \cdot \hat{\vec{\sigma}} \mid C, d_{yz}, \downarrow \rangle \neq 0$ [124]. However, the SOC Hamiltonian Eq. (6.9) is diagonal in spin for the d_{xz} and d_{yz} orbitals. In order to obtain a minimal model with just these two orbitals which exhibit DMI, the spin quantization axis is rotated. Following [124] we transform $\hat{\vec{\sigma}} \rightarrow \hat{\vec{\sigma}}'$, where $\hat{\vec{\sigma}}'$ has the x-axis as spin quantization axis. In this basis, $\langle C, d_{xz}, \uparrow \mid \vec{L}_C \cdot \hat{\vec{\sigma}}' \mid C, d_{yz}, \downarrow \rangle$ is a nonzero matrix element for the spin-orbit coupling.

To describe the magnetic moments of atom A and B, electrons correlations are included using a Stoner model:

$$\hat{H}_{\rm mag} = -\frac{I}{2}(\vec{m}_A \cdot \hat{\vec{\sigma}}' + \vec{m}_B \cdot \hat{\vec{\sigma}}'), \tag{6.10}$$

where I is the Stoner parameter. The orientation and magnitude of the classical magnetic moments at sites i=A, B: $\vec{m}_i$=m_i(cosϕ $\vec{e}_x$±sinϕ $\vec{e}_y$), where ϕ is the angle of the spins with respect to the x axis. We take I=0.96 eV and m_A=m_B=1.2 [124]. We note that, despite the presence of SO coupling, the system does not exhibit a preferential axis *i.e.* no magnetic anisotropy. Therefore, the only important parameter is the angle ϕ which is responsible for the relative canting of the magnetic moments.

We write the electronic Hamiltonian $\hat{H}_{\rm elec}$ using the basis states $\{|A, d_{xz}, \uparrow \rangle, |B, d_{xz}, \uparrow \rangle, |C, d_{xz}, \uparrow \rangle, |C, d_{yz}, \uparrow \rangle, |A, d_{xz}, \downarrow \rangle, |B, d_{xz}, \downarrow \rangle, |C, d_{xz}, \downarrow \rangle, |C, d_{yz}, \downarrow \rangle\}$. This yields

$$\hat{H}'_{\text{elec}} =$$

$$\begin{pmatrix}
E_A - \frac{Im}{2}\cos\phi & 0 & t_1 & t_2 & i\frac{Im}{2}\sin\phi & 0 & 0 & 0 \\
0 & E_B - \frac{Im}{2}\cos\phi & t_1 & -t_2 & 0 & -i\frac{Im}{2}\sin\phi & 0 & 0 \\
t_1 & t_1 & E_C & 0 & 0 & 0 & 0 & i\xi/2 \\
t_2 & -t_2 & 0 & E_C & 0 & 0 & -i\xi/2 & 0 \\
-i\frac{Im}{2}\sin\phi & 0 & 0 & 0 & E_A + \frac{Im}{2}\cos\phi & 0 & t_1 & t_2 \\
0 & i\frac{Im}{2}\sin\phi & 0 & 0 & 0 & E_B + \frac{Im}{2}\cos\phi & t_1 & -t_2 \\
0 & 0 & 0 & i\xi/2 & t_1 & t_1 & E_C & 0 \\
0 & 0 & -i\xi/2 & 0 & t_2 & -t_2 & 0 & E_C
\end{pmatrix}. \tag{6.11}$$

The spectrum of the trimer system is obtained by diagonalizing the above Hamiltonian and is displayed in Figure 6.2b, where the red (green) line shows the contribution of A and B (C) atom.

6.2.2 *Exchange interactions*

In this section, we extract the DMI (D) as well as the Heisenberg exchange interaction (J) from the trimer system and we study their behavior as a function of the hybridization.

A well-developed approach to evaluate D and J is from electronic structure calculations, which rely on small-angle variations with respect to a collinear ground state [38, 125, 126]. Although generalizations to non-collinear configurations have been developed as well [39], the simplicity of the model allows us to *(i)* directly evaluate the total energy E_{tot} as a function of the canting angle, and *(ii)* extract D and J from small angle variations with respect to the numerically obtained non-collinear ground state by comparison to a static spin model:

$$H_{\text{spin}} = J\vec{S}_A \cdot \vec{S}_B + \vec{D} \cdot \vec{S}_A \times \vec{S}_B. \tag{6.12}$$

In order to obtain a good understanding of the DMI, we use classical unit vectors for the spins $\vec{S}_i = (\cos\phi_i, \sin\phi_i)$, where $\phi_i = +(-)\phi$ for A (B). The energy of the spins system reads

$$\hat{E}_{\text{spin}} = J\cos\phi - D\sin\phi, \tag{6.13}$$

Below we first explain how we evaluate E_{tot} self-consistently, subsequently we explain how the mapping is established by considering small-angle variations around around the noncollinear ground state at $\phi = \phi_0$ for which the total energy $E_{\text{tot}}(\phi)$ has a minimum.

(a)

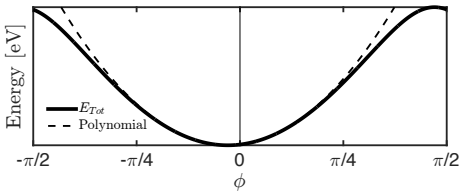

(b)

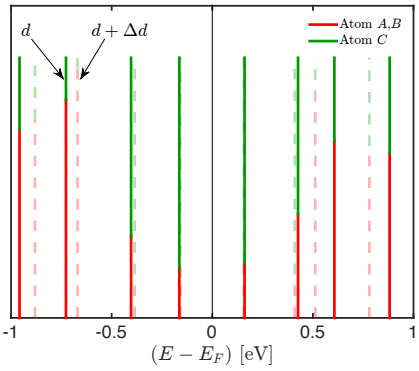

Figure 6.2: (a) The total energy E_{tot} as a function of the canting angle ϕ (solid line). The dashed line represents a fit of E_{tot} with a second order polynomial. (b) Illustration of the influence of a displacement Δd on the electronic spectrum. Full lines correspond to state energies at the equilibrium value of d while dashed semi-transparent lines correspond to eigen states for $d+\Delta d$, where a large Δd=100 pm is chosen for clarity. Note that the spectra are displayed for the ground state at ϕ_0, see subsection 6.2.2. Red (green) colors indicate the relative contribution of A, B (C) atoms to the states. Parameters of the system: E_A=0 eV, E_C=0.1 eV and ξ=0.6 eV.

To calculate the Fermi energy self-consistently, we use the Fermi-Dirac function to describe the distribution of electrons over the states in the system:

$$N = \sum_{\lambda=1}^{8} [e^{\beta(\epsilon_\lambda - E_F)} + 1]^{-1}, \tag{6.14}$$

where ϵ_λ are the eigenenergies of Eq. 6.1. The Fermi energy E_F is increased until the number of electrons N reaches the requested value where an occupation N=4 electrons of the system is assumed. Since ϵ_λ depend on ϕ, we obtain a Fermi energy that depends on the canting angle E_F=$E_F(\phi)$, ensuring charge conservation in the system. In order to obtain a Fermi function which can be well approximated by a step function, we take an energy smearing β=100 eV^{-1} *i.e.* a temperature $T\simeq$116 K. Following the Fermi energy calculation, we sum up the energies of the electrons in the system using the Fermi function:

$$E_{\rm tot} = \sum_{\lambda=1}^{8} \frac{\epsilon_\lambda}{e^{\beta(\epsilon_\lambda - E_F)} + 1} \tag{6.15}$$

The total energy $E_{\rm tot}$ is plotted with a black solid line in Figure 6.2a, it shows that the system is in a ferromagnetic state with a canting angle ϕ of about $\pi/40$. We fit the total energy of the system using the second order polynomial $E_{\rm tot}(\phi)$=c_0+$c_1\phi$+$c_2\phi^2$, indicated by the dashed line in Figure 6.2a, where the coefficients c_0,c_1 and c_2 are extracted from the fit. Using a small angle variation $\delta\phi$, the total energy variation is mapped onto the energy variation of the spin model

$$E_{\rm tot}(\phi_0+\delta\phi) = E_{\rm spin}(\phi_0+\delta\phi), \tag{6.16}$$

This leads to the equalities

$$-J\sin\phi_0 - D\cos\phi_0 = c_1 + 2c_2\phi_0, \tag{6.17}$$

$$-J\cos\phi_0 + D\sin\phi_0 = 2c_2, \tag{6.18}$$

from which an equation for J and D is obtained as a function of the coefficients c_1, c_2.

We show the behavior of D and J as a function of the hybridization $|E_C-E_A|$ in Figure 6.3. The results are plotted for three different values of the SOC ξ=0.4, 0.5 and 0.6 eV. Note that the canting angle of the magnetic moments increases with increasing $|E_C-E_A|$. We see that $|D|$ as well as $|J|$ can take a broad range of values from $\simeq$28 meV to $\simeq$0.1 meV. In addition, for each SOC strength studied and for most of the hybridization strength, $|D|>|J|$. This could originate from the strong sensitivity of J to hybridization. Indeed, in the regime studied the dependence of J on $|E_A-E_C|$ is so strong that even the sign of J changes while the system posess a Stoner spliting I. In the strong hybridization regime, the system is in a regime for which $|D|<|J|$. Such values of exchange are reminiscent to those found with more advanced ab initio calculations [110] and those deduced from experiments [127, 128]. Below we restrict ourselves to the regime for which $|D|\sim|J|/5$ that is indicated by the light grey region in Figure 6.3. Specifically, we choose $|E_C-E_A|$=0.1 eV for which we obtain $D\simeq-5$ meV and $J\simeq-26.5$ meV. Accordingly, the spins on site A and B are slightly canted away from ferromagnetic alignment by an angle of about 10°.

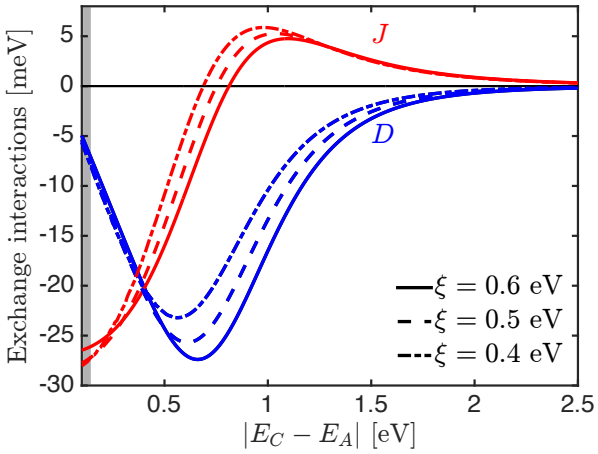

Figure 6.3: Heisenberg exchange interaction (red) and DMI (blue) as a function of the electronic hybridization $|E_C - E_A|$ for different SOC strength ξ=0.4, 0.5 and 0.6 eV, in dashed dots, dash-dotted, dashed and solid line, respectively. The shaded yellow region represents values of D and J that are accessible experimentaly. The system is filled with four electrons.

In order to have an understanding of the physics near the transition from $J<0$ to $J>0$, we consider the case where ξ=0. In this case, the system does not exhibit DMI, therefore, there is no intermediate canting angle between spins of atom A and B apart from ϕ=0 and ϕ=$\pi/2$. Nonetheless, a transition from $J<0$ to $J>0$ configuration can still be observed. The parallel ($J<0$) and antiparallel ($J>0$) configurations at ξ=0 are displayed in Figures 6.4a and c where the spin up and down contribution to the spectrum of atom A and B are shown in red and blue, respectively. We observe in Figure 6.4a that below the Fermi level, the spin majority is up. However, in Figure 6.4c, the spin up and down momentum have the same amplitude therefore, the net magnetization is nearly zero. This two cases can be understood from the Stoner model, Eq. (6.10). When $|E_C - E_A|$ is small, the system is in the Stoner limit which favors a net spin moment per site by inducing a splitting between minority and majority electrons. When the hybridization is such that $J>0$, the Stoner splitting is not strong enough to induce such a splitting, leading to a net magnetization per site which is nearly zero. Note that, in Figure 6.4b, states have the same energy leading to the observation of only four states in total *i.e.* each state which we observe in Figure 6.4c are two degenerate states with the same amplitude. In addition, unlike in Figure 6.2, in Figure 6.4, the spin momentum of atom C is not taken into account leading to states with different amplitudes.

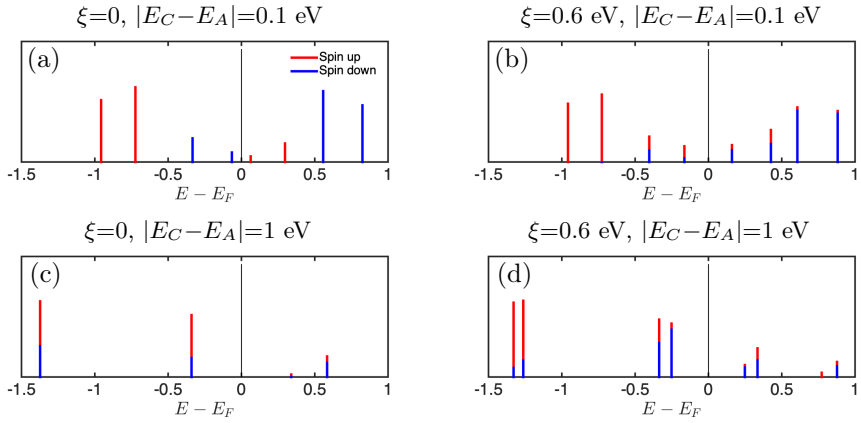

Figure 6.4: Spin up (red) and down (blue) contribution to the spectrum of atom A and B in the parallel configuration ($|E_C - E_A|$=0.1 eV) (a) for ξ=0, (b) for ξ=0.6 eV and in the antiparallel configuration ($|E_C - E_A|$=1 eV) (c) for ξ=0, (d) for ξ=0.6 eV.

Figures 6.4b and d show the spin momentum on the magnetic atoms when SOC is included in the model (ξ=0.6 eV). In this case, the SOC allows for spin up and down mixing, leading to spin mixed states in the parallel configuration, see Figure 6.4b. For the case of the antiparallel configuration, Figure 6.4d, we can see that, unlike for the case in which ξ=0, the states are not degenerated in energy. In addition, the net magnetization per site is not zero. However, the larger ξ, the larger the net magnetization in the antiparallel configuration. This can be partially explained by the fact that the hybridization for which J=0 increases for increasing ξ. Besides, in the presence of SOC, the competition betweeen the hybridization, the Stoner splitting and the SOC lead to non-trivial spin occupation on sites A and B both in the parallel and antiparallel configuration.

Summarizing, we obtained formulas for the exchange interactions by mapping the electronic model of the trimer system onto a spin model. In the regime of strong hybridization we recover values of D and J reminiscent to more advanced calculations and experiments, despite the simplicity of the model. In addition, we discussed the J<0 to J>0 transition for the case with and without spin-orbit coupling.

6.2.3 *Modification of the exchange interactions*

In this Section, we use the trimer system in order to study the modification of DMI as a function of the displacement d. Firstly, we illustrate the influence of the variation of d on the electronic spectrum. Secondly, we study the modifications of D and J up to ±5pm displacement.

Figure 6.2b illustrates the influence of a variation of d on the electronic spectrum. The equilibrium spectrum is plotted with full lines while the spectrum with an exagerated displacement Δd=100 pm is ploted with dashed semi-transparent lines. One can see that the differences in the spectrum after Δd are the energy distribution of the states as well as the contribution of each atom to the state. By increasing d, the hybridization between atoms A/B and atom C decreases. For instance, when a state has a minority of atom C contribution at d (see first two states at the low energy part of the spectrum), this contribution is further reduced at $d+\Delta d$. This comes from the fact that the hopping amplitudes, Eqs. (6.6) and (6.7), decrease with decreasing d.

Results for the modification of D, J and the ratio D/J as a function of the displacement d are shown in Figure 6.5. The exchange interactions modifications are computed for ξ=0.4, 0.5 and 0.6 eV. Figure 6.5 shows that for all SOC strength studied, D and J are reduced by increasing d. Similar as for the orbital resolved occupation, this can be explained by the reduction of hopping with the increase of d. However, D and J are not reduced in the same way: for a displacement of 5 pm, D changes up to 2.3% while the change of J goes up to 3.9%. Since $J>D$ in equilibrium, the modification of D/J ($\Delta(D/J)$) we observe in Figure 6.5c is mainly due to the large modification of J. The strongest $\Delta(D/J)$ is observed for ξ=0.6 eV: $\Delta(D/J)=3.1\times10^{-3}$. In absolute units, we obtain $\Delta D\propto10^{-4}$ eV which is in the range of what has been previously found with hydrogen pressure in a Fe double layer on Ir(111) [129]. Note that, while the trimer system captures the main features of DMI which have been found in *ab initio* results [124], we do not claim that the results for Heisenberg exchange can be quantitatively compared to results found with *ab initio* calculations.

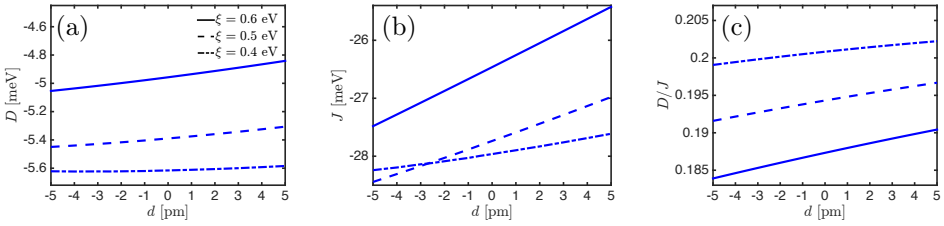

Figure 6.5: (a) D in meV, (b) J in meV and (c) D/J as a function of the displacement d in pm for three different SOC strength ξ=0.4, 0.5 and 0.6eV.

Summarizing, we investigated the influence of displacement on the exchange interactions. We find that D as well as J can be modified in the order of a few percent for Δd=5pm.

6.3 STRAIN-INDUCED MODIFICATION OF DZYALOSHINSKII-MORIYA INTERACTION

In the previous section we studied the changes of DMI due to displacement. In this section, we investigate how such displacements can be generated by the laser-induced excitation of a quasi-unipolar strain-wave.

The study of (quasi-)unipolar strain gives rise to a non-zero net effect on the displacement and therefore, would allow a non-zero net effect on the DMI. While the effects of a unipolar strain-wave has been studied in terfenol-D [122], it has never been investigated in magnets with sizable DMI. Here, we study the net effect of a quasi-unipolar strain-wave on the modifications of DMI at the interface of an Fe/Pt thin film.

First, we introduce the multilayer device used for the strain-wave generation. Second, we simulate the generation and the propagation strain through the device using an existing wave-propagation code [130]. Third, we extract the time-dependent displacements in order to evaluate the changes of DMI induced at the Fe/Pt interface.

6.3.1 *Multilayer structure for strain-wave generation*

We use a multilayer structure similar to what has previously been used to generate and propagate strain-waves [122, 130–132], see Figure 6.6. The ultrashort laser pulse penetrates a 100 nm sapphire layer which is used as an opto-accoustic transducer. The heat of the laser is deposited in a 35 nm cobalt layer where a strain-wave is created via a thermo-elastic mechanism. The strain-wave has a quasi-unipolar shape which follows the temperature profile in the cobalt layer. The 100 nm gold layer serves as an intermediate medium for propagation of the strain towards the magnetic thin film made of 3 nm iron on top of a 7 nm platinum layer.

We use the model described in [130] for the generation of the strain-wave:

$$\eta(t_0, z) = \alpha \Delta T(z), \tag{6.19}$$

where $\Delta T(z)$ is the temperature profile created in the cobalt layer by the laser pulse at t_0=0, $\eta(t_0, z)$ is the strain and α is the coefficient of linear thermal expansion. The temperature profile reads

$$\Delta T(z) = \frac{(1-R)q}{C_{\text{heat}}\delta} e^{-z/\delta}, \tag{6.20}$$

where R is the reflectance/reflection coefficient of cobalt, q is the laser fluence (mJ/cm^2), C_{heat} is the heat capacity of cobalt and δ=15 nm is the optical skin depth [132]. It was shown that dispersion effects in a 120 nm gold layer reduces by about 30% the amplitude of the strain [132].

However, for simplicity, we do not consider dispersion in the current model and use a simple Matlab algorithm given in [122] in order to propagate the strain-wave

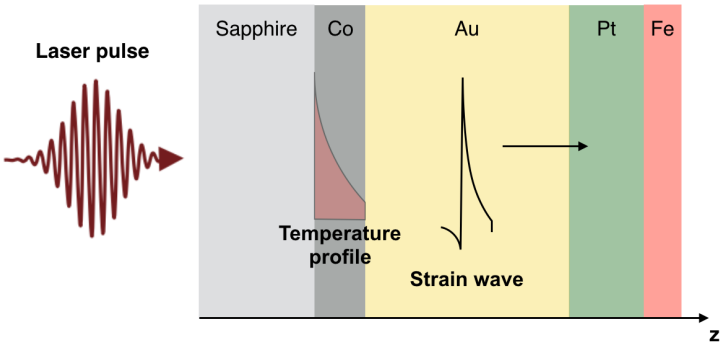

Figure 6.6: Opto-accoustic device used for the propagation of strain. It consists in five layers Sapp/Co/Au/Pt/Fe with thickness 100 nm/35 nm/100 nm/7 nm/3 nm respectively. The ultrashort laser pulse displayed on the left hand side deposits heat which is absorbed by the cobalt layer, generating the temperature profile Eq. (6.20). This launches a nearly unipolar strain-wave which propagates in the gold layer towards the magnetic thin film. Displacement induced at the Pt/Fe interface will cause a modification of the DMI.

through the multilayer structure. The algorithm is based on the finite-difference method which is an approximation for solving the wave equation

$$\frac{\partial^2 \eta}{\partial t^2} = c^2 \frac{\partial^2 \eta}{\partial z^2}, \tag{6.21}$$

where c is the speed of sound of the material. This algorithm can be used for strain propagation in nanostructures for which good agreements with experiments were found [130, 132]. The finite-difference algorithm separates the strain propagating forward $\eta_+(t,z)$ and the strain propagating backward $\eta_-(t,z)$. The total strain $\eta(t,z)$=$\eta_+(t,z)$+$\eta_-(t,z)$ is obtained using the following transmission and reflexion coefficient [130]

$$T_{12} = \frac{c_1}{c_2}\frac{2Z_1}{Z_1+Z_2}, \qquad T_{21} = \frac{c_2}{c_1}\frac{2Z_2}{Z_1+Z_2}, \tag{6.22}$$

$$R_{12} = \frac{Z_2-Z_1}{Z_1+Z_2}, \qquad R_{21} = \frac{Z_1-Z_2}{Z_1+Z_2}, \tag{6.23}$$

where Z_i is the accoustic impedance and c_i is the speed of sound of the material in the layer. Note that the ratios c_1/c_2 and c_2/c_1 are included in the transmission coefficients in order to satisfy the energy conservation law [130, 133]. This strain propagation is illustrated in Figure 6.7 as snapshots of the strain in the multilayers device at different times. The dynamics starts at t_0=0 ps where the initial unipolar strain in cobalt starts to propagate. At t=8 ps, part of the strain propagates in the gold layer with a small negative tail coming from the reflection at the

cobalt-sapphire interface while the other part of the strain propagates backward to the sapphire layer. At t∼30 ps, the strain enters the Fe/Pt thin film. After its propagation through the platinum layer, the strain enters the iron layer. At the Pt/Fe interface, about 30% of the wave is reflected back to the platinum layer. At t=37 ps, the strain propagates in the iron layer with an amplitude of about 4×10^{-4}. For simplicity, we do not account for the reflection at the right hand iron interface *i.e.* we assume total transmission of the strain-wave at the end of the multilayer structure.

Note that the finite-difference method ensures that the distance δz should be covered by the pulse in a time δt according to the speed of sound c in the material *i.e.*

$$\delta z = \delta t \times c. \tag{6.24}$$

This can be illustrated by comparing the width of the pulse in cobalt and in sapphire. Indeed, since the speed of sound is larger in sapphire than in cobalt, the strain pulse in the sapphire layer has a larger width than in the cobalt layer.

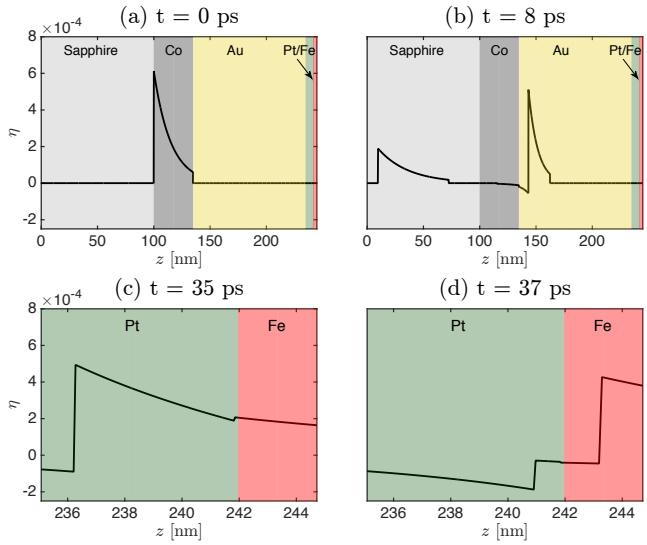

Figure 6.7: Strain profile in the multilayer structure: (a) in the cobalt layer at t_0 and (b) in the gold layer at t=8 ps. The strain profile in the Fe/Pt thin film: (c) in the platinum layer at t=35 ps and (d) in the iron layer at t=37 ps. The laser fluence is 1 mJ/cm^2 and the reflectance is R∼0.7 at the cobalt interface for an optical wavelength of 800 nm.

To summarize, we have introduced the multilayer structure in which a strain-wave is generated. In addition, we discussed the finite-difference method which is used to propagate the strain-wave through the structure.

6.3.2 *Strain-induced modification of exchange interactions*

In this subsection, we discuss the displacment induced by the strain-wave in the Fe/Pt thin film. Then, we discuss the DMI and Heisenberg exchange modifications resulting from the displacement at the Pt/Fe interface.

Using the relation between the strain and the displacement $d(t, z)$

$$\eta(t, z) = \frac{\partial d(t, z)}{\partial z}, \tag{6.25}$$

we first calculate the displacement induced by the strain in the cobalt layer at $t{=}t_0$. The profile of the displacement pulse is illustrated in Figure 6.8a and directly follows from the integral of the strain Eq. (6.25). Then, the displacement wave is propagated similarly as what is done for the strain-wave. This leads the displacement at the Pt/Fe interface shown in Figure 6.8a. From these calculations, it is found that that the displacement appears as a quasi-unipolar pulse which amplitude reaches up to 6 pm at the interface with a total duration of about 11 ps.

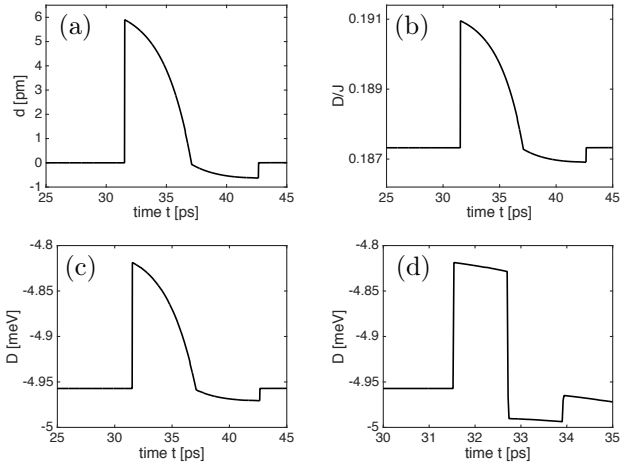

Figure 6.8: (a) Displacement d, (b) D/J and (c) D modifications at the Pt/Fe interface as a function of time. (d) D modifications accounting for the reflected wave at the iron/air interface. The SOC strenght is ξ=0.6 eV in (b)-(d).

To evaluate the corresponding changes of D and J, we also show $D[d(t, z)]$ as well as the ratio $D[d(t, z)]/J[d(t, z)]$ at the Pt/Fe interface. The results are displayed in Figures 6.8b and 6.8c. Following what is found for the displacement, Figure 6.8a, the exchange interaction quantities D and D/J have the shape of a quasi-unipolar pulse. Moreover, the modification of the exchange interactons is linear with the displacement which is expected from what we find in the previous calculations for ξ=0.6 eV, see Figure 6.9.

As last part of this section, we show that the unipolar shape of the DMI pulse can be further optimized by adding additional reflective layers. We illustrate this by adding an Fe/air interface. In this case, due to the large contrast of the acoustic impedance, almost complete reflection of the strain-wave is expected. As shown in Figure 6.8d, the interference of both waves causes a nearly perfectly rectangular pulse. The width and height of the pulse can be further optimized by controlling the Fe layer thickness and the laser fluence. Note that the rectangular pulse is followed by additional low amplitude pulses which can be seen at larger time. These additional pulses arise due to multiple reflections in the thin film and are not shown here.

To summarize, using a simplified model for strain generation, we demonstrated that a quasi-unipolar strain-wave can be generated in the Fe/Pt bilayer. This leads a nearly unipolar pulse of DMI changes with a duration of about 11 ps. In addition, accounting for large reflexion at the iron interface, the shape of the DMI pulse can be tuned to ressemble a rectangular pulse.

6.3.3 *Dispersion effects*

In the previous section, effects of dispersion in the propagation of the acoustic waves were argued to be negligible. Here we discuss this assumption in more detail.

It was found that phonon dispersion leads to a ∼30% reduction of the amplitude of a strain-wave propagating in a 120 nm gold layer [132]. Therefore, accounting for the phonon dispersion in gold would reduce the maximum displacement obtained at the Pt/Fe interface to 4 pm.

There are several ways to compensate for this reduction. First, since the displacement amplitude is linear in the regime explored, only a moderately increase of laser fluence (∼3 mJ/cm^2) is enough to counteract the 30% reduction of the displacement amplitude. Second, since the effect of dispersion increases with propagation length, a reduction of the gold layer thickness, down to at most the electron diffusion length of ∼40 nm [131], can remedy the effect of phonon dispersion. Another effect of phonon dispersion is high-frequency oscillations arising in the tail of the strain-wave which affect the quasi-unipolar characteristic of the strain [132]. However, this effect is strongly reduced with the calculation of the displacement, see Eq. (6.25). Hence, the high frequency oscillations should not affect the modification of exchange interactions.

Summarizing, including the effect of phonon dispersion is not expected to alter the main conclusions obtained before and can be mitigated with simple methods.

6.4 EFFECTS OF STRAIN-INDUCED CHANGES OF DMI ON NUCLEATION OF SKYRMIONS

Atomistic simulations revealed that by perturbing D (and the anisotropy K) across the boundary separating the Skyrmion stability region and the region where the

FM state is unstable, nucleation and annihilation of Skyrmions is possible. An example of such dynamics is shown in Figure 6.9. The details of the nucleation and annihilation will be discussed in [134], here we focus on the feasibility of such nucleation/annihilation for the strain-induced changes of D obtained in the preceding section.

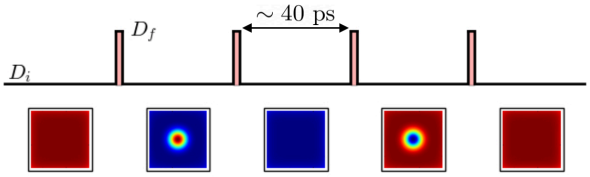

Figure 6.9: Toggle switching of a magnetic Skyrmion with DMI pulses as a function of time. Upper part of the figure represents 2 ps DMI pulse where D_i is the equilibrium and D_f is the maximum value of the DMI. Lower part of the figure is the spin texture observed on a magnetic sample 100×100, red and blue represent spins up and down, respectively. The magnetic Skyrmion is nucleated from a FM ground state and anihilated back to the FM state after each DMI pulse. Credit: Matteo Stifano

Using a system of 100×100 classical spins [123], M. Stifano obtained a Skyrmion stability diagram, see Figure 6.10. As a function of D and K, both in units of J, this diagram displays the unstable FM phase (yellow region) and the Skyrmion stability (Sk stability) phase.

The equilibrium quantity $D/J \simeq 0.187$ is obtained using the trimer system, with ξ=0.6 eV. For this equilibrium value, even changes $\Delta(D/J) \simeq 3\times10^{-3}$ obtained would allow the system to, starting from the Sk stability phase, go to the FM instability phase with a magnetic anisotropy of about $10^{-2}J$.

In addition, the nucleation/annihilation can proceed with rather small energy load. For example, according to our calculations, modification $\Delta D \propto 10^{-4}$ eV can be achieved with a laser fluence of about 3 mJ/cm^2. For a system of 100×100 spins and lattice spacing 2.77 Å, this yields an energy absorption per nucleation/annihilation event of 18 fJ. In addition, the strain-wave Skyrmion switching is predicted to occure within the timescale of picoseconds.

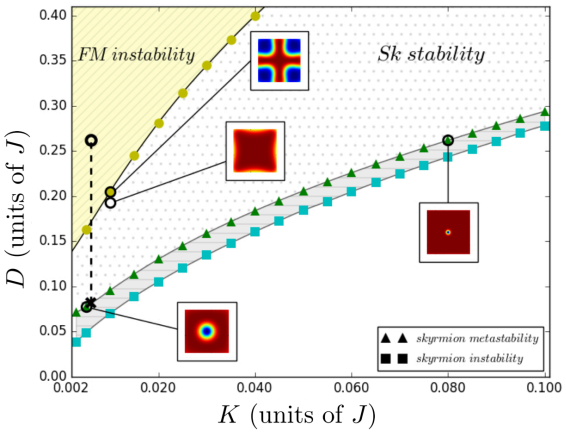

Figure 6.10: Skyrmion stability diagram computed using atomistic simulations [123]. DMI (in units of J) as a funtion of the magnetic anysotropy K (in units of J). Inserts show the static spin texture observed on a magentic sample of 100×100 atoms at specific points in the diagram. Black dashed lines represents the amplitude of the DMI pulse used for the toggle switching of Skyrmions illustrated in Figure 6.9. Credit: Matteo Stifano.

To conclude, we have discuss the feasibility of nucleation and annihilation of magnetic Skyrmions using the strain-induced modification of D obtained in the previous section.

7

SUMMARY AND OUTLOOK

Magnetism has been discovered and first used in ancient Greece, India as well as in China. It was applied for multiple purposes from the magnetic needle compass used in navigation to the magnetite used in erstwhile medical treatments. The scientific explaination of magnetism came much later with the work of Ampère, Gauss and Maxwell. Magnetism can be explained with quantum mechanics. Especially, the magnetic ordering in materials is determined by a force called the exchange interaction which is a result of the interaction between the charge of the electrons and the symmetry of the quantum mechanical wavefunction under exchanging the position of electrons. Nowadays, there is a huge interest among the scientific community in order to study this exchange interaction under non-equilibrium conditions aiming for the possibility of directly control this interaction, and thereby the magnetic order, on ultrafast time scales. In this thesis, we study the exchange interactions, especially their competition and the competition of electronic interactions in magnetic systems out of equilibrium.

In chapter 1, we introduce the concept of magnetism in materials. We discuss the spin of the electrons which is the smallest magnetic moment at the origin of the magnetism observed and used in our daily life. In addition, we introduce the exchange interaction which is the strongest force in magnetic materials and at the very origin of the magnetic ordering of spins. Then, we discuss the key role of magnetism in data storage technology and mention physical limitations in speed and energy consumption of current magnetic hard drives. This leads us to the field of ultrafast magnetism which recently attracted a lot of attention due to the possibility of controlling magnetism with laser pulses at the femtosecond time scale. Therefore, ultrafast magnetism is a prospective alternative to conventional magnetic dynamics. We discuss the high potential of a direct control of the exchange interaction as a candidate for controlling magnetism at the ultimate time scale with potential low energy dissipation. However, while theoretical and experimental advances in the direct control of the exchange have been made, little is known about the competition between multiple exchange interactions. In addition, the competition between electronic interactions in materials inducing screening effects on the exchange interaction is not yet explored. Out of equilibrium, these electronic interactions have their own dynamics and compete with each other leading to dynamical screening effects on the exchange which remain to be understood.

In chapter 2, we explain different methods which are used in the thesis in order to obtain the exchange interactions. We introduce the Hubbard model which we use in order to describe the different systems studied in this thesis. Then, we discuss the advantages and limitations of the exact diagonalization technique to solve

the model. In addition, we describe two techniques which give an approximate description of physical systems. First, the extended time-dependent canonical transformation which is a powerful technique that gives an analytical solution for time-dependent systems up to a specific order. The higher the order, the more precise the solution. However, this method is restricted to situations where there is a small ratio of different electronic interactions. Second, we sketch the key points of the extended dynamical mean-field theory which is a numerical method that, unlike the canonical transformation, may be used for any interaction regime. We end this chapter with a dicsussion on the exchange mechanism as well as two ways to evaluate the formula for the exchange interaction.

In chapter 3, we study a system of atoms with two electronic orbitals as minimal model for competing exchange interactions. This orbital degree of freedom gives rise to two type of exchange interactions; the Heisenberg exchange which sign determines whether the spins are arranged in a parallel or antiparallel way and the biquadratic exchange interaction which sign determines either a collinear or non-collinear spin allignment. With this system, we study the direct control of the exchange interactions by an external electric field using the extended time-dependent canonical transformation introduced in chapter 2. We find that both the Heisenberg as well as the biquadratic exchange can be controlled by the electric field parameters. In addition, despite the fact that in equilibrium, the biquadratic exchange is much weaker than the Heisenberg exchange interaction, we show that out of equilibrium, there is a field regime for which the exchange interactions have similar values and therefore strongly compete.

In chapter 4, we study the same system as in chapter 3. However, we go beyond the description of the exchange interactions and discovered a novel spin-charge coupling phenomenon. The spin-charge coupling is a purely non-equilibrium phenomenon and is specific to multi-orbital systems. Practically, it allows the non-resonant and reversible hybridization of a spin and a charge state which, in equilibrium, are separated by a large energy gap.

The scope of chapter 5 is the enhancement of screening effects on the exchange interaction out of equilibrium. In this chapter, we discuss the screening effects due to competition between electronic interactions. We study the screening using the extended dynamical mean-field theory introduced in chapter 2. In equilibrium, we find that screening effects lead to only small corrections to the exchange interaction. In addition, we find that these results do not correspond to what is predicted by the canonical transformation. Out of equilibrium, we see that the dynamical exchange reaches a quasi-thermal state for long time dynamics. In this quasi-equilibrium state, we observe that the screening effects are up to 10 times stronger to what is found in equilibrium. This shows that the physics of dynamical screening goes beyond what is expected from the equilibrium results.

In chapter 6, we study the Dzyaloshinskii-Moriya interaction (DMI). Unlike the Heisenberg exchange, the DMI is an antisymmetric interaction which favors the canting of spins. Here, we study the possibility of modifying the competing DMI

and Heisenberg exchange with an accoustic wave. This is aimed to support the feasibility of strain-induced magnetic Skyrmion creation and annihilation. Using a minimal model for magnetic thin films, we studied the modification of DMI as well as Heisenberg exchange interaction as a function of displacement at the thin film interface. To support the feasibility of such displacement, we propose to generate accoustic waves in a multi-layer device using an ultrashort laser pulse. The simulation of the strain-wave propagation showed that it is possible to generate a few pm displacement at the thin film interface with a moderate laser fluence. This displacement gives rise to a DMI modification which, according to atomistic simulations, might be sufficiently large to enable the creation and annihilation of a magnetic Skyrmion. Interestingly, this strain-induced Skyrmion switching is expected to take tens of ps with an energy disipation which goes down to the femtojoule range.

To conclude, we studied the influence of orbital degrees of freedom on the control of exchange interactions. We did not only obtain a better understanding of the competition between the exchanges interactions under an external driving field, but we also discovered a novel spin-charge coupling phenomenon generic to multi-orbital systems. In addition, we discovered non-trivial screening effects on the dynamical exchange interaction. Finally, we proposed to switch a magnetic Skyrmion by controlling the exchange interactions at the interface of a magnetic thin film using strain-waves. We anticipate that the work presented in this thesis will stimulate further studies on multi-orbital systems out of equilibrium. Indeed, non-equilibrium multi-orbital systems do not only exhibit competing exchange interactions but we believe that they give rise to a broad range of novel physics such as the spin-charge coupling discussed in this thesis. In addition, our work on the dynamical screening of exchange opens new ways for studying competing electronic interactions. Despite previous work on the subject, creation of magnetic Skyrmions using strain-waves is a rather new idea. The main interest of this technique is that it is predicted to lead to a very fast and energy-efficient Skyrmion switching. Therefore, we expect that the results presented in this thesis will stimulate the scientific community to look for similar techniques involving strain-waves and prospectively, reduce the time and energy scale of Skyrmion switching.

8

SAMENVATTING

Magnetisme is ontdekt en voor het eerst gebruikt in het oude Griekenland, India en China. Het werd voor meerdere doeleinden toegepast, van navigeren met een magnetisch naaldkompas tot vroegere medische behandelingen met magnetiet. De wetenschappelijke verklaring van magnetisme kwam veel later met het werk van Ampère, Gauss en Maxwell. De microscopisch oorsprong van magnetisme kan verklaard worden met kwantummechanica. In het bijzonder wordt de magnetische ordening in materialen bepaald door een kracht die de exchange interactie (letterlijk: uitwisselingsinteractie) wordt genoemd. Deze is het resultaat is van de wisselwerking tussen de lading van de elektronen gecombineerd met de symmetrie van de golffunctie onder het verwisselen van de positie van de elektronen. Tegenwoordig is er een enorme belangstelling in de wetenschappelijke gemeenschap om deze exchange interactie onder niet-evenwichtsomstandigheden te bestuderen, met het oog op de mogelijkheid om deze interactie, en daarmee de magnetische orde, direct te controleren op ultrakorte tijdschaal. In dit proefschrift bestuderen we de exchange interacties, in het bijzonder de competitie tussen verschillende soorten magnetische interacties in magnetische systemen buiten evenwicht.

In hoofdstuk 1 introduceren we de basis van magnetisme in materialen. We bespreken de spin van het elektron, het kleine magnetische moment dat aan de oorsprong ligt van het magnetisme dat we waarnemen en gebruiken in het dagelijks leven. Daarnaast introduceren we de exchange interactie, de sterkste kracht in een magnetisch materiaal die verantwoordelijk is voor magnetische ordening. Vervolgens bespreken we de sleutelrol van magnetisme in dataopslagtechnologie en bespreken we fysieke beperkingen in snelheid en energieverbruik van de huidige magnetische harde schijven. Dit brengt ons op het gebied van ultrasnel magnetisme dat recentelijk veel aandacht trok vanwege de mogelijkheid om magnetisme te controleren met laserpulsen op de femtoseconde tijdschaal. Daarom is ultrasnel magnetisme een aantrekkelijk alternatief voor conventionele magnetische dynamica. We bespreken de hoge potentie van een directe controle van de exchange interactie als een kandidaat voor het controleren van magnetisme op de aller kortste tijdschaal met minimaal energieverlies. Hoewel er theoretische en experimentele vorderingen zijn gemaakt bij de directe controle van de exchange interactie, is er weinig bekend over de competitie tussen verschillende soorten exchange interacties. Bovendien is de competitie tussen verschillende elektronische interacties in materialen, die lading-afschermingseffecten op de exchange interactie kunnen veroorzaken, nog niet onderzocht. Buiten het evenwicht hebben deze elektronische interacties hun eigen dynamica, die leidt tot een dynamische bijdrage van de ladingsafscherming aan de exchange interactie die tot dusver niet begrepen is.

In hoofdstuk 2 leggen we verschillende theoretische en computationele methoden uit die in het proefschrift worden gebruikt om de exchange interacties te berekenen. We introduceren het Hubbard-model dat we gebruiken om de verschillende systemen die in dit proefschrift worden bestudeerd te beschrijven. Vervolgens bespreken we de voordelen en beperkingen van exacte diagonalisatie om het model op te lossen. Daarnaast beschrijven we twee methodes die bij benadering een oplossing geven van de natuurkundige modellen. Ten eerste de uitgebreide tijdsafhankelijke canonieke transformatie, een krachtige techniek die een analytische oplossing biedt voor tijd-periodieke systemen als een storingsreeks in een kleine parameter. Hoe meer termen worden meegenomen, hoe nauwkeuriger de oplossing kan worden. Deze methode is echter beperkt tot situaties waarin de verhouding tussen verschillende elektronische interacties klein is. Ten tweede schetsen we de belangrijkste punten van de uitgebreide dynamische velden theorie, een numerieke methode die, in tegenstelling tot de canonieke transformatie, kan worden gebruikt voor elk interactieregime. We besluiten dit hoofdstuk met een discussie over het mechanisme achter de exchange interactie en twee manieren om de formule voor de exchange interactie numeriek te evalueren.

In hoofdstuk 3 bestuderen we een systeem van atomen met twee elektronische orbitalen als minimaal model voor wedijverende exchange interacties. Deze extra vrijheidsgraad in de orbitale beweging geeft aanleiding tot twee soorten exchange interacties: de Heisenberg-interactie wiens teken bepaalt of de spins parallel of antiparallel zijn gerangschikt in evenwicht en de bi-kwadratische wisselwerking wiens teken collineaire of niet-collineaire oriëntatie van spins bevoordeelt. Met dit systeem bestuderen we de directe controle van de exchange interacties door een extern elektrisch veld met behulp van de uitgebreide tijdsafhankelijke canonieke transformatie geïntroduceerd in hoofdstuk ref ch: Methods. We vinden dat zowel de Heisenberg als de bi-kwadratische interactie gecontroleerd kan worden door de parameters van het elektrische veld. Bovendien, ondanks het feit dat in evenwicht de bi-kwadratische uitwisseling veel zwakker is dan de Heisenberg-wisselinteractie, laten we zien dat er buiten het evenwicht een regime bestaat waarvoor deze interacties vergelijkbare waarden hebben en daarom sterk met elkaar in competitie zijn.

In hoofdstuk 4 wordt hetzelfde systeem als in hoofdstuk 3 bestudeerd. We gaan echter verder dan de beschrijving van spin-spin interacties alleen en voorspellen een nieuwe vorm van spin-ladingskoppeling. De koppeling is een puur niet-evenwichtsfenomeen en is generiek voor systemen met meerdere orbitalen. Praktisch gezien maakt het de niet-resonante en omkeerbare overdracht mogelijk tussen een spin en een ladingstoestand, welke in evenwicht worden gescheiden door een grote bandkloof.

Het onderwerp van hoofdstuk 5 is de bestudering van het effect van de landingsafscherming op de exchange interactie buiten evenwicht. In dit hoofdstuk bespreken we deze landingsafscherming als gevolg van competitie tussen twee verschillende elektronische interacties. We bestuderen de landingsafscherming met de uitgebreide

dynamische gemiddelde veldentheorie die in hoofdstuk 2 is geïntroduceerd. In evenwicht vinden we dat de invloed van ladingsafscherming slechts leidt tot kleine correcties op de exchange interactie. Bovendien vinden we dat deze resultaten niet overeenkomen met wat wordt verwacht op basis van analytische resultaten verkregen met de canonieke transformatie. Buiten evenwicht zien we dat de tijdsafhankelijke exchange interactie een quasi-evenwichtstoestand bereikt op een tijdschaal lang vergeleken met de laser puls. In deze quasi-evenwichtstoestand zien we dat de effecten van ladingsafscherming tot 10 keer sterker zijn dan in evenwicht.

In hoofdstuk 6 bestuderen we de Dzyaloshinskii-Moriya interactie (DMI). In tegenstelling tot de Heisenberg-interactie, is de DMI een antisymmetrische interactie die niet-collineaire oriëntatie van spins bevoordeelt. Hier bestuderen we de mogelijkheid om de competitie van de DMI en Heisenberg-interactie te veranderen met een akoestische golf. Dit is bedoeld om de haalbaarheid van creatie en annihilatie van Skyrmion-creatie en annihilatie door een akoestische drukgolf te ondersteunen. Met behulp van een minimaal model voor magnetische dunne films bestudeerden we de verandering van zowel DMI als Heisenberg exchange interacties als functie van de verplaatsing van de dunne-film grenslaag. Om de haalbaarheid van een dergelijke verplaatsing te ondersteunen, bestuderen we de excitatie van akoestische golven in een multilaag systeem met een ultrakorte laserpuls. Numerieke simulatie van de golfvoortplanting laat zien dat het met een gangbare lasersterkte mogelijk is om de grenslaag kortstondig met enkele picometers te verplaatsen. Deze verplaatsing geeft aanleiding tot een verandering van DMI die volgens atomistische simulaties voldoende groot zou kunnen zijn om de creatie en annihilatie van een magnetische Skyrmion mogelijk te maken. Gecombineerd voorspellen deze berekeningen en simulaties dat opto-akoestisch geïnduceerde Skyrmion-schakeling slechts tientallen picoseconde zal vergen, met een energiedissipatie in het femtojoule regime.

Samengevat hebben we de invloed van orbitale vrijheidsgraden op de controle van exchange interacties bestudeerd. We verkregen niet alleen een beter begrip van de competitie tussen de exchange interacties ten gevolge van een tijd-periodiek elektrisch veld, maar we ontdekten ook een nieuw type spin-ladingkoppeling dat generiek is voor systemen met meerdere orbitalen. Daarnaast ontdekten we niet-triviale landing-afschermingseffecten op de dynamische exchange interactie. Tenslotte hebben we voorspeld dat magnetische Skyrmions geschakeld kunnen worden door de exchange interacties aan de grenslaag van een magnetische dunne film te controleren met optisch geïnduceerde akoestische golven. We verwachten dat het werk dat in dit proefschrift wordt gepresenteerd, verdere studies aan systemen met meerdere orbitalen buiten evenwicht zal stimuleren. Deze systemen vertonen niet alleen competitie tussen verschillende exchange interacties, maar we verwachten eveneens dat dit aanleiding zal geven tot een breed scala aan nieuwe fysica, zoals de spin-ladingskoppeling die in dit proefschrift wordt besproken. Bovendien opent ons werk aan de dynamische ladingsafscherming nieuwe manieren om met elkaar wedijverende elektronische interacties te bestuderen. Het schakelen van magnetische Skyrmions met behulp van akoestische golven is een relatief nieuw idee, ondanks

eerder werk over dit onderwerp. Een belangrijk voordeel van deze techniek is dat het kan leiden tot een zeer energiezuinige en snelle Skyrmion-schakeling. Daarom verwachten we dat de resultaten die in dit proefschrift worden gepresenteerd, de wetenschappelijke gemeenschap zullen stimuleren om te zoeken naar vergelijkbare technieken met akoestische golven om de tijd- en energieschaal van Skyrmion schakeling in de toekomst te verkleinen.

9

RÉSUMÉ

Le magnétisme à été découvert et et utilisé pour la première fois dans la Grèce antique, en Inde et en Chine. Ce phénomène était utilisé de multiple manières, du compas magnétique en navigation à la magnétite utilisé dans les traitements médicaux. L'explication scientifique du magnétisme est apparu bien plus tard avec le travail d'Ampère, Gauss et Maxwell. Le magnétisme peut être expliqué grâce à la mécanique quantique. En effet, l'ordre magnétique au sein des matériaux est déterminé par une force appelée l'interaction d'échange qui est le résultat des interactions entre la charge et la position des électrons au sein du système. De nos jours, il y a un énorme intérêt de la part de la communauté scientifique quant à l'étude de cette interaction d'échange dans des conditions hors équilibre. Le but étant de pouvoir contrôler cette interaction, et donc de contrôler le magnétisme, à des échelles de temps de l'ordre du millionième de milliardième de seconde. Dans cette thèse, nous étudions différentes interactions d'échange, en particulier, leur compétition entre elles ainsi que la compétition entre les interactions électroniques dans des systèmes magnétiques hors d'équilibre.

Dans le chapitre 1, il est introduit le concept de magnétisme au sein des matériaux. On y présente le spin de l'électron qui est la plus petite quantité magnétique à l'origine du magnétisme observé et utilisé dans notre vie quotidienne. De plus, nous introduisons l'interaction d'échange qui est la force la plus intense dans les matériaux et à l'origine d'un ordre magnétique. Ensuite, nous discutons du rôle clé du magnétisme dans les technologies de stockage de données ainsi que les limitations physiques au regard de la vitesse et de la consommation d'énergie des disques durs. Cela nous mène au domaine de recherche du magnétisme ultra-rapide qui a récemment attiré beaucoup d'attention dû aux possibilités de contrôle du magnétisme avec des pulses laser d'une durée de quelques femtosecondes. En conséquent, le magnétisme ultra-rapide est une alternative prometteuse au contrôle conventionnel de la dynamique des moments magnétiques dans les matériaux. Nous mettons en lumière le potentiel d'un contrôle directe de l'interaction d'échange comme candidat au contrôle du magnétisme à la vitesse ultime avec, en toute probabilité, une faible dissipation énergétique. Cependant, bien que des avancements théoriques et expérimentaux quant au contrôle direct de l'interaction d'échange ont été fait, la compétition entre de multiples interaction d'échanges est encore peu connu. De plus, la compétition entre les interactions électroniques dans les matériaux induisant des effets d'écrantage de l'interaction d'échange n'a pas encore été exploré. Hors d'équilibre, ces interactions électroniques ont leur propre dynamique et sont en compétition. Ceci conduit à un effet d'écrantage dynamique de l'interaction d'échange qui reste à comprendre.

Dans le chapitre 2, il est expliqué les différentes méthodes qui sont utilisé dans cette thèse afin d'obtenir l'interaction d'échange. Nous introduiront le modèle de Hubbard que nous utilisons pour décrire les différents systèmes étudiés dans cette thèse. Ensuite, nous discutons des avantages et limitations de la technique de diagonalisation exacte pour obtenir une solution aux différents modèle. De plus, nous décrivons deux techniques qui donnent une solution approximée de systèmes physiques. Premièrement, la transformation canonique étendue dépendante du temps qui est une technique puissante donnant un résultat analytique, pour des systèmes dépendant du temps de manière périodique, à l'ordre désiré. Plus l'ordre est élevé, plus le résultat est précis. Cependant, cette méthode est restreinte aux situations où il y a possibilité d'un faible ratio entre différentes interactions électroniques. Deuxièmement, nous décrivons les points clé de la théorie du champ moyen dynamique étendu qui est une méthode numérique qui, par opposition à la transformation canonique, peut être utilisée pour tout régime d'interactions. Nous terminons ce chapitre avec une discussion sur le mécanisme d'échange ainsi que deux façons d'évaluer la formule d'interaction d'échange.

Dans le chapitre 3, nous étudions un système d'atomes avec deux orbitales électroniques comme modèle minimal qui donne lieu à une compétition entre les interactions d'échange. Ce degré de liberté orbital donne naissance à deux interactions d'échange: l'interaction de Heisenberg dont le signe détermine si les spins sont organisés de manière parallèle ou anti-parallèle, et l'interaction bi-quadratique dont le signe détermine si les spins sont colinéaires ou non-colinéaires entre eux. Avec ce système, nous étudions le contrôle direct des interactions d'échange avec un champ électrique externe en utilisant la transformation canonique étendue dépendante du temps introduite dans le chapitre 2. Nous trouvons que l'interaction de Heisenberg ainsi que l'interaction bi-quadratique peuvent toutes deux être contrôlées par les paramètres du champ électrique. De surcroît, malgré le fait que, en situation d'équilibre, l'interaction bi-quadratique est beaucoup plus faible que l'interaction de Heisenberg, nous montrons que, hors de l'équilibre, il existe un régime de champ électrique pour lequel les interactions d'échange ont des valeurs similaires et ainsi sont en compétition.

Dans le chapitre 4, nous étudions le même système que dans le chapitre 3. Cependant, nous allons au delà de la description des interactions d'échange et découvrons un nouveau phénomène de couplage entre le spin et un état de charge électronique. Ce couplage spin-charge est un phénomène purement hors d'équilibre et est spécifique aux systèmes avec de multiples orbitales. De manière plus pratique, ce couplage permet une hybridation non-résonante et réversible d'un état de spin et de charge qui, en situation d'équilibre, sont fortement séparés en énergie.

Le chapitre 5 met en lumière l'augmentation des effets d'écrantage sur l'interaction d'échange dans des conditions hors d'équilibre. Dans ce chapitre, nous discutons des effets d'écrantage dû à la compétition entre les interactions électroniques. Nous étudions l'écrantage grâce à la méthode du champ moyen dynamique étendu introduit dans le chapitre 2. Dans des conditions d'équilibre, nous observons que les effets

d'écrantage n'induisent que des petites modifications de l'interaction d'échange. De surcroit, nous découvrons que ces résultats ne correspondent pas à ce qui est prédit par la formule pour l'interaction d'échange obtenu avec une transformation canonique. Hors équilibre, nous observons que l'interaction d'échange dynamique atteint un état quasi-thermal au bout d'un long temps de dynamique. Dans cet état de quasi-équilibre, nous découvrons que les effets d'écrantage sont 10 fois supérieurs à ce qui est observé à l'équilibre. Cela montre que la physique de l'écrantage dynamique va au delà de ce que l'on attendait par rapport aux résultats obtenus à l'équilibre.

Dans le chapitre 6, nous étudions l'interaction de Dzyaloshinskii-Moriya (DM). Par opposition à l'interaction de Hesienberg, l'interaction DM est une interaction anti-symétrique dont l'intensité détermine l'inclinaison des spins. Ici, nous étudions la possibilité de modifier la compétition entre l'interaction DM et Heisenberg avec une onde acoustique. Ceci a pour but de soutenir la possibilité de créer et annihiler des Skyrmions magnétiques grâce à des déformations géométriques au sein du système. En utilisant un modèle minimal pour un film magnétique fin, nous étudions la modification de l'interaction DM ainsi que l'interaction de Heisenberg en fonction du déplacement à l'interface du film magnétique. Pour soutenir la possibilité de réaliser un tel déplacement, nous proposons de générer une onde acoustique dans un matériau multi-couche en utilisant un pulse laser ultra-rapide. La simulation de la propagation de l'onde de déformation montre qu'il est possible de générer un déplacement de quelques picomètres à l'interface du film fin avec une puissance laser modérée. Ce déplacement entraine une modification de l'interaction DM qui, en accord avec des simulations atomiques, peut être suffisamment large pour donner lieu à la création et à l'annihilation d'un Skyrmion magnétique. Étonnement, la transition d'un Skyrmion par déformation ne devrait pas prendre plus d'une dizaine de pisosecondes avec une dissipation d'énergie de l'ordre du femtojoule.

En conclusion, nous avons étudié dans cette thèse l'influence du degré de liberté orbital sur le contrôle des interactions d'échange. Nous n'avons pas seulement obtenu une meilleure compréhension de la compétition entre les interactions d'échange sous l'effet d'un champ électrique externe, mais nous avons aussi découvert un nouvel effet de couplage spin-charge spécifique aux systèmes multi-orbitalaires. De plus, nous avons découvert un effet d'écrantage non-trivial de l'interaction d'échange. Enfin, nous avons proposé de faire transiter un Skyrmion magnétique en contrôlant les interactions d'échange à l'interface d'un film fin magnétique en utilisant une onde de déformation. Nous pensons que le travail présenté dans cette thèse stimulera des études additionnelles sur les systèmes multi-orbitalaires hors d'équilibre. En effet, les systèmes multi-orbitalaires hors d'équilibre ne démontrent pas seulement des interactions d'échange en compétition mais nous pensons que ces systèmes peuvent donner naissance à une large gamme de nouvelle physique comme le couplage spin-charge discuté dans cette thèse. De surcroit, notre travail sur l'écrantage dynamique de l'interaction d'échange ouvre la voie à de nouvelle façon d'étudier les interactions électroniques en compétition dans les matériaux.

En dépit des travaux précédents sur le sujet, la création des Skyrmion magnétique via des ondes de déformation est une idée relativement nouvelle. L'intérêt principal de cette technique est qu'elle prédit la transition d'un Skyrmion en utilisant peu d'énergie. En conséquent, nous pensons que les résultats présentés dans cette thèse stimulerons la communauté scientifique à utiliser des techniques similaires incluant des ondes de déformation et possiblement, réduire le temps et l'énergie dépensés à faire transiter un Skyrmion.

10

ACKNOWLEDGMENTS

With the completion of my thesis, I realized one of my childhood dream to become a Physicist. However, this journey could not have had been possible without the help of my supervisors, my colleagues, my friends and familly. Therefore, I want to thank these people who helped me to make this dream possible.

First of all, I am and will be eternally greatful for the opportunity which my supervisors, Johan Mentink and Mikhail Katsnelson, gave me to work as a PhD student in their group. Then, I want to thank my supervisor Johan Mentink for the tremendous amount of time, work and effort he put in the supervision of my thesis. Despite his (very) busy schedule, Johan always found time for me to answer my questions and guide me on the path of understanding and solving physical problem. His enthousiasm and passion for physics always inspired me. In addition, he truly helped me to build myself as an independent scientist. Moreover, in difficult moments, he would always genuinely listen to me and try to find solutions. Last but not least, he taught me how to write and explain my research in the best way he could (which is quite an achievement because we started from scratches). Then, I would like to thank my thesis advisor Mikhail Katsnelson for inspiring discussions and for helping me to find specific litterature which is commonly hard to find online. Indeed, Misha can be way more efficient than Google Scholar. Appart from work, I always found myself stimulated by his anecdotes and stories about life and science during the Soviet time. As a matter of fact, I learned more about the USSR in a couple of months at TCM than in my entire school years. Note that Mikhail Titov also contributed to my current knowledges about the soviet time. Lastly, I want to thank Theo Rasing (as well as Johan) for giving me the opportunity to stay a little longer in the SSI group in order to complete this thesis.

Then, I would like to thank my coleagues who always have been interesting to be around. Especially, I would like to thank Koen whose moral support and interest in my mental health has been of great help. Then I would like to thank Robert for being Robert and for always awkwardly waving at me. In addition, now that I will be gone, he will not be cappable to steal the food on my desk! Beuuuh! Next, I would like to thank Edo for introducing me to Cat Poke, helping me to reduce my aweful French accent and inprove my English. I want to thank Lennert for our usual great discussion about everything but mainly religion and philosophy. Lennert, I hope you will find happiness with your growing familly and I wish that you will find satisfaction from a professional point of view because you deserve it so much! Last but not least, I would like to thank the rest of the TCM group as well as the SSI group members; Belinda, Marilou, Anna P., Anna G., Askar, Bektur, Guodong, Peiliang, Analisa, Malte (for taking care of the cluster nodes), Achille, Ivan (for being Ivan), Kiran, Irina, Kshiti, Albert, Guus, Erik, Jin, Tom...

Next, I want to thank the staff members of C&CZ which have been of great help with any informatic problem I encountered. In addition, they gave me the privilege to visit the cluster nodes installation, nodes on which I did some of my calculations. I want to give a special thank to Ben without whom I would have never been cappable to run the EDMFT codes. Ben, you are a programming magician!

This part of the aknowledgments is dedicated to my familly and therefore, written in French. Je voudrais remercier ma maman qui, toujours, m'a soutenu et encouragé dans tout ce que j'ai entrepris. Elle m'a écouté et soutenu pendant cette thèse, dans des moments (incroyablement) difficiles. Elle a toujours été fière de moi quoi que je fasse, quelque soit mes décisions. Sans elle, je ne serais pas la personne que je suis actuellement. Merci maman. Ensuite, je voudrais remercier ma petite soeur qui est tout juste extraordinaire (il n'y a pas d'autres mots). Je t'ai toujours admiré, et je t'admire toujours. J'admire ta confiance en toi, ta repartie et ta capacité à garder ton sang-froid. Merci d'avoir et de toujours essayer de me comprendre, de comprendre mes difficultés. PS: si tu vas à aux pages 28 et 29 de ma thèse, tu verras que j'utilise l'abréviation HP comme pour Harry Potter ;) . Je voudrais remercier mon papa pour sa patience (plus ou moins forcée). Malgré sa réluctance quant à la poursuite de mes études, je pense qu'il est fier de moi. J'aimerais remercier mes grands-parents, tout particulièrement mon grand-père. En effet, il est comme mon guide dans la vie; il me dit: "va à droite!" DONC je vais à gauche! C'est certainement grâce à mon caractère entêté et têtu (qu'apparemment j'aurais hérité de lui) que j'ai déjà accompli beaucoup de choses dans ma vie, en particulier ce doctorat!

Then, I would like to thank my fluffy. He is my daily companion in life and brings me so much happiness. I learn so much from him and he is always with me when I am down. I love youshka!

The final acknowledgement goes to whom I consider as my best friend; Jordan. We met when we were both doing our bachelor studies in Tour. I remember that at the time, I wanted to go to an engineer school because I thought myself incappable to achieve a master degree. At the last year of our bachelor, you not only told me that I was cappable to do master studies, but you prooved it to me. You proved me that I was not more stupid than anyone else and that I could go for it and eventually go for a PhD. Without you, I would have never achieved what I achieved. Therefore, I dedicate this thesis to you.

11

RESEARCH DATA MANAGEMENT

This thesis research has been carried out in accordance with the research data management policy of the Institute for Molecules and Materials of Radboud University, the Netherlands.[1]

The following datasets have been produced during this research:

- **Chapter 3 and 4:** Marion M.S. Barbeau, Martin Eckstein, Mikhail I. Katsnelson, Johan H. Mentink. Optical control of competing exchange interactions and coherent spin-charge coupling in two-orbital Mott insulators. SciPost Phys. 6, 027 (2019), doi: `https://scipost.org/10.21468/SciPostPhys.6.3.027`.
- **Chapter 5:** Marion M.S. Barbeau, D. Golež, J.H. Mentink. Calculations of exchange interactions using EDMFT.
- **Chapter 6:** Marion M.S. Barbeau, J.H. Mentink. Calculations of strain-control of antisymmetric exchange interactions.

1 https://www.ru.nl/rdm/vm/policy-documents/policy-imm/, last accessed 24 January 2020.

12

PUBLICATIONS

M.M.S. Barbeau, M. Eckstein, M.I. Katsnelson and J.H. Mentink,
"Optical control of competing exchange interactions and coherent spin-charge coupling in two-orbital Mott insulators",
SciPost Phys. **6**, 027 (2019)

M.M.S. Barbeau, D. Golež, P. Werner and J.H. Mentink,
"Effect of dynamical screening on the exchange interactions"
in preparation

M. Stifano, **M.M.S. Barbeau**, J.H. Mentink,
"Ultrafast toggle switching of magnetic skyrmions"
in preparation

13

CURRICULUM VITAE

NAME: Marion Michelle Séverine Barbeau
DATE OF BIRTH: 30 June 1992
PLACE OF BIRTH: Nantes, France

2007–10 High School in the scientific cursus, speciality: Physics
LYCÉE SAINTE MARIE DU PORT, Olonnes sur Mer (France)

2010–13 Bachelor in Matter Science
UNIVERSITÉ FRANÇOIS RABELAIS, Tours (France)

2013–15 Master in Matter Physics
UNIVERSITÉ PAUL SABATIER, Toulouse (France)

2015 Master Thesis
UPPSALA UNIVERSITY, Uppsala (Sweden)

2015–19 PhD in the Theory of Condensed Matter Physics Group
RADBOUD UNIVERSITY, Nijmegen (The Netherlands)

2020–current PostDoctoral position at QuSpin
NTNU,
NORWEGIAN UNIVERSITY OF SCIENCE AND TECHNOLOGY
Trondheim (Norway)

BIBLIOGRAPHY

[1] W. Van Heddeghem, S. Lambert, B. Lannoo, D. Colle, M. Pickavet, and P. Demeester, Comput. Commun. **50**, 64–76 (2014).

[2] E. Beaurepaire, J.-C. Merle, A. Daunois, and J.-Y. Bigot, Phys. Rev. Lett. **76**, 4250–4253 (1996).

[3] C. D. Stanciu, F. Hansteen, A. V. Kimel, A. Kirilyuk, A. Tsukamoto, A. Itoh, and T. Rasing, Phys. Rev. Lett. **99**, 047601 (2007).

[4] T. Ostler, J. Barker, R. Evans, R. Chantrell, U. Atxitia, O. Chubykalo-Fesenko, S. El Moussaoui, L. Le Guyader, E. Mengotti, L. Heyderman, F. Nolting, A. Tsukamoto, A. Itoh, D. Afanasiev, B. Ivanov, A. Kalashnikova, K. Vahaplar, J. Mentink, A. Kirilyuk, T. Rasing, and A. Kimel, Nat. Commun. **3**, 666 (2012).

[5] A. R. Khorsand, M. Savoini, A. Kirilyuk, A. V. Kimel, A. Tsukamoto, A. Itoh, and T. Rasing, Phys. Rev. Lett. **108**, 127205 (2012).

[6] C.-H. Lambert, S. Mangin, B. S. D. C. S. Varaprasad, Y. K. Takahashi, M. Hehn, M. Cinchetti, G. Malinowski, K. Hono, Y. Fainman, M. Aeschlimann, and E. E. Fullerton, Science **345**, 1337–1340 (2014).

[7] J. Zhao, A. V. Bragas, D. J. Lockwood, and R. Merlin, Phys. Rev. Lett. **93**, 107203 (2004).

[8] S. Wall, D. Prabhakaran, A. T. Boothroyd, and A. Cavalleri, Phys. Rev. Lett. **103**, 097402 (2009).

[9] M. Först, R. I. Tobey, S. Wall, H. Bromberger, V. Khanna, A. L. Cavalieri, Y.-D. Chuang, W. S. Lee, R. Moore, W. F. Schlotter, J. J. Turner, O. Krupin, M. Trigo, H. Zheng, J. F. Mitchell, S. S. Dhesi, J. P. Hill, and A. Cavalleri, Phys. Rev. B **84**, 241104(R) (2011).

[10] T. Li, A. Patz, L. Mouchliadis, J. Yan, T. A. Lograsso, I. E. Perakis, and J. Wang, Nature **496**, 69–73 (2013).

[11] R. R. Subkhangulov, A. B. Henriques, P. H. O. Rappl, E. Abramof, T. Rasing, and A. V. Kimel, Sci. Rep. **4**, 4368 (2015).

[12] M. Matsubara, A. Schroer, A. Schmehl, A. Melville, C. Becher, M. Trujillo-Martinez, D. G. Schlom, J. Mannhart, J. Kroha, and M. Fiebig, Nat. Commun. **6**, 6724 (2015).

[13] R. Mikhaylovskiy, E. Hendry, A. Secchi, J. Mentink, M. Eckstein, A. Wu, R. Pisarev, V. Kruglyak, M. Katsnelson, T. Rasing, and A. Kimel, Nat. Commun. **6**, 8190 (2015).

[14] D. Bossini, S. Dal Conte, Y. Hashimoto, A. Secchi, R. V. Pisarev, T. Rasing, G. Cerullo, and A. V. Kimel, Nat. Commun. **7**, 10645 (2016).

[15] S. Trotzky, P. Cheinet, S. Folling, M. Feld, U. Schnorrberger, A. M. Rey, A. Polkovnikov, E. A. Demler, M. D. Lukin, and I. Bloch, Science **319**, 295–299 (2008).

[16] Y.-A. Chen, S. Nascimbène, M. Aidelsburger, M. Atala, S. Trotzky, and I. Bloch, Phys. Rev. Lett. **107**, 210405 (2011).

[17] F. Görg, M. Messer, K. Sandholzer, G. Jotzu, R. Desbuquois, and T. Esslinger, Nature **553**, 481–485 (2018).

[18] J. H. Mentink, K. Balzer, and M. Eckstein, Nat. Commun. **6**, 6708 (2015).

[19] J. M. Losada, A. Brataas, and A. Qaiumzadeh, arXiv: 1904.01270 (2019).

[20] J. H. Mentink and M. Eckstein, Phys. Rev. Lett. **113**, 057201 (2014).

[21] M. Eckstein, J. H. Mentink, and P. Werner, arXiv:1703.03269 (2017).

[22] V. A. Gavrichkov, S. I. Polukeev, and S. G. Ovchinnikov, Phys. Rev. B **95**, 144424 (2017).

[23] J. Liu, K. Hejazi, and L. Balents, Phys. Rev. Lett. **121**, 107201 (2018).

[24] S.-S. B. Lee, J. von Delft, and A. Weichselbaum, Phys. Rev. B **96**, 245106 (2017).

[25] A. M. Oleś, Phys. Rev. B **41**, 2562 (1990).

[26] M. Bukov, M. Kolodrubetz, and A. Polkovnikov, Phys. Rev. Lett. **116**, 125301 (2016).

[27] S. Kitamura, T. Oka, and H. Aoki, Phys. Rev. B **96**, 014406 (2017).

[28] M. Bukov, "Floquet engineering in periodically driven closed quantum systems from dynamical localization to ultracold topological matter," PhD thesis (Boston University, 2017).

[29] M. Jarrell, Phys. Rev. Lett. **69**, 168 (1992).

[30] M. Caffarel and W. Krauth, Phys. Rev. Lett. **72**, 1545 (1994).

[31] O. Sakai and Y. Kuramoto, Solid State Commun. **89**, 307–311 (1994).

[32] A. Georges, G. Kotliar, W. Krauth, and M. J. Rozenberg, Rev. Mod. Phys. **68**, 13 (1996).

[33] R. O. Jones, Rev. Mod. Phys. **87**, 897 (2015).

[34] R. Chitra and G. Kotliar, Phys. Rev. Lett. **84**, 3678 (2000).

[35] D. Golež, M. Eckstein, and P. Werner, Phys. Rev. B **92**, 195123 (2015).

[36] M. I. Katsnelson and A. I. Lichtenstein, Phys. Rev. B **61**, 8906 (2000).

[37] M. Katsnelson and A. Lichtenstein, Eur. Phys. J. B **30**, 9–15 (2002).

[38] M. I. Katsnelson, Y. O. Kvashnin, V. V. Mazurenko, and A. I. Lichtenstein, Phy. Rev. B **82**, 100403(R) (2010).

[39] A. Secchi, S. Brener, A. Lichtenstein, and M. Katsnelson, Ann. Phys. (N. Y). **333**, 221–271 (2013).

[40] M. C. Gutzwiller, Phys. Rev. Lett. **10**, 159 (1963).

[41] J. Kanamori, Prog. Theor. Phys. **30**, 275–289 (1963).

[42] J. Hubbard, Proc. R. Soc. London. Ser. A. Math. Phys. Sci. **276**, 238 (1963).

[43] J. Hubbard, Proc. R. Soc. London. Ser. A. Math. Phys. Sci. **281**, 401 (1964).

[44] M. Cyrot, Solid State Commun. **62**, 821–823 (1987).

[45] I. Affleck and J. B. Marston, Phys. Rev. B **37**, 3774(R) (1988).

[46] L. Tarruell and L. Sanchez-Palencia, Comptes Rendus Phys. **19**, 365–393 (2018).

[47] N. F. Mott, Rev. Mod. Phys. **40**, 677 (1968).

[48] R. Peierls, Zeitschrift für Phys. **80**, 763–791 (1933).

[49] J. M. Luttinger, Phys. Rev. **84**, 814 (1951).

[50] V. M. Pereira, F. Guinea, J. M. B. Lopes dos Santos, N. M. R. Peres, and A. H. Castro Neto, Phys. Rev. Lett. **96**, 036801 (2006).

[51] M. Barbeau, M. Eckstein, M. Katsnelson, and J. Mentink, SciPost Phys. **6**, 027 (2019).

[52] K. A. Chao, J. Spałek, and A. M. Oleś, Phys. Status Solidi **84**, 747–759 (1977).

[53] K. A. Chao, J Spalek, and A. M. Oles, J. Phys. C Solid State Phys. **10**, L271 (1977).

[54] K. A. Chao, J. Spałek, and A. M. Oleś, Phys. Rev. B **18**, 3453 (1978).

[55] J. Zaanen and A. M. Oleś, Phys. Rev. B **37**, 9423 (1988).

[56] M. S. Laad and D. K. Ghosh, J. Phys. Condens. Matter **3**, 9723 (1991).

[57] A. Eckardt and E. Anisimovas, New J. Phys. **17**, 093039 (2015).

[58] M. Bukov, L. D'Alessio, and A. Polkovnikov, Adv. Phys. **64**, 139–226 (2015).

[59] A. H. MacDonald, S. M. Girvin, and D. Yoshioka, Phys. Rev. B **37**, 9753 (1988).

[60] A. P. Itin and M. I. Katsnelson, Phys. Rev. Lett. **115**, 075301 (2015).

[61] P. Sun and G. Kotliar, Phys. Rev. B **66**, 085120 (2002).

[62] L. Huang, T. Ayral, S. Biermann, and P. Werner, Phys. Rev. B **90**, 195114 (2014).

[63] A. Amaricci, A. Camjayi, K. Haule, G. Kotliar, D. Tanasković, and V. Dobrosavljević, Phys. Rev. B **82**, 155102 (2010).

[64] H. Terletska, T. Chen, and E. Gull, Phys. Rev. B **95**, 115149 (2017).

[65] T. Ayral, S. Biermann, and P. Werner, Phys. Rev. B **87**, 125149 (2013).

[66] A. A. Abrikosov, L. P. Gorkov, and I. E. Dzyaloshinski, *Methods of quantum field theory in statistical physics*, Dover Books on Physics Series (Dover Publications, 1975).

[67] P. Werner and M. Casula, J. Phys. Condens. Matter **28**, 383001 (2016).

[68] W. Metzner and D. Vollhardt, Phys. Rev. Lett. **62**, 324 (1989).

[69] P. W. Anderson, Phys. Rev. **124**, 41 (1961).

[70] T. Holstein, Ann. Phys. **8**, 325–342 (1959).

[71] A. C. Hewson and D Meyer, J. Phys. Condens. Matter **14**, 427 (2002).

[72] G. Li, "Non-local correlations within dynamical mean-field theory," PhD thesis (Bonn University, 2009).

[73] H. Aoki, N. Tsuji, M. Eckstein, M. Kollar, T. Oka, and P. Werner, Rev. Mod. Phys. **86**, 779 (2014).

[74] M. Eckstein and P. Werner, Phys. Rev. B **82**, 115115 (2010).

[75] R. Bersohn, Science **139**, 399–400 (1963).

[76] P. W. Anderson, Solid State Phys., 99–214 (1963).

[77] T. Holstein and H. Primakoff, Phys. Rev. **58**, 1098 (1940).

[78] J. H. Mentink, "Magnetism on the timescale of the exchange interaction: explanations and prediction," PhD thesis (Radboud University, 2012).

[79] J. Hellsvik, M. Balestieri, T. Usui, A. Stroppa, A. Bergman, L. Bergqvist, D. Prabhakaran, O. Eriksson, S. Picozzi, T. Kimura, and J. Lorenzana, Phys. Rev. B **90**, 014437 (2014).

[80] F. Haldane, Phys. Lett. A **93**, 464–468 (1983).

[81] F. D. M. Haldane, Phys. Rev. Lett. **50**, 1153 (1983).

[82] S. R. Manmana, A. M. Läuchli, F. H. L. Essler, and F. Mila, Phys. Rev. B **83**, 184433 (2011).

[83] I. d. P. R. Moreira, N. Suaud, N. Guihéry, J. P. Malrieu, R. Caballol, J. M. Bofill, and F. Illas, Phys. Rev. B **66**, 134430 (2002).

[84] K. Takasan and M. Sato, Phys. Rev. B **100**, 060408(R) (2019).

[85] V. Y. Irkhin and Y. P. Irkhin, Phys. status solidi (b) **183**, 9–58 (1994).

[86] L. Landau, Phys. Z. Sowjetunion **46**, 2 (1932).

[87] C. Zener, Proc. R. Soc. A Math. Phys. Eng. Sci. **137**, 696 (1932).

[88] A. Sibille, J. F. Palmier, and F. Laruelle, Phys. Rev. Lett. **80**, 4506 (1998).

[89] B. Rosam, D. Meinhold, F. Löser, V. G. Lyssenko, S. Glutsch, F. Bechstedt, F. Rossi, K. Köhler, and K. Leo, Phys. Rev. Lett. **86**, 1307 (2001).

[90] T. Oka, R. Arita, and H. Aoki, Phys. Rev. Lett. **91**, 066406 (2003).

[91] P. W. Anderson and P. Morel, Phys. Rev. **123**, 1911 (1961).

[92] P. W. Anderson, Science **235**, 1196–1198 (1987).

[93] A. Alvermann and H. Fehske, J. Comput. Phys. **230**, 5930–5956 (2011).

[94] L. D'Alessio and M. Rigol, Phys. Rev. X **4**, 041048 (2014).

[95] P. Weinberg, M. Bukov, L. D'Alessio, A. Polkovnikov, S. Vajna, and M. Kolodrubetz, Phys. Rep. **688**, 1–35 (2017).

[96] H. U. R. Strand, D. Golež, M. Eckstein, and P. Werner, Phys. Rev. B **96**, 165104 (2017).

[97] P. Werner, H. U. R. Strand, S. Hoshino, Y. Murakami, and M. Eckstein, Phys. Rev. B **97**, 165119 (2018).

[98] J. Li, H. U. R. Strand, P. Werner, and M. Eckstein, Nat. Commun. **9**, 4581 (2018).

[99] P. Soltan-Panahi, D.-S. Lühmann, J. Struck, P. Windpassinger, and K. Sengstock, Nat. Phys. **8**, 71–75 (2012).

[100] Z. Zhang, H.-H. Hung, C. M. Ho, E. Zhao, and W. V. Liu, Phys. Rev. A **82**, 033610 (2010).

[101] N. Tancogne-Dejean, M. A. Sentef, and A. Rubio, arXiv: 1906.11316 (2019).

[102] E. A. Stepanov, E. G. C. P. van Loon, A. A. Katanin, A. I. Lichtenstein, M. I. Katsnelson, and A. N. Rubtsov, Phys. Rev. B **93**, 045107 (2016).

[103] E. G. C. P. van Loon, M. Schüler, M. I. Katsnelson, and T. O. Wehling, Phys. Rev. B **94**, 165141 (2016).

[104] D. Medvedeva, S. Iskakov, F. Krien, V. V. Mazurenko, and A. I. Lichtenstein, Phys. Rev. B **96**, 235149 (2017).

[105] R. Eder, J. van den Brink, and G. A. Sawatzky, Phys. Rev. B **54**, R732(R) (1996).

[106] A. Fert, V. Cros, and J. Sampaio, Nat. Nano. **8**, 152–156 (2013).

[107] A. Fert, N. Reyren, and V. Cros, Nat. Rev. Mat. **2**, 17031 (2017).

[108] Y. Zhou, National Sci. Rev. **6**, 210–212 (2018).

[109] N. Romming, C. Hanneken, M. Menzel, J. E. Bickel, B. Wolter, K. von Bergmann, A. Kubetzka, and R. Wiesendanger, Science **341**, 636–639 (2013).

[110] J. Sampaio, V. Cros, S. Rohart, A. Thiaville, and A. Fert, Nat. Nano. **8**, 839–844 (2013).

[111] W. Jiang, P. Upadhyaya, W. Zhang, G. Yu, M. B. Jungfleisch, F. Y. Fradin, J. E. Pearson, Y. Tserkovnyak, K. L. Wang, O. Heinonen, S. G. E. te Velthuis, and A. Hoffmann, Science **349**, 283–286 (2015).

[112] P.-J. Hsu, A. Kubetzka, A. Finco, N. Romming, K. von Bergmann, and R. Wiesendanger, Nat. Nano. **12**, 123–126 (2017).

[113] Y. Liu, H. Du, M. Jia, and A. Du, Phy. Rev. **91**, 094425 (2015).

[114] C. Heo, N. S. Kiselev, A. K. Nandy, S. Blügel, and T. Rasing, Sci. Rep. **6**, 27146 (2016).

[115] M. Finazzi, M. Savoini, A. R. Khorsand, A. Tsukamoto, A. Itoh, L. Duò, A. Kirilyuk, T. Rasing, and M. Ezawa, Proc. SPIE, Spintronics VI, 07 (2013).

[116] G. Berruto, I. Madan, Y. Murooka, G. M. Vanacore, E. Pomarico, J. Rajeswari, R. Lamb, P. Huang, A. J. Kruchkov, Y. Togawa, T. LaGrange, D. McGrouther, H. M. Rønnow, and F. Carbone, Phys. Rev. Lett. **120**, 117201 (2018).

[117] S.-G. Je, P. Vallobra, T. Srivastava, J.-C. Rojas-Sánchez, T. H. Pham, M. Hehn, G. Malinowski, C. Baraduc, S. Auffret, G. Gaudin, S. Mangin, H. Béa, and O. Boulle, Nano Lett. **18**, 7362–7371 (2018).

[118] J.-M. Hu, T. Yang, and L.-Q. Chen, npj Comput. Mat. **4**, 62 (2018).

[119] S. C. Masmanidis, H. X. Tang, E. B. Myers, M. Li, K. D. Greve, G. Vermeulen, W. V. Roy, and M. L. Roukes, Phy. Rev. Lett. **95**, 187206 (2005).

[120] A. V. Scherbakov, A. S. Salasyuk, A. V. Akimov, X. Liu, M. Bombeck, C. Brüggemann, D. R. Yakovlev, V. F. Sapega, J. K. Furdyna, and M. Bayer, Phys. Rev. Lett. **105**, 117204 (2010).

[121] J.-W. Kim, M. Vomir, and J.-Y. Bigot, Phy. Rev. Lett. **109**, 166601 (2012).

[122] O. Kovalenko, T. Pezeril, and V. V. Temnov, Phy. Rev. Lett. **110**, 266602 (2013).

[123] M. Stifano, "Skyrmion Manipulation in Ultrathin Films by Modification of Exchange Interactions", Master Thesis (Radboud University, 2017).

[124] V. Kashid, T. Schena, B. Zimmermann, Y. Mokrousov, S. Blügel, V. Shah, and H. G. Salunke, Phy. Rev. B **90**, 054412 (2014).

[125] A. Liechtenstein, M. Katsnelson, V. Antropov, and V. Gubanov, JMMM **67**, 65–74 (1987).

[126] K. Sato, L. Bergqvist, J. Kudrnovský, P. H. Dederichs, O. Eriksson, I. Turek, B. Sanyal, G. Bouzerar, H. Katayama-Yoshida, V. A. Dinh, T. Fukushima, H. Kizaki, and R. Zeller, Rev. Mod. Phys. **82**, 1633–1690 (2010).

[127] A. Soumyanarayanan, M. Raju, A. L. Gonzalez Oyarce, A. K. C. Tan, M.-Y. Im, A. P. Petrović, P. Ho, K. H. Khoo, M. Tran, C. K. Gan, F. Ernult, and C. Panagopoulos, Nat. Mater. **16**, 898–904 (2017).

[128] K. Zakeri, J. Phys. Condens. Matter **29**, 013001 (2017).

[129] P.-J. Hsu, L. Rózsa, A. Finco, L. Schmidt, K. Palotás, E. Vedmedenko, L. Udvardi, L. Szunyogh, A. Kubetzka, K. von Bergmann, and R. Wiesendanger, Nat. Commun. **9**, 1571 (2018).

[130] V. Shakagatskyi, "Ultrafast acoustics in hybrid and magnetic structures," PhD thesis (Thèse de doctorat du Maine, 2015).

[131] V. V. Temnov, Nat. Photonics **6**, 728–736 (2012).

[132] V. V. Temnov, C. Klieber, K. A. Nelson, T. Thomay, V. Knittel, A. Leitenstorfer, D. Makarov, M. Albrecht, and R. Bratschitsch, Nat. Commun. **4**, 1468 (2013).

[133] H. N. Lin., R. J. Stoner, H. J. Maris, and J. Tauc, J. Appl. Phys. **69**, 3816 (1991).

[134] M. Stifano et al., *"Ultrafast toggle switching of magnetic skyrmions", in preparation.*